國 立 交 通 大 學

土木工程學系

碩 士 論 文

外源界面活性劑在呼吸道黏性薄膜上傳輸之理論探討

Exogenous Surfactant Transport on the Viscous Thin Film within a Pulmonary Airway: a Theoretical Study

研究生: 劉俐鈺

指導教授: 蔡武廷 教授

中華民國九十二年七月

外源界面活性劑在呼吸道黏性薄膜上傳輸之理論探討

Exogenous Surfactant Transport on the Viscous Thin Film within a Pulmonary Airway: a Theoretical Study

研究生: 劉俐鈺 Student: Li-Yu Liu

指導教授: 蔡武廷 教授 Advisor: Professor Wu-ting Tsai

國立交通大學

土木工程學系

碩士論文

A Thesis

Submitted to Department of Civil Engineering

College of Engineering

National Chiao Tung University

in Partial Fulfillment of the Requirements

of the Degree of

Master

in

Civil Engineering

July 2003

Hsinchu, Taiwan, Republic of China

中華民國九十二年七月

外源界面活性劑在呼吸道黏性薄膜上傳輸之理論探討

研究生: 劉俐鈺　　指導教授: 蔡武廷 教授

國立交通大學
土木工程研究所碩士班

摘　　要

本研究以潤滑理論推導之運動與傳輸模式, 配合數值計算, 模擬外源界面活性劑在呼吸道黏性薄膜上之傳輸, 以及其所造成的黏膜擾動。其研究目的爲探討影響「界面活性劑療法」治療新生兒「呼吸窘迫症候群」之相關參數, 包括: 黏膜厚度與呼吸道半徑比、外源界面活性劑強度、原有界面活性劑、薄膜黏滯性、呼吸道氣流、以及界面活性劑之可溶性。數值模擬結果發現; 外源界面活性劑在低級數呼吸道 (較高之黏膜厚度與呼吸道半徑比值) 中所造成之薄膜擾動幅度較高級數呼吸道中明顯, 但呼吸道半徑對界面活性劑傳輸之影響極小。外源界面活性劑初始強度愈強, 則所造成的薄膜擾動波與界面活性劑之傳輸速率亦愈快。原有界面活性劑的存在對薄膜擾動與外源界面活性劑傳輸皆產生極大的影響; 原有界面活性劑降低薄膜之擾動幅度, 然而卻提高界面活性劑波前傳播之速率。此波前傳播速率之提高乃因外源活性劑推擠原有界面活性劑, 使原有界面活性劑局部濃度增加並往前推進, 然而外源界面劑之傳輸速率則因此降低。呼吸道氣流在黏膜表面所造成之剪力對界面活性劑之傳輸影響極小。界面活性劑之可溶性質減緩表面界面活性劑之濃度梯度, 進而減弱表面張力梯度引起的流場, 降低表面界面活性劑之傳輸速率, 但黏膜擾動波波高則明顯增大。

Exogenous Surfactant Transport on the Viscous Thin Film within a Pulmonary Airway: a Theoretical Study

Student: Li-Yu Liu Advisor: Professor Wu-ting Tsai

Department of Civil Engineering

National Chiao Tung University

Abstract

The transport of the exogenous surfactant in a pulmonary airway lining is analyzed using the theoretical model developed based on the lubrication theory. The primary objective of the model is to study the parameters involved in surfactant replacement therapy for neonatal respiratory distress syndrome, including the ratio of film thickness to airway radius, the strength of exogenous surfactant dose, the presence of preexisting surfactant, the film viscosity, the shear stress due to air flow, and the surfactant solubility. Numerical simulation of the model indicates that the film disturbance induced by the Marangoni effect in low-generation airways (larger ratio of film thickness to airway radius) is more significant than that in high-generation airways. However, the surfactant spreading is virtually unaffected. Increasing the initial local exogenous concentration enhances the surfactant transport and also accelerates the propagation of film disturbance. The presence of preexisting surfactant tends to moderate the shock-like film disturbance and also prolongs the extent of surfactant monolayer front. This, however, does not mean that the spreading of exogenous surfactant is enhanced by the presence of preexisting surfactant. The extended monolayer is attributed to the compression of the preexisting surfactant in regions ahead of the advancing exogenous surfactant front. The shear stress induced by the air flow within the airway has very little effect on the surfactant transport. If the surfactant is soluble, the gradient in the surface concentration distribution as well as the induced Marangoni effect diminish, and the surfactant transport is slowed down. The shock-like film disturbance, however, is elevated significantly.

Acknowledgments

First and foremost, I would like to thank my advisor Prof. Wu-ting Tsai for his encourage and guidance. He makes me think, even when I do not want to, and pushes me to my best. In many ways, he reaches me more about myself than about the topic at hand. Thanks to the professors Jui-Ying Tasi, Hsien-Hung Wei, Liang-Cheng Chang and Chih-Ping Wang for providing insightful advice to my search. Special thanks to Dr. Pei-Chieh Sun for assistance with physiological and clinical informations.

In these two years, I have benefited from working with all members in the lab. Li-Ping Hung and Mei-Ying Lin provide me with many suggestions and continuous encouragement. Shi-Ming Chen, Meng-Kang Yeh, Kuo-Hui Wen work with me to solve many challenging problems in classes. Efforts of Shi-Ming Chen as a system manager also give us stable computing resources. They are not only partners in work but also good friends.

Finally, I would like to express my appreciate to my wonderful friends and family who have continued to support and encourage me, especially during times of slow progress.

Li-Yu Liu

July 2003

Contents

摘 要 i

Abstract ii

Acknowledgments iii

Contents iv

List of Tables v

List of Figures vi

1 Introduction 1

1.1 Pulmonary Anatomy and Physiology 1

1.2 Surface Tension and Surfactant 4

1.3 Pulmonary Surfactant 7

1.4 Neonatal Respiratory Distress Syndrome 8

1.5 Surfactant Replacement Therapy 10

1.6 Previous Studies on Surfactant-Driven Thin-Film Flows 13

1.7 Outline of the Present Study 16

2 Model Formulation 18

2.1 Governing Equations 18

2.1.1 Momentum and mass conservation 18

2.1.2 Boundary conditions . . . 19
2.1.3 Transport equations for the surfactant . . . 21
2.1.4 Equation of state . . . 22
2.2 Non-dimensionalization . . . 23
2.3 Lubrication Approximation . . . 27
2.4 Cross-sectional Average . . . 30

3 Numerical Method **33**
3.1 Time Integration Scheme . . . 33
3.2 Initial Conditions . . . 34
3.3 Boundary Conditions . . . 36

4 Results **37**
4.1 Film Disturbance and Surfactant Spread in Various Generations of Airways 37
4.2 Effect of the Initial Exogenous Surfactant Strength . . . 47
4.3 Effect of the Preexisting Surfactant . . . 52
4.4 Effect of the Film Viscosity . . . 58
4.5 Effect of the Air-Flow Induced Shear Stress . . . 64
4.6 Effect of the Surfactant Solubility . . . 73
4.6.1 Effect of the diffusion-adsorption ratio . . . 73
4.6.2 Effect of the kinetic nonlinearity . . . 80

5 Conclusions **89**

Bibliography **93**

A Stress Boundary Conditions for a Newtonian Interface **101**
A.1 Normal-stress Boundary Condition . . . 101
A.2 Tangential-stress Boundary Condition . . . 104

B Cross-sectional Average of Bulk Surfactant Transport Equation **106**

C Shear Stress Due to Air Flow **109**

List of Tables

1.1 Dimensions of the first 16 generations of airways [from Weibel, 1963]. . . . 3

2.1 Order-of-magnitude estimates for the physical constants in the human airways and the physicochemical constants associated with the pulmonary surfactant. 24

2.2 Non-dimensional parameters considered in the formulation and the ranges of the values estimated using the physical and physicochemical constants listed in Table **??**. 28

List of Figures

1.1 Organization of the respiratory system [from Vander *et al.*, 1994]. 2

1.2 Relationships between blood vessels and airways. A small section of (A) is enlarged in (B) to show the continuation of the airways and the clusters of alveoli at their end. The Alveolus are surrounded by capillaries [from Vander *et al.*, 1994]. 4

1.3 Anatomy of the respiratory membrane. The respiratory membrane is composed of epithelial cells of the alveoli, the capillary endothelium, and the basement membranes between. Surfactant-secreting cells are also shown. Diffusion of oxygen occurs from the alveolar air into the pulmonary capillary blood; carbon dioxide diffuses from the pulmonary blood into the alveolus [from Marieb, 2000]. 5

1.4 At the interface with no surfactant molecules, liquid molecules are attracted to each other and to molecules below, creating a force to contract the surface. 6

1.5 Surfactant molecules form a monolayer at the gas-liquid interface and reduce the surface tension between the liquid molecules at the interface. . . . 6

1.6 A comparison of pressure-volume curves for cat lungs inflated with air or saline [from Clements & Tierney, 1965]. 7

1.7 Mean concentrations of lecithin and sphingomyelin in amniotic fluid during gestation [from Gluck *et al.*, 1971]. 10

1.8 An oral endotracheal tube in position [from Barnes, 1994]. 11

1.9 Schematic of Marangoni effect. 12

2.1 The geometry of a lined airway with soluble surfactants distributed. 19

3.1 Initial conditions for (a) the film thickness $h(z,0)$ and (b) the surfactant surface concentration $\Gamma(z,0)$ for $\Gamma_{exo} = 1.0$ and $\Gamma_{pre} = 0.1$. In Figure (b), the dashed line represents the surfactant distribution described by (**??**), and the dotted line represents that described by (**??**). 35

4.1 Time varying profiles of film thickness $h(z,t)$ for the ratio of film thickness to airway radius ϵ = (a) 0.001, (b) 0.01, (c) 0.05 and (d) 0.1, at time $t = 0$ (dashed line), 1, 5, 10, 20 and 40. Parameter values are $\Gamma_{exo} = 1$, $\Gamma_{pre} = 0$, $\mu = 0.01$ g/cm s, $\tau_{air} = 0$ and $\mathcal{G}_r = \mathcal{G}_z = 0$. 41

4.2 Time varying profiles of surface surfactant concentration $\Gamma(z,t)$ for the ratio of film thickness to airway radius ϵ = (a) 0.001, (b) 0.01, (c) 0.05 and (d) 0.1, at time $t = 0$ (dashed line), 1, 5, 10, 20 and 40. Parameter values are $\Gamma_{exo} = 1$, $\Gamma_{pre} = 0$, $\mu = 0.01$ g/cm s, $\tau_{air} = 0$ and $\mathcal{G}_r = \mathcal{G}_z = 0$. 42

4.3 Temporal evolutions of (a) the peak film thickness, h_{peak}, (b) the axial position of peak film thickness, z_{peak}, and (c) the trough film thickness, h_{trough}, for various ratios of film thickness to airway radius $\epsilon = 0.001$, 0.01, 0.05 and 0.1. 43

4.4 Temporal evolutions of (a) the length of surfactant monolayer, L_{mono}, (b) the spreading velocity of surfactant monolayer, $\mathrm{d}L_{mono}/\mathrm{d}t$, (c) the surfactant concentration at $z = 0$, $\Gamma(0,t)$, and (d) the dropping rate, $\mathrm{d}\Gamma(0,t)/\mathrm{d}t$, for various ratios of film thickness to airway radius $\epsilon = 0.001$, 0.01, 0.05 and 0.1. 44

4.5 Time varying profiles of film thickness $h(z,t)$ for the ratio of film thickness to airway radius ϵ = (a) 0.001, (b) 0.01, (c) 0.05 and (d) 0.1, at time $t = 0$ (dashed line), 1, 5, 10, 20 and 40. Parameter values are $\Gamma_{exo} = 1$, $\Gamma_{pre} = 0$, $\mu = 0.01$ g/cm s, $\tau_{air} = 0$ and $\mathcal{G}_r = \mathcal{G}_z = 0$. 45

4.6 Time varying profiles of surface surfactant concentration $\Gamma(z,t)$ for the ratio of film thickness to airway radius ϵ =1 (a) 0.00, (b) 0.01, (c) 0.05 and (d) 0.1, at time $t = 0$ (dashed line), 1, 5, 10, 20 and 40. Parameter values are $\Gamma_{exo} = 1$, $\Gamma_{pre} = 0$, $\mu = 0.01$ g/cm s, $\tau_{air} = 0$ and $\mathcal{G}_r = \mathcal{G}_z = 0$. 46

4.7 Time varying profiles of film thickness $h(z,t)$ for the concentration of exogenous surfactant Γ_{exo} = (a) 1, (b) 0.8, (c) 0.6 and (d) 0.4, at time $t = 0$ (dashed line), 1, 5, 10, 20, 40 and 100. Parameter values are $\epsilon = 0.01$, $\Gamma_{pre} = 0$, $\mu = 0.01$ g/cm s, $\tau_{air} = 0$ and $\mathcal{G}_r = \mathcal{G}_z = 0$. 48

4.8 Time varying profiles of surface surfactant concentration $\Gamma(z,t)$ for the concentration of exogenous surfactant Γ_{exo} = (a) 1, (b) 0.8, (c) 0.6 and (d) 0.4, at time $t = 0$ (dashed line), 1, 5, 10, 20, 40 and 100. Parameter values are $\epsilon = 0.01$, $\Gamma_{pre} = 0$, $\mu = 0.01$ g/cm s, $\tau_{air} = 0$ and $\mathcal{G}_r = \mathcal{G}_z = 0$. 49

4.9 Temporal evolutions of (a) the peak film thickness, h_{peak}, (b) the axial position of peak film thickness, z_{peak}, and (c) the trough film thickness, h_{trough}, for various initial concentrations of exogenous surfactant $\Gamma_{exo} = 1$, 0.8, 0.6 and 0.4. 50

4.10 Temporal evolutions of (a) the length of surfactant monolayer, L_{mono}, (b) the spreading velocity of surfactant monolayer, $\mathrm{d}L_{mono}/\mathrm{d}t$, (c) the surfactant concentration at $z = 0$, $\Gamma(0,t)$, and (d) the dropping rate, $\mathrm{d}\Gamma(0,t)/\mathrm{d}t$, for various initial concentrations of exogenous surfactant $\Gamma_{exo} = 1$, 0.8, 0.6 and 0.4. 51

4.11 Time varying profiles of film thickness $h(z,t)$ for the concentrations of preexisting surfactant Γ_{pre} = (a) 0, (b) 0.01, (c) 0.05 and (d) 0.1, at time $t = 0$ (dashed line), 1, 5, 10, 20 and 40. Parameter values are $\epsilon = 0.01$, $\Gamma_{exo} = 1$, $\mu = 0.01$ g/cm s, $\tau_{air} = 0$ and $\mathcal{G}_r = \mathcal{G}_z = 0$. 54

4.12 Time varying profiles of surface surfactant concentration $\Gamma(z,t)$ for the concentrations of preexisting surfactant Γ_{pre} = (a) 0, (b) 0.01, (c) 0.05 and (d) 0.1, at time $t = 0$ (dashed line), 1, 5, 10, 20 and 40. Parameter values are $\epsilon = 0.01$, $\Gamma_{exo} = 1$, $\mu = 0.01$ g/cm s, $\tau_{air} = 0$ and $\mathcal{G}_r = \mathcal{G}_z = 0$. 55

4.13 Temporal evolutions of (a) the peak film thickness, h_{peak}, (b) the axial position of peak film thickness, z_{peak}, and (c) the trough film thickness, h_{trough}, for various concentrations of preexisting surfactant $\Gamma_{pre} = 0$, 0.01, 0.05 and 0.1. 56

4.14 Temporal evolutions of (a) the length of surfactant monolayer, L_{mono}, (b) the spreading velocity of surfactant monolayer, $\mathrm{d}L_{mono}/\mathrm{d}t$, (c) the surfactant concentration at $z = 0$, $\Gamma(0,t)$, and (d) the dropping rate, $\mathrm{d}\Gamma(0,t)/\mathrm{d}t$, for various concentrations of preexisting surfactant $\Gamma_{pre} = 0$, 0.01, 0.05 and 0.1. 57

4.15 Time varying profiles of film thickness $h(z,t)$ for the film viscosity μ = (a) 0.01, (b) 1, (c) 10 and (d) 100 g/cm s, at time $t = 0$ (dashed line), 1, 5, 10, 20, 40 and 80. Parameter values are $\epsilon = 0.01$, $\Gamma_{exo} = 1$, $\Gamma_{pre} = 0$, $\tau_{air} = 0$ and $\mathcal{G}_r = \mathcal{G}_z = 0$. 60

4.16 Time varying profiles of surface surfactant concentration $\Gamma(z,t)$ for the film viscosity μ = (a) 0.01, (b) 1, (c) 10 and (d) 100 g/cm s, at time $t = 0$ (dashed line), 1, 5, 10, 20, 40 and 80. Parameter values are $\epsilon = 0.01$, $\Gamma_{exo} = 1$, $\Gamma_{pre} = 0$, $\tau_{air} = 0$ and $\mathcal{G}_r = \mathcal{G}_z = 0$. 61

4.17 Temporal evolutions of (a) the peak film thickness, h_{peak}, (b) the axial position of peak film thickness, z_{peak}, and (c) the trough film thickness, h_{trough}, for various film viscosities $\mu = 0.01$, 1, 10 and 100 g/cm s. 62

4.18 Temporal evolutions of (a) the length of surfactant monolayer, L_{mono}, (b) the spreading velocity of surfactant monolayer, $\mathrm{d}L_{mono}/\mathrm{d}t$, (c) the surfactant concentration at $z = 0$, $\Gamma(0,t)$, and (d) the dropping rate, $\mathrm{d}\Gamma(0,t)/\mathrm{d}t$, for various film viscosities $\mu = 0.01$, 1, 10 and 100 g/cm s. 63

4.19 Schematic of an asymmetric breathing cycle with the inspiration fraction $f = 0.25$, the breathing period τ_0 and the tidal volume $2V_T$: (a) the time varying lung volume and (b) the air flux in the airway. 65

4.20 Time varying profiles of film thickness $h(z,t)$ with no shear stress (solid line) and considering forward shear stress (dash-dotted line) and backward shear stress (dashed line) in the airway at generation $n =$ (a) 1, (b) 5, (c) 10 and (d) 14, at time $t = 0$, 1, 5, 10, 20 and 40. The dimensional parameters of the air flow are: $2V_T \times R^3 = 6.6$ ml, $\tau_0 \times \mathcal{T} = 2$ s and $f = 0.25$. Other parameter values are fixed as $\Gamma_{exo} = 1$, $\Gamma_{pre} = 0$, $\mu = 100$ g/cm s and $\mathcal{G}_r = \mathcal{G}_z = 0$. 68

4.21 Time varying profiles of surface surfactant concentration $\Gamma(z,t)$ with no shear stress (solid line) and considering forward shear stress (dash-dotted line) and backward shear stress (dashed line) in the airway at generation $n =$ (a) 1, (b) 5, (c) 10 and (d) 14, at time $t = 0$, 1, 5, 10, 20 and 40. The dimensional parameters of the air flow are: $2V_T \times R^3 = 6.6$ ml, $\tau_0 \times \mathcal{T} = 2$ s and $f = 0.25$. Other parameter values are fixed as $\Gamma_{exo} = 1$, $\Gamma_{pre} = 0$, $\mu = 100$ g/cm s and $\mathcal{G}_r = \mathcal{G}_z = 0$. 69

4.22 Time varying profiles of (a) film thickness $h(z,t)$ and (b) surface surfactant concentration $\Gamma(z,t)$ considering forward shear stress with the tidal volume $2V_T \times R^3$ (ml) = 0 (solid line), 6.6 (dashed line) and 12 (dash-dotted line), and $\tau_0 \times \mathcal{T} = 2$ s, $f = 0.25$ in generation 1 airway, at time $t = 0$, 1, 5, 10, 20, 40 and 80. Other parameter values are fixed as $\Gamma_{exo} = 1$, $\Gamma_{pre} = 0$, $\mu = 100$ g/cm s and $\mathcal{G}_r = \mathcal{G}_z = 0$. 70

4.23 Temporal evolutions of (a) the peak film thickness, h_{peak}, (b) the axial position of peak film thickness, z_{peak}, and (c) the trough film thickness, h_{trough}, for various shear stresses with the tidal volume $2V_T \times R^3 = 0$, 6.6 and 12 ml. 71

4.24 Temporal evolutions of (a) the length of surfactant monolayer, L_{mono}, (b) the spreading velocity of surfactant monolayer, $\mathrm{d}L_{mono}/\mathrm{d}t$, (c) the surfactant concentration at $z = 0.0$, $\Gamma(0,t)$, and (d) the dropping rate, $\mathrm{d}\Gamma(0,t)/\mathrm{d}t$, for various shear stresses with the tidal volume $2V_T \times R^3 = 0$, 6.6 and 12 ml. 72

4.25 Time varying profiles of film thickness $h(z,t)$ for the diffusion-adsorption ratio $\mathcal{J}$ = (a) 100, (b) 1 and (c) 0.01, illustrated at times $t = 0$ (dashed line), 1, 5, 10, 20, 40, 80. Other parameter values are fixed and chosen as $\beta \to \infty$, $\mathcal{K} = 1$, $\Gamma_{exo} = 1$, $\Gamma_{pre} = 0$, $\mu = 100$ g/cm s, $\tau_{air} = 0$ and $\mathcal{G}_r = \mathcal{G}_z = 0$. 75

4.26 Time varying profiles of surface surfactant concentration $\Gamma(z,t)$ for the diffusion-adsorption ratio $\mathcal{J}$ = (a) 100, (b) 1 and (c) 0.01, illustrated at times $t = 0$, 1 (dashed), 5 (dash-dotted), 10 (long-dashed line), 20, 40, 80. Other parameter values are fixed and chosen as $\beta \to \infty$, $\mathcal{K} = 1$, $\Gamma_{exo} = 1$, $\Gamma_{pre} = 0$, $\mu = 100$ g/cm s, $\tau_{air} = 0$ and $\mathcal{G}_r = \mathcal{G}_z = 0$. 76

4.27 Time varying profiles of bulk surfactant concentration $\bar{C}(z,t)$ for the diffusion-adsorption ratio $\mathcal{J}$ = (a) 100, (b) 1 and (c) 0.01, illustrated at times $t = 0$, 1 (dashed), 5 (dash-dotted), 10 (long-dashed line), 20, 40, 80. Other parameter values are fixed and chosen as $\beta \to \infty$, $\mathcal{K} = 1$, $\Gamma_{exo} = 1$, $\Gamma_{pre} = 0$, $\mu = 100$ g/cm s, $\tau_{air} = 0$ and $\mathcal{G}_r = \mathcal{G}_z = 0$. 77

4.28 Temporal evolutions of (a) the bulk surfactant concentration at $z = 0$, $\bar{C}(0,t)$, (b) the surface surfactant concentration at $z = 0$, $\Gamma(0,t)$, and (c) the monolayer length, L_{mono}, for $\mathcal{J} = 100$, 1 and 0.01. 78

4.29 Temporal evolutions of (a) the peak film thickness, h_{peak}, and (b) the axial position of peak film thickness, z_{peak}, for $\mathcal{J} = 100$, 1 and 0.01. 79

4.30 The equilibrium relation between the average bulk concentration $\bar{C}$ and the surface concentration Γ, based on the nonlinear (Langmuir) isotherm (**??**) for varying kinetic nonlinearity β. 81

4.31 Surface tension σ as a function of surface concentration Γ for varying kinetic nonlinearity β according to the nondimensional nonlinear equation of state (**??**), and the Marangoni number $\mathcal{M}a = 0.6$. 81

4.32 Time varying profiles of film thickness $h(z,t)$ for the kinetic nonlinearity (a) $\to \infty$ (linear), and $\beta =$ (b) 5, (c) 1, (d) 0.5, illustrated at times $t = 0$ (dashed line), 1, 5, 10, 20, 40, 100. Other parameter values are fixed and chosen as $\mathcal{J} = \mathcal{K} = 1$, $\Gamma_{exo} = 1$, $\Gamma_{pre} = 0$, $\mu = 100$ g/cm s, $\tau_{air} = 0$ and $\mathcal{G}_r = \mathcal{G}_z = 0$. 83

4.33 Time varying profiles of surface surfactant concentration $\Gamma(z,t)$ for the kinetic nonlinearity (a) $\to \infty$ (linear), and $\beta =$ (b) 5, (c) 1, (d) 0.5, illustrated at times $t = 0$, 1 (dashed), 5 (dash-dotted), 10 (long-dashed line), 20, 40, 100. Other parameter values are fixed and chosen as $\mathcal{J} = \mathcal{K} = 1$, $\Gamma_{exo} = 1$, $\Gamma_{pre} = 0$, $\mu = 100$ g/cm s, $\tau_{air} = 0$ and $\mathcal{G}_r = \mathcal{G}_z = 0$. 84

4.34 Time varying profiles of bulk surfactant concentration $\bar{C}(t)$ for the kinetic nonlinearity (a) $\to \infty$ (linear), and $\beta =$ (b) 5, (c) 1, (d) 0.5, illustrated at times $t = 0$, 1 (dashed), 5 (dash-dotted), 10 (long-dashed line), 20, 40, 100. Other parameter values are fixed and chosen as $\mathcal{J} = \mathcal{K} = 1$, $\Gamma_{exo} = 1$, $\Gamma_{pre} = 0$, $\mu = 100$ g/cm s, $\tau_{air} = 0$ and $\mathcal{G}_r = \mathcal{G}_z = 0$. 85

4.35 Time varying profiles of surface tension $\sigma(z,t)$ for the kinetic nonlinearity (a) $\to \infty$ (linear), and $\beta =$ (b) 5, (c) 1, (d) 0.5, illustrated at times $t = 0$, 1 (dashed), 5 (dash-dotted), 10 (long-dashed line), 20, 40, 100. Other parameter values are fixed and chosen as $\mathcal{J} = \mathcal{K} = 1$, $\Gamma_{exo} = 1$, $\Gamma_{pre} = 0$, $\mu = 100$ g/cm s, $\tau_{air} = 0$ and $\mathcal{G}_r = \mathcal{G}_z = 0$. 86

4.36 Temporal evolutions of (a) the peak film thickness, h_{peak}, and (b) the axial position of peak film thickness, z_{peak}, for $\beta \to \infty$ (linear), 5, 1 and 0.5. . . . 87

4.37 Temporal evolutions of (a) the bulk surfactant concentration at $z = 0$, $\bar{C}(0,t)$, (b) the surface surfactant concentration at $z = 0$, $\Gamma(0,t)$, and (c) the monolayer length, L_{mono}, for $\beta \to \infty$ (linear), 5, 1 and 0.5. 88

Chapter 1

Introduction

1.1 Pulmonary Anatomy and Physiology

The main function of the lung is to provide a pathway for the environmental air to reach the circulatory system for the gas exchange with the blood cells. As shown in Figure 1.1, the air is breathed through either the nose or the mouth and enters the pharynx. The pharynx then branches into two tubes, the esophagus and the larynx. Food from the mouth passes the esophagus to the stomach. Through the larynx the air reaches the trachea. The trachea separates into the left and right bronchi, which are the starting airways of the left and right lungs. The two main bronchi continue bifurcating into narrower, shorter and more branches. Beginning from the trachea the branching structure consists of approximately 23 generations [Weibel, 1963], which is called the tracheobronchial tree. The trachea is supported by C-shaped cartilage and smooth muscle. The walls of bronchi contain semicircular cartilage. As the bronchi branch, the cartilage rings are replaced by irregular-shaped cartilage plates. These cartilages support the large airways and give them cylindrical shapes. The cartilages diminish in the airway when the diameter is about 1 mm. The first airway branch that no longer contains cartilages is termed bronchiole. The first sixteen generations form the conducting zone consisting of the airways from the trachea to the terminal bronchioles, which contains no alveoli and across which no gas exchange occurs. The dimensions of the first 16 generations are listed

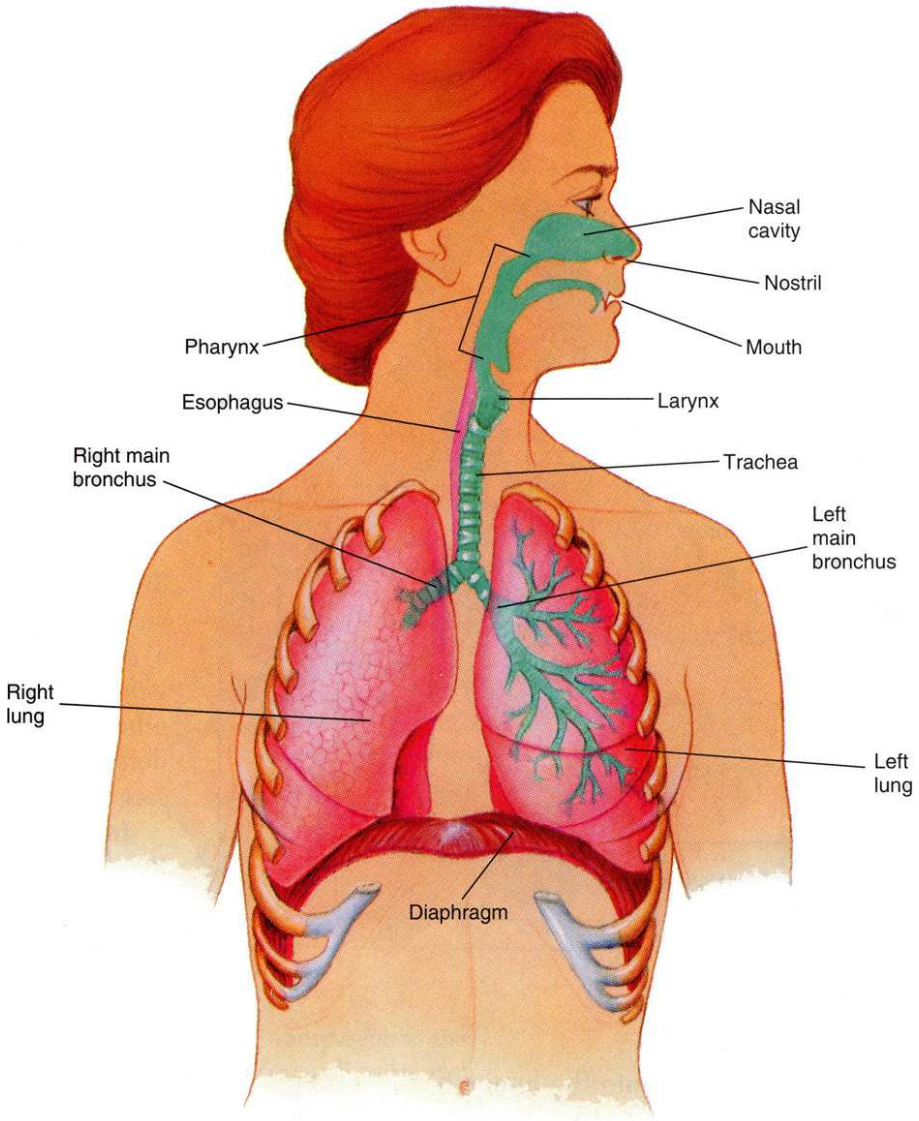

Figure 1.1: Organization of the respiratory system [from Vander *et al.*, 1994].

in Table 1.1. The last seven generations are called the respiratory zone, which contains alveoli and is the main site for gas exchange. Alveoli begin to appear in the bronchioles called respiratory bronchioles. The number of the alveoli increases in the alveolar ducts and the airways end in grape-like clusters of alveoli called alveolar sacs.

The interior surface of the airway is lined with a thin layer of liquid, which moisturizes the air entering the airways. The epithelial surfaces of the trachea and bronchi contain cilia and goblet cells. These goblet cells and the mucous glands secrete mucus onto the surface of the airways. Surrounding the cilia is the watery periciliary sol, and over this

Generation	Number	Radius (mm)	Length (mm)
0	1	9.000	120.0
1	2	6.100	47.6
2	4	4.150	19.0
3	8	2.400	6.5
4	16	1.950	10.9
5	32	1.500	9.2
6	64	1.200	7.7
7	128	1.000	6.5
8	256	0.800	5.5
9	512	0.650	4.6
10	1024	0.550	3.9
11	2048	0.465	3.3
12	4096	0.405	2.8
13	8192	0.350	2.3
14	16384	0.315	2.0
15	23000	0.280	1.7
16	46000	0.255	1.4

Table 1.1: Dimensions of the first 16 generations of airways [from Weibel, 1963].

layer of sol is a viscous gel layer of mucus [Beachey, 1998]. Inhaled particles, such as dust contained in the inspired air, stick to the mucus. These inhaled particles are moved slowly and continually by the cilia to the pharynx and then swallowed. Such a process, called the mucociliary escalator, makes the inhaled air clean. Furthermore, the vessels around the airways help warm up the air. After passing through the conducting zone the air becomes cleaner, moister, warmer and suitable for gas exchange.

In the respiratory zone, the alveoli are embraced by the pulmonary capillaries, as shown in Figure 1.2. There are more than three million alveoli providing a surface area approximately fifty to one hundred square meters for gas exchange. Although the respiratory membrane between the alveoli and pulmonary capillaries is multi-layered (Figure 1.3), it is normally 0.2 to 0.5 μm thick [Levitzky, 1999]. The extensive area as well as the extremely thin blood-air barrier allow rapid exchange of large quantities of oxygen

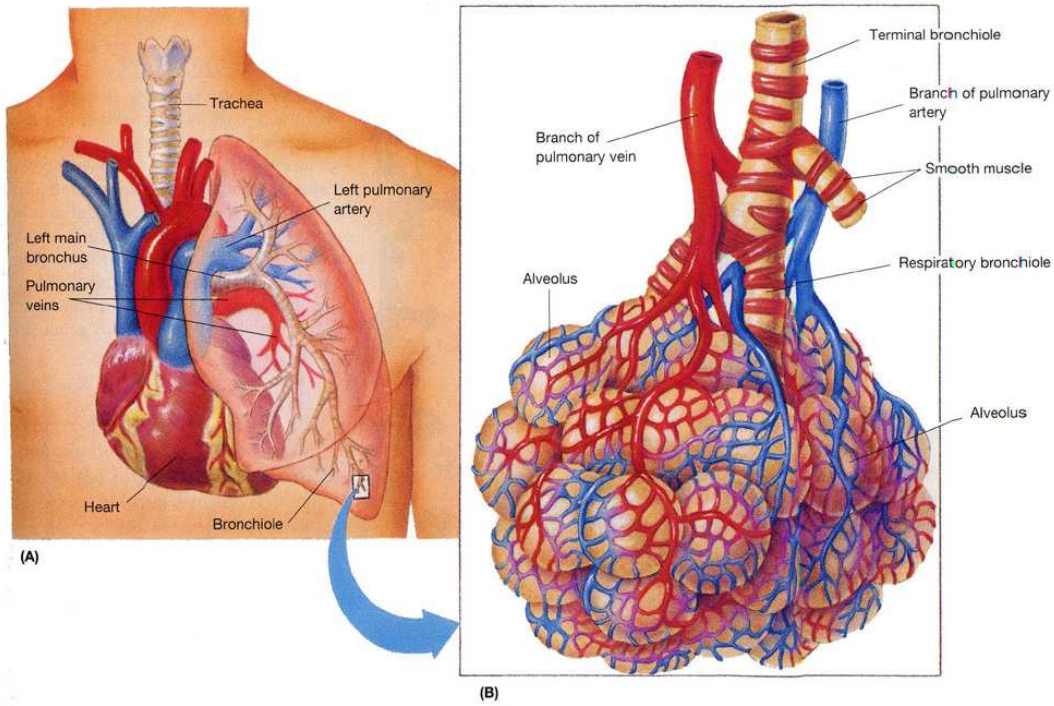

Figure 1.2: Relationships between blood vessels and airways. A small section of (A) is enlarged in (B) to show the continuation of the airways and the clusters of alveoli at their end. The Alveolus are surrounded by capillaries [from Vander *et al.*, 1994].

and carbon dioxide by diffusion. The alveolar epithelial surface mainly consists of the flat type I alveolar cells and the type II cells. The type I cells make up 90 to 95 percent of the alveolar surface, although the number of type II cells is twice of that of type I cell. The type II alveolar cells produce and secrete the pulmonary surfactant, which will be discussed in the following section. In addition, the alveolar walls also contain macrophages. The number of the macrophages is much less than the alveolar cells, but the macrophages engulf microorganisms and foreign materials and play an important role in the alveolar clearance.

1.2 Surface Tension and Surfactant

Surface-tension forces occur at gas-liquid interfaces or interfaces between two immiscible liquids. The liquid molecules in the bulk phase are attracted by the surrounding molecules

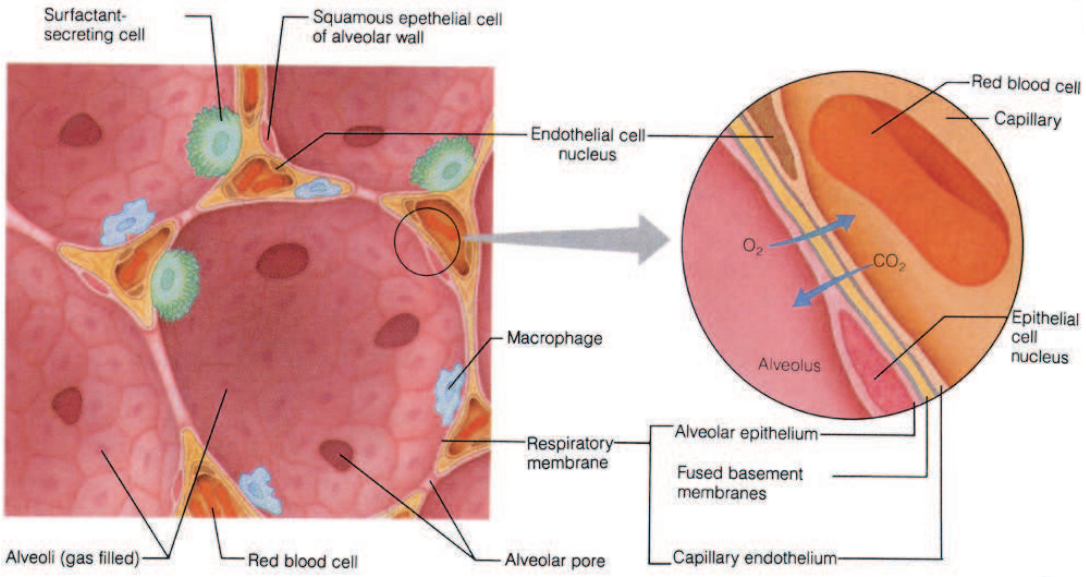

Figure 1.3: Anatomy of the respiratory membrane. The respiratory membrane is composed of epithelial cells of the alveoli, the capillary endothelium, and the basement membranes between. Surfactant-secreting cells are also shown. Diffusion of oxygen occurs from the alveolar air into the pulmonary capillary blood; carbon dioxide diffuses from the pulmonary blood into the alveolus [from Marieb, 2000].

and are in an equilibrium state. However, for the liquid molecules at the gas-liquid interface, the attraction caused by the liquid molecules below and beside are higher than that by the gas molecules above. As a result, the gas-liquid interface has a tendency to contract toward the liquid phase as shown in Figure 1.4.

SURFace-ACTive agANTS, called surfactants, which are adsorbed at the interface will lower the surface tension as depicted in Figure 1.5. Because of the amphiphilic structure of the surfactant molecules, they are adsorbed at the gas-liquid interface with the hydrobolic (water-hating) tails up and the hydrophilic (water-loving) heads down. The surfactant molecules replace the surface liquid molecules forming a monolayer (single molecule layer) at the gas-liquid interface. The presence of surfactant molecules decreases the attraction forces along the interface, and consequently reduces the surface tension.

The surfactant molecules can also exist in the bulk phase of a liquid as micelles if

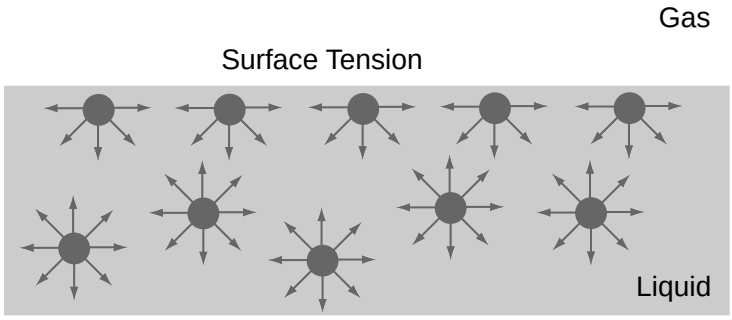

Figure 1.4: At the interface with no surfactant molecules, liquid molecules are attracted to each other and to molecules below, creating a force to contract the surface.

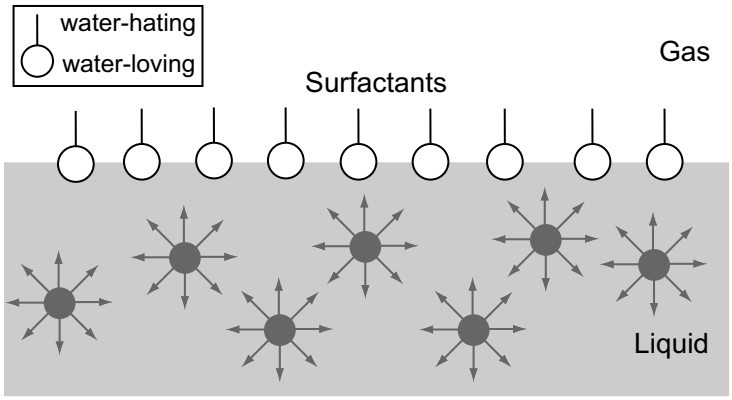

Figure 1.5: Surfactant molecules form a monolayer at the gas-liquid interface and reduce the surface tension between the liquid molecules at the interface.

insoluble or as monomers (single molecules) if soluble. The micelle is roughly spherical or cylindrical in shape and contains about 50 to 100 surfactant molecules that aggregate with their polar head in contact with the liquid and the tails inward. The concentration at which the micelles begin to form is called the critical micelle concentration. Above the critical micelle concentration, the surfactant concentration at the interface is essentially unchanged and so is the surface tension. Any further addition of surfactant molecules will only form micelles [Hiemenz, 1986; Probstein, 1994].

If the surfactant is soluble, there exists a dynamic equilibrium between the surfactants at the interface and those in the bulk. The surfactant will continuously adsorb from the bulk phase to the interface and desorb from the interface to the bulk phase [Clint, 1992].

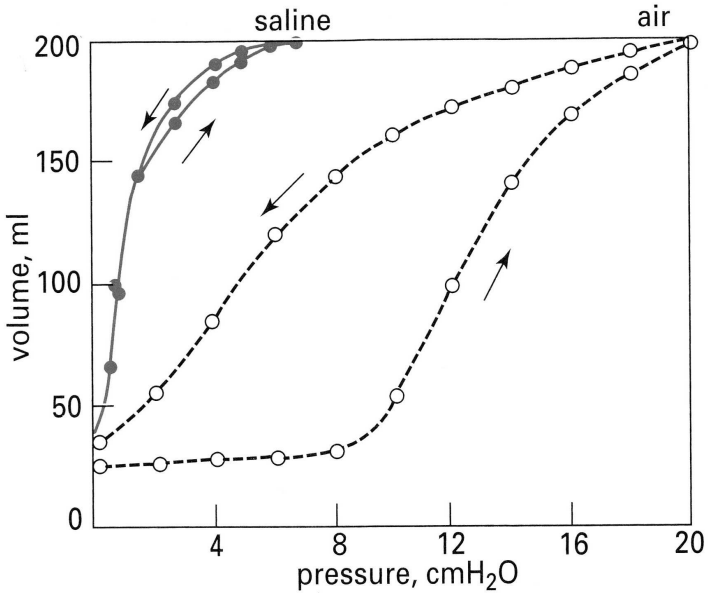

Figure 1.6: A comparison of pressure-volume curves for cat lungs inflated with air or saline [from Clements & Tierney, 1965].

1.3 Pulmonary Surfactant

The elastic recoil of lung is generated by the elastic and collagen fibers of the lung tissues and the surface-tension forces along the air-liquid interface of film lining the alveoli. The function of the surface-tension forces in the elastic recoil has been demonstrated in the experiment by Clements & Tierney [1965], in which a cat lung is inflated first with air and then with saline as shown in Figure 1.6. The experiment reveals that saline inflation requires much less external pressure than air inflation to achieve a given volume. When the lung is inflated with air, the air-liquid interface is formed, and the surface tension contributes to the elastic recoil of lung. However, when the lung is inflated with saline, there is no air-liquid interface, and the elastic recoil is only due to the lung tissues.

The pulmonary surfactant in the alveoli forms a monolayer at the air-liquid interface in the alveoli and helps to regulate the elastic recoil of lung. During the period of expiration this monolayer is compressed and the surfactant concentration at the interface increases. As a result, the surface tension in the alveoli is the lowest at the end of expiration and the

lung can be easily expanded afterward. On the contrary, during the period of inspiration, the surfactant concentration decreases and the elastic recoil due to the surface tension reverts. Therefore, the alveoli have a tendency to contract at the end of inspiration. Because of the presence of pulmonary surfactant the air can be easily inspired into and expired from the lung.

The pulmonary surfactant is a complex mixture consisting of about 90% lipids and 10% proteins. The lipids portion contains 80% phospholipid and 20% neutral lipid. Dipalmitoyl phosphatidylcholine (DPPC) comprises approximately 50% content of the phospholipids [Boncuk-Dayanikli & Taeusch, 1995; Beachey, 1998; Levitzky, 1999]. However, DPPC molecules are very insoluble, and hence need other phospholipids and proteins for surface spreading and adsorption to the interface. The pulmonary surfactant contains four specific proteins: surfactant protein(SP)-A, SP-B, SP-C, and SP-D, which aid the interfacial kinetic behavior of surfactant [Hawgood, 1989; Possmayer, 1990; Weaver & Whitsett, 1991].

1.4 Neonatal Respiratory Distress Syndrome

In 1959, Avery & Mead [1959] first provided the evidence that the respiratory distress syndrome (RDS) in premature newborn infants is caused by the lack of surfactant in their lungs. When a newborn infant takes the first breath to inflate the lung, an air-liquid interface is created in the alveoli. If there exists insufficient level of surfactant or functionally impaired surfactant, the surface tension along the air-liquid interface is so high that the infant has difficulty inflating the alveoli. The infant suffering from RDS has dyspnoea after birth and makes tremendous efforts just to keep reinflating the alveoli, which collapse after each breath. In addition to strenuous breath, neonatal RDS is characterized by nasal flaring, grunting noise with each breath, and blue around lips and nail beds, which indicates a lack of oxygen[1].

[1]http://www.lungusa.org

The full term pregnancy is defined as lasting between 37 and 42 weeks. The pulmonary surfactant secreted by the type II alveolar cells only begins to emerge on the 32nd week of gestation and achieves adequate concentration after 36 weeks. Thus, the incidence of neonatal RDS declines with the gestational age. It occurs in 60% of infants born at less than 28 weeks gestation, 30% of those born at 28 to 34 weeks, and 5% of those born after 34 or more weeks[2].

The infants will be born safely if there is sufficient pulmonary surfactant in their alveoli, which can be measured from the amniotic fluids. Gluck *et al.* [1971] measured the lecithin/sphingomyelin (L/S) ratio of the amniotic fluid to help to make the clinical decision whether the fetus is ready to be born. Figure 1.7 shows the mean concentrations of lecithin and sphingomyelin in the amniotic fluid during gestation. There is a rapid growth in the concentration of lecithin at 35 weeks gestation, which indicates the maturity of the lung of the fetus.

The prevention of a premature birth is the primary mean to reduce the cause of neonatal RDS. However, when a premature birth can not be prevented, giving corticosteroids to mothers before deliveries has been shown to dramatically lower the risk and severity of neonatal RDS in the infants. The medications are often given between 24 and 34 weeks gestation to mothers at risk of early delivery[3]. Nevertheless, since it takes at least 48 to 72 hours for the corticosteroids to become effective, mothers who suddenly go to uncontrolled delivery get no benefit from taking corticosteroids[4]. The most common and effective technique for the prevention and treatment of neonatal RDS is surfactant replacement therapy, which will be discussed in the following section.

[2]http://www.lungusa.org

[3]http://www.lpch.org/DiseaseHealthInfo/HealthLibrary/hrnewborn

[4]http://www.geocities.com/HotSprings/Chalet/4121

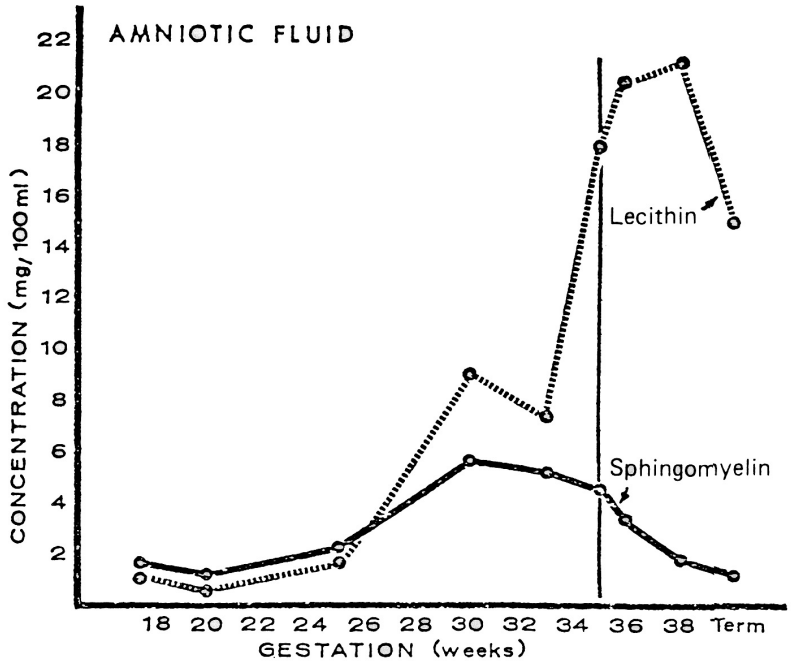

Figure 1.7: Mean concentrations of lecithin and sphingomyelin in amniotic fluid during gestation [from Gluck *et al.*, 1971].

1.5 Surfactant Replacement Therapy

Fujiwara *et al.* [1980] were among the first attempts to successfully treat premature infants with a modified surfactant extract. The treatment, which is usually called surfactant replacement therapy (termed SRT), is now the standard treatment for infants suffering from RDS [Corbet *et al.*, 1991; Jobe, 1993; Kendig *et al.*, 1991; Long *et al.*, 1991; Robertson & Taeusch, 1995]. Clinical trials using SRT show significant improvements in pulmonary compliance, gas exchange, and complications of barotrauma [Mercier & Soll, 1993; Corbet, 1993]. The infant mortality is reduced about one half after the introduction of SRT [Long *et al.*, 1991; Soll & McQueen, 1992].

Two types of surfactant products have been tested and approved to treat infants with RDS. One type is natural surfactant, which is derived either from bovine lungs or from human amniotic fluid and porcine lungs. Surfactant TA, the first efficient surfactant developed by Fujiwara and coworkers [1980], and Survanta are representative natural

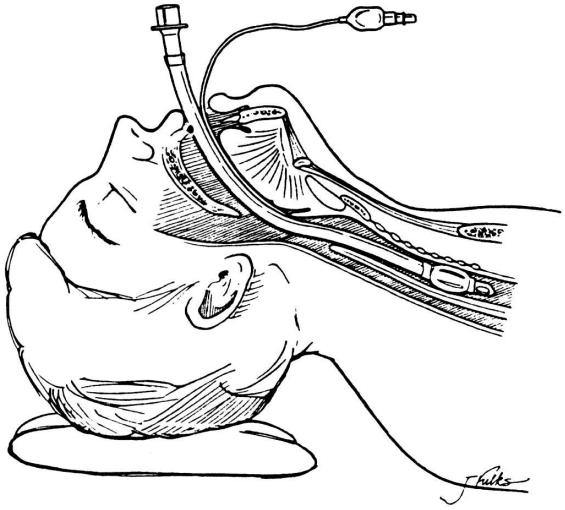

Figure 1.8: An oral endotracheal tube in position [from Barnes, 1994].

surfactants. The other type is synthetic surfactant such as Exosurf and ALEC, which are protein-free and so as not to cause allergic reactions [Morley, 1991; Soll & McQueen, 1992; Jobe, 1993].

The delivery method of the "exogenous" surfactant is either by instilling the surfactant bolus into the trachea or by inhalation as aerosol. The intra-tracheal bolus instillation is the more popular approach. For the common procedure of SRT, the dosage needed for an infant is 4 ml surfactant suspension each kg birth weight. Each ml of surfactant suspension contains 25 mg of phospholipids. The surfactant bolus is administered by the endotracheal tube inserted from the mouth to the trachea, as shown in Figure 1.8. Each surfactant dose is divided into four quarter-doses. These four quarter-doses are administered with the infant in four different positions: head up, left or right lateral, and head down, left and right lateral. After administration of each quarter-dose the infant is ventilated at a rate of 60 breaths per minute, and inspiratory time 0.5 second for at least 30 seconds. After completing the dosing procedure, the infant is returned to usual ventilator management and clinical care. In general, surfactant preparations are given to prevent or treat RDS. For infants of less than 1250 g birth weight or of less than 27 weeks

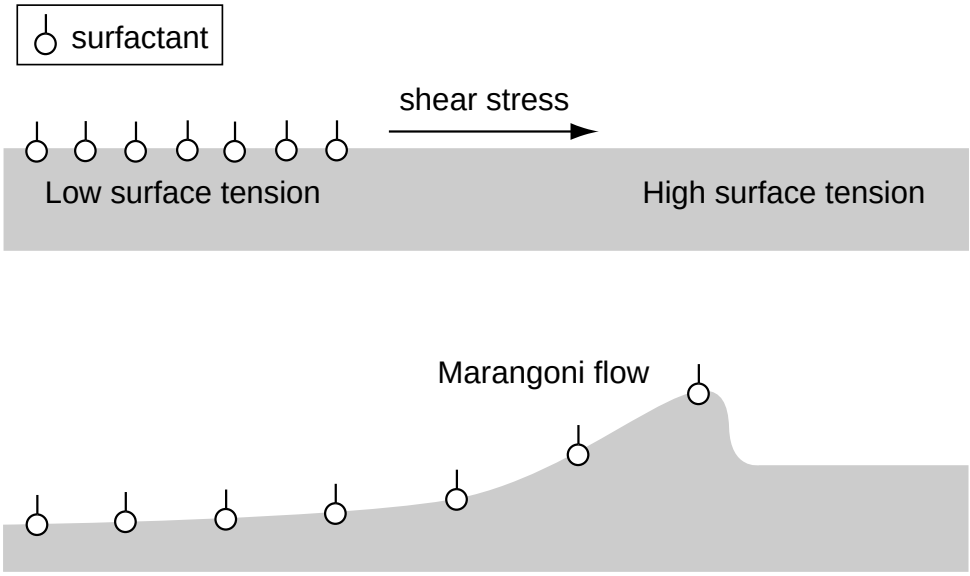

Figure 1.9: Schematic of Marangoni effect.

gestation prevention treatment is given as soon as possible after birth, preferably within 15 minutes[5].

An instilled bolus of surfactant in the trachea transports by a combination of various physical forces [Halpern *et al.*, 1998; Espinosa & Kamm, 1999]. At first, the bolus creates a liquid plug occluding the airway and is pushed into the lung during inspiration. When this plug progresses and finally ruptures, the bolus coats the airways with a layer of surfactant. In smaller airways, the surfactant lowers the local surface tension and forms a surface-tension gradient. The induced surface-tension gradient results in a flow, called Marangoni flow, in the direction toward the higher surface tension region, as shown in Figure 1.9. By such a Marangoni flow, the exogenous surfactants are delivered to the peripheries of airways. The surfactant, which finally reaches the alveoli, is absorbed by the cells in the alveoli.

The ultimate goal of the technique to administer surfactant for treating RDS is to achieve a homogenous distribution in the lung. Perfectly uniform surfactant administration into the lung would result in normal alveolar expansion [Jobe, 1993]. In contrast, if

[5]http://www.survanta.com

the distribution of surfactant is accumulated to one particular lung, the volume of this over-treated lung would expand attributed to low surface tension. If the pressure of ventilation is not reduced, this expanded lung will over expand and potentially be injured. On the other hand, if the pressure of the ventilation is decreased, the untreated lungs would lose the volume of air they are supposed to receive and become more atelectatic [Lewis *et al.*, 1993].

In addition to neonatal RDS, SRT has been used to treat other lung disorders, such as meconium aspiratory syndrome [Sun *et al.*, 1994; Wiswell *et al.*, 1994], congenital pneumonia [Khammash *et al.*] and acute respiratory distress syndrome (ARDS) [Lewis & Jobe, 1993; Spragg *et al.*, 1994]. ARDS is caused by various factors, such as aspiration, toxic inhalation, pulmonary inflection, near drowning, lung contusion and severe trauma [Pison *et al.*, 1995]. Additionally, the surfactant has also been employed as a spreading agent for drug delivery [Kharasch *et al.*, 1991; Haitsma *et al.*, 2001] and as a gene vector for gene therapy [Jobe *et al.*, 1996; Katkin *et al.*, 1997]. The optimal technique for delivery of surfactant into the lung depends on the particular application of SRT.

1.6 Previous Studies on Surfactant-Driven Thin-Film Flows

Being provoked by the need to improve techniques and efficiency for SRT, the transport of surfactant within the airways under the action of Marangoni effect has been a subject of extensive studies. The focus of these work is the efficiency of SRT through understanding of the detailed transport mechanisms and to have a better estimate of the transit time for the surfactant to reach the periphery of airway. These studies are primarily contributed by Grotberg and coworkers [e.g. Borgas & Grotberg, 1988; Jensen & Grotberg, 1992; Halpern & Grotberg, 1998], Espinosa, Kamm and coworkers [e.g. Espinosa *et al.*, 1993; Espinosa & Kamm, 1999], and Craster, Matar and coworkers [e.g. Craster & Matar, 2000; Zhang *et al.*, 2002; Zhang *et al.*, 2003]. By assuming a thin film, these studies employed

the lubrication approximation to analyze the transport of surfactant and the deformation of film lining the airway.

The early study by Borgas & Grotberg [1988] examined the spreading behavior of insoluble and non-diffusing surfactants on a planar thin liquid film. The surfactant spreads as a monolayer on the thin film. At the leading edge of this monolayer, the discontinuity in the shear stress causes a shock of film deformation with height twice that of the undisturbed film and thinning of the film behind the shock. Gaver & Grotberg [1992] observed experimentally that if the initial surface-tension gradients are sufficiently large, the deformation of film may be severe enough for the thinnest part of film to rupture, which leads to termination of the surfactant transport. The subsequent theoretical study by Jensen & Grotberg [1992] considered the additional effects of capillarity and van der Waals forces. Their study, however, indicated that the severe thinning due to Marangoni effect alone is insufficient to induce film rupture. They further demonstrated that the instability caused by van der Waals forces is a likely candidate for the dry out process. Jensen & Halpern [1998] also made detailed analyses of the shock structure and the induced flows. They found that in the flat interface limit, a spreading monolayer drives an unsteady return flow beneath most of the monolayer and creates a series of weak vortices ahead of the tip. Surface diffusion smooths the tip singularity and can ultimately destroy the vortices.

To consider the effect of surfactant solubility, models of soluble surfactant spreading on a thin liquid film were developed by Halpern & Grotberg [1992] and Jensen & Grotberg [1993]. Their model results reveal that the transient desorption of surfactant from the interface to the bulk causes the surfactant spreading rate to diminish. Nevertheless, the induced film deformations are more severe forming larger shock heights when the surfactant is soluble.

The surface-tension driven flow in an axisymmetric thin film lined airway was first studied by Davis *et al.* [1974] using the lubrication approximation. Espinosa *et al.* [1993] extended this model and examined the effects of various parameters, including the film

thickness to airway radius ratio, the initial concentration of exogenous surfactant, the bolus volume, the gravity and the endogenous surfactant, on the film deformation and the surfactant spreading. Their study showed that increasing the level of endogenous surfactant decreases the height of the shock but augments the spreading rate of exogenous surfactant. This is a contradictory result since the presence of endogenous surfactant reduces the surface-tension gradient and also the induced flow and is expected to decrease the surfactant spreading rate. Grotberg *et al.* [1995] clarified this contradictory issue by distinguishing the leading edge of exogenous surfactant from the disturbance front of endogenous monolayer. Their study demonstrated that the presence of endogenous surfactant indeed retards the spreading of exogenous surfactant.

Another group which has made significant contributions to this subject is Craster, Matar and coworkers. Craster & Matar [2000] considered the non-Newtonian properties of mucus and the bilayer structure of film lining in the airways. The thin film in their model consists of the non-Newtonian mucus and the periciliary liquid sublayer, which is primary Newtonian. Their study indicated that the two principle rheological properties of the mucus, the yield stress and the shear thinning, have the most significant influences on the transport rate of surfactant. Increasing the yield stress or decreasing the power-low exponent for a shear thinning fluid delays the progress of transport wave. Recently, Zhang *et al.* [2002] found that the presence of weak viscoelasticity also tends to retard the transport process.

The studies reviewed so far primarily focus on localized surfactant transport on a planar film or an axisymmetric lining. These localized transport models have also been extended to a surfactant bolus delivery in the whole realistic tracheobronchial tree, which helps obtain better estimates of the delivery time for the surfactant. The mechanisms of a bolus transport from the trachea to the peripheries of airway is distinguished into four regimes: air-blown plug, gravity-draining liquid coating, surfactant-driven flows and alveolar clearance [Halpern *et al.*, 1998]. The delivery time for the first dose to be com-

pletely transported to the peripheries of airway is about 24 hours, and is much longer for following doses because of the increasing level of preexisting surfactant. In the estimation of Espinosa & Kamm [1999], the additional effects, such as sorption kinetics, gravity and shear stress due to air flow, were also considered. In their model, it takes about 4 to 170 seconds for the leading edge of exogenous surfactant to reach the peripheries but considerably longer for the entire dose. For other applications of SRT such as drug delivery and gene therapy, Zhang *et al.* [2003] drew on these models but focused on the transient and final distribution of the chemical delivered using exogenous surfactant as a vehicle into the lung. Their results show that the exogenous surfactant can significantly enhance the delivery of chemicals into the lung.

1.7 Outline of the Present Study

Given the complexity of the pulmonary airways and the vast variety of parameters that can influence the underlying transport physics, contradictory conclusions are often reached by different models. This is primary attributed to the physical and physiological constants involved in the model, and also the treatments of real airway geometry that have profound effect on the behavior of the models. It is worthwhile to reappraise the problem of the surfactant spreading in an airway lining.

In the present study, we unify the models developed in the previous studies and integrate all the possible mechanisms that can affect the surfactant spreading and the induced film disturbance. A thin layer of Newtonian fluid lining in an axisymmetric airway is considered with a flow driven by the Marangoni effect. The surfactant-driven thin-film flow and the transport of surfactant are modeled using the lubrication theory. This comprehensive model is then solved numerically with the emphasis on examining the possible effects of various parameters on the film deformation and the surfactant spreading. The ultimate goal of this study is to clarify the underlying mechanisms that govern the exogenous surfactant, and to assess the possible impact of the surfactant redistribution on the

thin film lining in surfactant replacement therapy.

We begin the development of the theoretical model by deriving the governing equations and the boundary conditions for the interfacial flow and the surfactant transport from the conservation principles in Chapter 2. Lubrication approximation is then applied to derive the thin-film equation for the spatial-temporal evolution of the film disturbance. Cross-sectional averaging is employed to incorporate surfactant solubility in the surfactant transport equations. The final model consists of a coupled system of nonlinear partial differential equations. The numerical method used to solve these coupled nonlinear partial differential equations is then described in Chapter 3. Numerical results from the model simulation are presented and discussed in Chapter 4. The parameters considered in these simulations include: the ratio of film thickness to airway radius, the viscosity of thin film, the concentration of exogenous surfactant dose, the presence of preexisting surfactant, the gravitational forces, the shear stress due to air flow, the solubility of surfactant, and the nonlinearity of sorption kinetics. The thesis is concluded with discussion and recommendation for further studies in Chapter 5.

Chapter 2

Model Formulation

2.1 Governing Equations

We focus on localized transport of exogenous surfactant within a single airway lined with a thin liquid layer. An axisymmetric airway of circular cross section with radius R and length L is considered. A schematic of the model geometry and the cylindrical coordinate system is shown in Figure 2.1. The r-axis is along the airway radial direction, and the z coordinate coincides with the airway centerline. The corresponding velocity components are $u(r, z, t)$ and $w(r, z, t)$, and t is the time. Initially, the interior of the airway is covered with an undisturbed, thin layer of liquid film with a uniform thickness h_0. The liquid is assumed to be incompressible with a constant density ρ and Newtonian with a constant viscosity μ. At the air-liquid interface of the thin film, the surface tension is σ. The surfactant distributes at the interface with a surface concentration $\Gamma(z, t)$ and in the bulk phase with a bulk concentration $C(r, z, t)$.

2.1.1 Momentum and mass conservation

For a Newtonian fluid, conservation of momentum requires that the radial and axial velocities u and w satisfy the Navier-Stokes equations

$$\rho\left(\mathbf{V}_t + \mathbf{V}\cdot\nabla\mathbf{V}\right) = -\nabla p + \mu\nabla^2\mathbf{V} + \mathbf{g}, \tag{2.1}$$

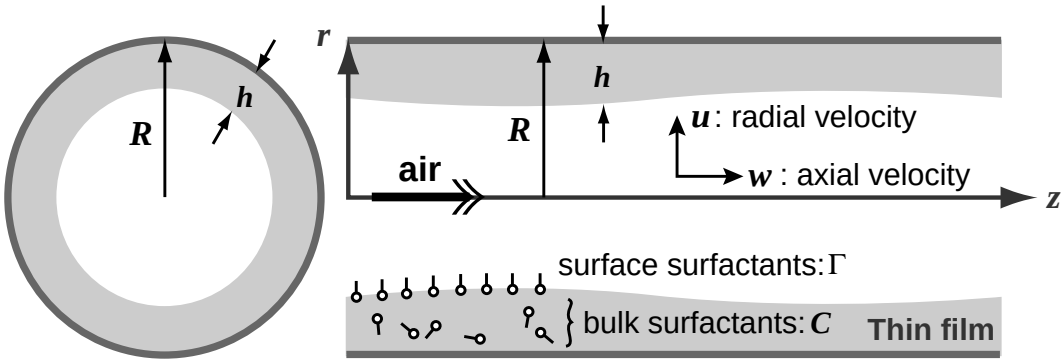

Figure 2.1: The geometry of a lined airway with soluble surfactants distributed.

where the pressure is denoted by p, the velocity vector $\mathbf{V} = (u, 0, w)$, and the gravitational acceleration $\mathbf{g} = (g_r, 0, g_z)$. The continuity equation for an incompressible fluid with a constant density considered here is

$$\nabla \cdot \mathbf{V} = 0. \tag{2.2}$$

Expressing (2.1) and (2.2) in terms of the cylindrical-coordinate variables, these equations become

$$\rho(u_t + uu_r + wu_z) = -p_r + \mu \left[r^{-1}(ru_r)_r + u_{zz} - u_{rr}\right] + \rho g_r, \tag{2.3}$$

$$\rho(w_t + uw_r + ww_z) = -p_z + \mu \left[r^{-1}(rw_r)_r + w_{zz}\right] + \rho g_z, \tag{2.4}$$

and

$$r^{-1}(ru)_r + w_z = 0. \tag{2.5}$$

2.1.2 Boundary conditions

At the airway wall, the boundary is regarded as no-slip, and the conditions of the velocities are

$$u = w = 0 \qquad \text{at } r = R. \tag{2.6}$$

At the interface, the boundary moves as a material surface, and the fluid particles there will stay on the surface, which results in the kinematic condition. Defining the interfacial

function $F(r,z,t) = r - [R - h(z,t)]$, the kinematic boundary condition is given by

$$\frac{\mathrm{D}F(r,z,t)}{\mathrm{D}t} = 0 \qquad \text{at } r = R - h(z,t).$$

This leads to the condition for the interfacial height h that

$$h_t + u + wh_z = 0 \qquad \text{at } r = R - h(z,t). \tag{2.7}$$

At the air-liquid interface, momentum conservation is also required which gives rise to the dynamic interfacial boundary conditions. These conditions are typically expressed in the normal and tangential directions following the boundary. The normal stress exerted at the interface by the underlying fluids must balance the air normal stress and the stress induced by surface tension σ attributed to the surface curvature H, therefore [Scriven, 1960; Edwards *et al.*, 1991]

$$-\mathbf{n}\cdot\mathbf{P}\cdot\mathbf{nn} = \mathbf{F}^s\cdot\mathbf{nn} + 2H\sigma\mathbf{n} \qquad \text{at } r = R - h(z,t), \tag{2.8}$$

where the pressure tensor $\mathbf{P} = -p\,\mathbf{I} + \mu(\nabla\mathbf{V} + \nabla\mathbf{V}^{\intercal})$, the external force $\mathbf{F}^s = (0, 0, \tau_{air})$ and the normal vector at the interface is defined as

$$\mathbf{n} = (n_r, 0, n_z) = \frac{(1, 0, h_z)}{(1 + h_z^2)^{1/2}}.$$

Here we have neglected the effects of dilatational and shear surface viscosities. In the tangential direction, the interfacial tangential stress also needs to balance the shear stresses induced by the surface-tension gradient and the air flow:

$$\mathbf{n}\cdot\mathbf{P}\cdot\mathbf{I}_s = \mathbf{F}^s\cdot\mathbf{I}_s + \nabla_s\sigma \qquad \text{at } r = R - h(z,t), \tag{2.9}$$

where the dyadic surface idemfactor $\mathbf{I}_s = (\mathbf{I} - \mathbf{nn})$, with $\mathbf{I}$ the identity tensor, and ∇_s is the surface operator, $\nabla_s = (\mathbf{I} - \mathbf{nn})\cdot\nabla$. In (2.8) and (2.9), the normal and tangential stress conditions are represented in tensor forms, which can be further expressed in vector forms in the cylindrical coordinate system. Details of the derivation are given in Appendix A.

The final normal and tangential stress boundary conditions at the interface $z = R - h(z,t)$ are

$$n_r p - 2\mu \left[n_r^3 u_r + n_r n_z^2 w_z + n_r^2 n_z (w_r + u_z) \right] = n_r n_z \tau_{air} - \left(n_r \frac{\partial n_z}{\partial z} + \frac{n_r^2}{r} \right) \sigma, \tag{2.10}$$

and

$$-2\mu n_r^2 n_z (u_r + w_z) - \mu (n_r^3 - n_r n_z^2)(w_r + u_z) = n_r^2 \tau_{air} + n_r^2 \sigma_z, \tag{2.11}$$

respectively.

2.1.3 Transport equations for the surfactant

In this study, the surfactant is considered to be either insoluble or soluble in the bulk phase. The surfactant transport equation governing the surface concentration along the interface $\Gamma(z,t)$ is [Stone, 1989]

$$\Gamma_t + \nabla_s \cdot (\mathbf{V}^s \Gamma) + \Gamma (\nabla_s \cdot \mathbf{n})(\mathbf{V} \cdot \mathbf{n}) = D_s \nabla_s^2 \Gamma + J, \tag{2.12}$$

where $\mathbf{V}^s = (u^s, 0, w^s)$ is the surface velocity, D_s is the surface diffusivity, and J is the desorption/adsorption flux to/from the bulk phase. For insoluble surfactant, there is no sorption flux, i.e. $J = 0$. The transport mechanisms involved in (2.12) include the convection along the surface, the changes in surface area, the surface diffusion and the sorption flux. For soluble surfactant, the transport equation governing the dissolved bulk concentration $C(r,z,t)$ is

$$C_t + \mathbf{V} \cdot \nabla C = D_b \nabla^2 C, \tag{2.13}$$

where D_b is the bulk diffusivity of dissolved surfactant. Expressing the transport equations for the surface and bulk concentrations in cylindrical coordinate, (2.12) and (2.13) become

$$\Gamma_t + \left[\frac{u^s \Gamma}{r} + n_r^2 (w^s \Gamma)_z - n_r n_z (u^s \Gamma)_z \right] + \Gamma (n_r u^s + n_z w^s) \left(\frac{n_r}{r} + \frac{\partial n_z}{\partial z} \right) = D_s n_r^2 \Gamma_{zz} + J, \tag{2.14}$$

and

$$C_t + (u C_r + w C_z) = D_b \left[r^{-1} (r C_r)_r + C_{zz} \right]. \tag{2.15}$$

The sorption flux J is proportional to the difference in concentrations between the surface, $\Gamma(z,t)$, and the substrate immediately beneath the surface, $C_s(z,t) = C(r = R-h(z,t), z, t)$. Following Tsai & Yue [1995], we model this relationship with a nonlinear (Langmuir) isotherm,

$$J = k_a C_s(\Gamma^* - \Gamma) - k_d\Gamma = \left[D_b(\mathbf{n}\cdot\nabla)C\right]_{\,r=R-h(z,t)}\,, \tag{2.16}$$

where Γ^* is the saturated surfactant concentration. The sorption flux 2.16 includes two components: an upward adsorption flux with a rate constant k_a and a downward desorption flux with a rate constant k_d. This sorption flux equation couples the surface surfactant transport equation (2.14) with the bulk transport equation (2.15).

2.1.4 Equation of state

In the presence of surfactant at the interface, the surface tension σ is reduced, and the surface-tension variation is related to the surfactant surface concentration Γ through an equation of state. This relationship between the surface tension and the surface concentration is in general nonlinear and empirically determined as shown in Otis *et al.* [1994] and Krueger & Gaver [2000]. In the study of Krueger & Gaver [2000], the experimental measurements of the σ-Γ data is fitted to obtain a single equation divided into three regimes: the Frumkin equation at high surface tension (low surfactant concentration), a logistic equation for the collapse region at the lowest surface tension (the highest surfactant concentration), and a linear region linking the two. In this study, we follow the model of Tsai & Yue [1995] and adopt the Gibbs' adsorption equation to provide an equilibrium relationship between the surface tension and the surface concentration for soluble surfactant as

$$\sigma = \sigma_m + \mathcal{R}\,T\int_0^{C_s}\Gamma\,\frac{\mathrm{d}C_s}{C_s}, \tag{2.17}$$

where the bulk concentration at the interface C_s is related to the surface concentration Γ by the sorption kinetics (2.16), σ_m is the surface tension of the surfactant-free interface, $\mathcal{R}$ is the gas constant, and T is the temperature.

For the case of insoluble surfactant, previous studies using the nonlinear equation of state [Borgas & Grotberg, 1988; Gaver & Grotberg, 1992] indicate that only the disturbance of film may be affected. The transport of surfactant, however, is virtually independent on the choice of the equation of state. Accordingly, for the model of insoluble surfactant, a linear equation of state is employed, which is expressed as

$$\sigma = \sigma_m + \left(\frac{\mathrm{d}\sigma}{\mathrm{d}\Gamma}\right)_{\Gamma=0} \Gamma = \sigma_m + \frac{\sigma^* - \sigma_m}{\Gamma^*}\ \Gamma, \tag{2.18}$$

where σ^* is the saturated surface tension as the surfactant surface concentration reaches the saturated concentration Γ^*.

2.2 Non-dimensionalization

By assuming the condition that the ratio of initial film thickness to airway radius, $\epsilon = h_0/R$, is very small, i.e. $\epsilon \ll 1$, lubrication approximation may be used to extract the leading-order physics. In order to employ the lubrication approximation, the variables of the geometry and the flow are nondimensionalized using the following characteristic scales: the undisturbed film height h_0; the airway radius R; the characteristic radial and axial velocities $\mathcal{U}$ and $\mathcal{W}$; the maximum surface tension σ_m. The typical values of these characteristic scales in the human airways and some other physicochemical constants associated with the pulmonary surfactant are listed in Table 2.1. The spatial derivatives with respective to r and z are nondimensionalized by h_0^{-1} and R^{-1}, respectively. In this model the dominant physics involves the balance between the shear stress at the interface and the surface-tension gradient, i.e. $\mu w_r \sim \sigma_z$. Consequently, we choose $\mathcal{W} = \sigma_m \epsilon/\mu$ as the characteristic axial velocity. By use of the continuity equation (2.5), the radial and axial velocities can be related by $\mathcal{U} = \epsilon\mathcal{W}$. The radial velocity is therefore nondimensionalized by $\sigma_m\epsilon^2/\mu$. The time scale is defined as the axial length scale divided by the axial velocity scale, $\mathcal{T} = R/\mathcal{W} = (\mu R^2)/(\sigma_m h_0)$. Accordingly, the following

Constant	Symbol	Typical value	Source
Initial film thickness	h_0	10^{-3} (cm)	Widdicombe [2002]
Airway radius	R	$10^{-2} \sim 1$ (cm)	Weibel [1963]
Density	ρ	1 (g/cm^3)	∼Water
Viscosity	μ	$10^{-2} \sim 10^2$ (g/cm s)	Silberberg [1983]
Gravity	g	981 (cm/s^2)	
Surface diffusivity	D_s	10^{-5} (cm^2/s)	Sakata and Berg [1969]
Bulk diffusivity	D_b	10^{-6} (cm^2/s)	Johannsen *et al.* [1991]
Maximum surface tension	σ_m	70 (dyne/cm)	Morris *et al.* [2001]
Saturated surface tension	σ^*	25 (dyne/cm)	Morris *et al.* [2001]
Saturated concentration	Γ^*	3×10^{-7} (g/cm^2)	Johannsen *et al.* [1991]
Adsorption rate constant	k_a	(cm^2/g s)	
Desorption rate constant	k_d	(1/s)	

Table 2.1: Order-of-magnitude estimates for the physical constants in the human airways and the physicochemical constants associated with the pulmonary surfactant.

nondimensional variables are introduced,

$$\begin{aligned} h &= h_0\tilde{h}, \quad r = h_0\tilde{r}, \quad z = R\tilde{z}, \\ w &= \mathcal{W}\tilde{w}, \quad u = \mathcal{U}\tilde{u}, \quad t = \mathcal{T}\tilde{t}, \\ \sigma &= \sigma_m\tilde{\sigma}, \quad p = \frac{\sigma_m}{R}\tilde{p}. \end{aligned} \tag{2.19}$$

On substituting the nondimensional variables (2.19) into the Navier-Stokes equations (2.3) and (2.4) and the continuity equation (2.5), and discarding the tilde, we arrive at the following nondimensional equations:

$$\mathcal{R}e\epsilon^3(u_t + uu_r + wu_z) = -p_r + \epsilon\left[r^{-1}(ru_r)_r + \epsilon^2 u_{zz} - \frac{u}{r^2}\right] + \mathcal{G}_r, \tag{2.20}$$

$$\mathcal{R}e\epsilon^2(w_t + uw_r + ww_z) = -\epsilon p_z + \left[r^{-1}(rw_r)_r + \epsilon^2 w_{zz}\right] + \mathcal{G}_z, \tag{2.21}$$

and

$$r^{-1}(ru)_r + w_z = 0. \tag{2.22}$$

Note that all the nondimensional variables and their derivatives in the above equations are of order one. The nondimensional parameters $\mathcal{R}e \equiv (\rho\sigma_m h_0)/\mu^2$ is the Reynolds number,

and the radial and axial Bond numbers, $\mathcal{G}_r \equiv (\rho g_r h_0^2)/(\epsilon\sigma_m)$ and $\mathcal{G}_z \equiv (\rho g_z h_0^2)/(\epsilon\sigma_m)$, represent the gravity forces in the radial and axial directions relative to the Marangoni stress, respectively. Substituting the nondimensional variables (2.19) into (2.7), (2.10) and (2.11), the surface boundary conditions become

$$h_t + w^s h_z + u^s = 0, \tag{2.23}$$

$$\begin{aligned} p \; &- 2\epsilon\mathcal{N}^2 \left[u_r + \epsilon^2 h_z^2 w_z + h_z(w_r + u_z)\right] \\ &= \epsilon\mathcal{N} h_z \tau_{air} - \left[\epsilon\mathcal{N}^3 h_{zz} + \mathcal{N}(1-\epsilon h)^{-1}\right](1+\sigma), \end{aligned} \tag{2.24}$$

and

$$-\mathcal{N}(w_r + \epsilon^2 u_z) - 2\epsilon^2 \mathcal{N} h_z (u_r + w_z) = \tau_{air} + \sigma_z, \tag{2.25}$$

satisfied at the interface, $r = (1/\epsilon) - h(z,t)$, where $\mathcal{N} = (1+\epsilon^2 h_z^2)^{-1/2}$. The nondimensional boundary condition at the airway wall, $r = 1/\epsilon$, remains the same as

$$u = 0 \quad \text{and} \quad w = 0. \tag{2.26}$$

In order to non-dimensionalize the transport equations for the surfactant, we consider the local equilibrium of the surface and bulk surfactant concentrations. For the balance of the adsorptive and desorptive fluxes, the nonlinear (Langmuir) isotherm (2.16) becomes

$$k_a C_0(\Gamma^* - \Gamma_0) = k_d \Gamma_0.$$

Therefore,

$$C_0 = \frac{k_d}{k_a}\frac{1}{\beta} \quad \text{and} \quad \Gamma_0 = \frac{\Gamma^*}{\beta+1},$$

where the kinetic nonlinearity $\beta = (\Gamma^*/\Gamma_0) - 1$. When $\beta \to \infty$, the nonlinear sorption kinetics becomes the linear kinetics. The equilibrium surface concentration Γ_0 and bulk concentration C_0 are then considered as the characteristic concentrations for Γ and C. With this scaling the sorption kinetics (2.16) becomes

$$\begin{aligned} J &= \frac{1}{\mathcal{P}e_b}\frac{1}{\mathcal{K}}\frac{1}{\mathcal{J}}\frac{1}{\epsilon}\left(\frac{\beta}{\beta+1}\right)\left[C_s\left(1+\frac{1-\Gamma}{\beta}\right)-\Gamma\right] \\ &= \frac{1}{\mathcal{P}e_b}\frac{1}{\mathcal{K}}\mathcal{N}\left(\frac{1}{\epsilon^2}C_r + h_z C_z\right)_{r=\frac{1}{\epsilon}-h}, \end{aligned} \tag{2.27}$$

and the nondimensional Langmuir isotherm gives

$$C_s = \frac{\beta\Gamma}{1+\beta-\Gamma}. \tag{2.28}$$

In the nondimensional kinetics above, the bulk Péclet number is defined as $\mathcal{P}e_b \equiv (\sigma_m h_0)/(\mu D_b)$, which measures the relative importance of convection versus bulk diffusivity. The equilibrium ratio $\mathcal{K}$ is equal to the ratio of adsorption to desorption rates,

$$\mathcal{K} \equiv \frac{\Gamma_0}{h_0 C_0} = \frac{k_a}{k_d}\frac{\Gamma^*}{h_0}\frac{\beta}{\beta+1}.$$

Note that $\mathcal{K}$ measures the degree of solubility: for $\mathcal{K} \to 0$, the surfactant is highly soluble in the substrate and adsorbs weakly at the interface; while for $\mathcal{K} \to \infty$, the surfactant adsorbs preferentially at the interface and has very low bulk solubility. In (2.27), the interfacial transport rate $\mathcal{J} \equiv D_b/(k_a R\Gamma^*)$. For small $\mathcal{J}$, the kinetics is the so-called diffusion-controlled adsorption. In this limit surfactant transport by diffusion is slow and adsorption can be considered to occur instantaneously relative to the diffusion process. In the limit of large $\mathcal{J}$, the surfactant is transported rapidly to the interface by diffusion and the kinetics is known as adsorption-controlled transport. The nondimensional transport equations for the bulk and surface surfactants (2.14) and (2.15) become

$$\begin{aligned}\Gamma_t + &\left[\frac{\epsilon}{(1-\epsilon h)}u^s\Gamma + \mathcal{N}^2(w^s\Gamma)_z + \epsilon^2\mathcal{N}^2(u^s\Gamma)_z\right] \\ &+ \Gamma(u^s + h_z w^s)\left[\frac{\epsilon}{(1-\epsilon h)}\mathcal{N}^2 + \epsilon^2\mathcal{N}^4 h_{zz}\right] = \frac{1}{\mathcal{P}e_s}\mathcal{N}^2\Gamma_{zz} + J,\end{aligned} \tag{2.29}$$

and

$$C_t + uC_r + wC_z = \frac{1}{\mathcal{P}e_b}\left[\frac{1}{\epsilon^2}r^{-1}(rC_r)_r + C_{zz}\right], \tag{2.30}$$

where the surface Péclet number is defined as $\mathcal{P}e_s \equiv (\sigma_m h_0)/(\mu D_s)$.

For the Gibbs' adsorption equation (2.17) governing the relationship between the surface tension and the surfactant surface concentration, the nondimensional form is

$$\sigma = 1 + \mathcal{R}T\frac{\Gamma_0}{\sigma_m}\int_0^\Gamma \frac{\Gamma}{C_s}\frac{\mathrm{d}C_s}{\mathrm{d}\Gamma}\mathrm{d}\Gamma. \tag{2.31}$$

Substituting the nondimensional Langmuir isotherm (2.28) into (2.31) gives rise to the nondimensional nonlinear equation of state for soluble surfactant as

$$\sigma = 1 - \mathcal{R}T\frac{\Gamma_0}{\sigma_m}(1+\beta)\ln\left(1-\frac{\Gamma}{1+\beta}\right) \equiv 1 - \mathcal{M}a(1+\beta)\ln\left(1-\frac{\Gamma}{1+\beta}\right). \tag{2.32}$$

In the above expression, we define the Marangoni number for soluble surfactant as $\mathcal{M}a \equiv \mathcal{R}T(\Gamma_0/\sigma_m)$. For insoluble surfactant, the nondimensional equation of state (2.18) becomes

$$\sigma = 1 + \frac{\Gamma_0}{\sigma_m}\left(\frac{d\sigma}{d\Gamma}\right)_{\Gamma=0}\Gamma \equiv 1 + \mathcal{M}a\Gamma, \tag{2.33}$$

where

$$\mathcal{M}a \equiv \frac{\Gamma_0}{\sigma_m}\left(\frac{d\sigma}{d\Gamma}\right)_{\Gamma=0} = \frac{(\sigma^* - \sigma_m)}{\Gamma^*}\frac{\Gamma_0}{\sigma_m}$$

is defined as the Marangoni number for insoluble surfactant.

In Table 2.2, we summarize the major nondimensional parameters considered in the formulation above with the estimated ranges of values based on the physical and physicochemical constants listed in Table 2.1.

2.3 Lubrication Approximation

In the nondimensional radial momentum equation (2.20), the inertial terms are of $O(\mathcal{R}e\epsilon^3)$ and the viscous terms of $O(\epsilon)$. Retaining only the first-order pressure-gradient term and the gravity term, the radial momentum equation becomes

$$p_r = \mathcal{G}_r. \tag{2.34}$$

For the axial momentum equation (2.21), neglecting the higher order inertial terms of $O(\mathcal{R}e\epsilon^2)$ and the viscous term of $O(\epsilon^2)$ results in the leading-order equation,

$$r^{-1}(rw_r)_r = \epsilon p_z - \mathcal{G}_z. \tag{2.35}$$

The pressure is found by integrating the radial momentum equation (2.34) with the normal stress boundary condition (2.24), to give

$$p\ (r,z,t) = \mathcal{G}_r\left[r - \left(\frac{1}{\epsilon} - h\right)\right] + \epsilon h_z\mathcal{N}\tau_{air} - \frac{1}{(1-\epsilon h)}\mathcal{N}\sigma - \epsilon h_{zz}\mathcal{N}^3\sigma. \tag{2.36}$$

Nondimensional parameter	Symbol	Representation	Range of value
Ratio of film thickness to airway radius	ϵ	$\dfrac{h_0}{R}$	$10^{-3} \sim 10^{-1}$
Reynolds number	$\mathcal{R}e$	$\dfrac{\rho\sigma_m h_0}{\mu^2}$	$7 \times 10^{-7} \sim 7 \times 10^{2}$
Radial Bond number	$\mathcal{G}_r$	$\dfrac{\rho g_r h_0^2}{\epsilon\sigma_m}$	$0 \sim 10^{-3}$
Axial Bond number	$\mathcal{G}_z$	$\dfrac{\rho g_z h_0^2}{\epsilon\sigma_m}$	$0 \sim 10^{-3}$
Surface Péclet number	$\mathcal{P}e_s$	$\dfrac{\sigma_m h_0}{\mu D_s}$	$7 \times 10^{1} \sim 7 \times 10^{5}$
Bulk Péclet number	$\mathcal{P}e_b$	$\dfrac{\sigma_m h_0}{\mu D_b}$	$7 \times 10^{2} \sim 7 \times 10^{6}$
Marangoni number	$\mathcal{M}a$	$\dfrac{(\sigma^* - \sigma_m)}{\Gamma^*}\dfrac{\Gamma_0}{\sigma^*}$	-0.6
Equilibrium ratio	$\mathcal{K}$	$\dfrac{k_a}{k_d}\dfrac{\Gamma^*}{h_0}\dfrac{\beta}{\beta+1}$	
Interfacial transport rate number	$\mathcal{J}$	$\dfrac{D_b}{k_a R\Gamma^*}$	
Kinetic nonlinearity	β		$0.5 \sim \infty$

Table 2.2: Non-dimensional parameters considered in the formulation and the ranges of the values estimated using the physical and physicochemical constants listed in Table 2.1.

Integrating the axial momentum equation (2.35) and imposing the interfacial tangential and airway wall no-slip boundary conditions, (2.25) and (2.26), the axial velocity profile is obtained readily as

$$w(r,z,t) = (\epsilon p_z - \mathcal{G}_z)\left[\frac{1}{4}\left(r^2 - \frac{1}{\epsilon^2}\right) - \frac{(1-\epsilon h)^2}{2\epsilon^2}\ln \epsilon r\right] - (\tau_{air} + \sigma_z)\frac{1-\epsilon h}{\epsilon}\mathcal{N}^{-1}\ln \epsilon r. \quad (2.37)$$

Integrating the continuity equation (2.22) with the no-slip boundary condition at the airway wall (2.26) and making use of the axial velocity (2.37), the radial velocity can be

obtained as

$$\begin{aligned}u(r,z,t) =&\epsilon p_{zz}\left[\left(\frac{-1}{16}r^3+\frac{r}{8\epsilon^2}+\frac{1}{16r\epsilon^4}\right)+\left(\frac{r}{2}\ln\epsilon r-\frac{r}{4}+\frac{1}{4r\epsilon^2}\right)\frac{(1-\epsilon h)^2}{2\epsilon^2}\right]\\&-\frac{(1-\epsilon h)}{\epsilon}h_z(\epsilon p_z-\mathcal{G}_z)\left(\frac{r}{2}\ln\epsilon r-\frac{r}{4}+\frac{1}{4r\epsilon^2}\right)\\&+\left[\frac{(1-\epsilon h)}{\epsilon}\mathcal{N}^{-1}\sigma_{zz}-h_z\mathcal{N}^{-1}(\tau_{air}+\sigma_z)\right]\left(\frac{r}{2}\ln\epsilon r-\frac{r}{4}+\frac{1}{4r\epsilon^2}\right).\end{aligned}\tag{2.38}$$

From (2.37) and (2.38), the axial and radial surface velocities can be expressed as

$$\begin{aligned}u^s(z,t) =&u\left(\epsilon^{-1}-h(z,t),z,t\right)\\=&\left(\frac{1}{2}\frac{\epsilon}{(1-\epsilon h)}h^2h_z\mathcal{N}-\frac{1}{2}\epsilon h^2h_z\mathcal{N}^{-1}\right)\sigma_z\\&+\left(\frac{1}{2}h^2\mathcal{N}^{-1}-\frac{1}{6}\epsilon h^3\mathcal{N}^{-1}+\frac{1}{3}\frac{\epsilon}{(1-\epsilon h)}h^3\mathcal{N}\right)\sigma_{zz}-\frac{1}{2}\epsilon h^2h_z\mathcal{N}^{-1}\tau_{air}\\&+\left(-\frac{1}{2}\epsilon h^2h_z^2-\frac{1}{3}\epsilon h^3h_{zz}\right)\mathcal{G}_r+\left(\frac{1}{2}h^2h_z-\frac{1}{6}\epsilon h^3h_z\right)\mathcal{G}_z,\end{aligned}\tag{2.39}$$

and

$$\begin{aligned}w^s(z,t) =&w\left(\epsilon^{-1}-h(z,t),z,t\right)\\=&\left(\frac{1}{2}\frac{\epsilon^2}{(1-\epsilon h)^2}h_z\mathcal{N}+\frac{1}{2}\epsilon^2h^2h_{zzz}\mathcal{N}^3\right)\sigma\\&+\left(h\mathcal{N}^{-1}-\frac{1}{2}\epsilon h^2\mathcal{N}^{-1}+\frac{1}{2}\frac{\epsilon}{(1-\epsilon h)}h^2\mathcal{N}-\frac{1}{6}\frac{\epsilon^2}{(1-\epsilon h)}h^3\mathcal{N}+\frac{1}{2}\epsilon^2h_{zz}\mathcal{N}^3\right)h^2\sigma_z\\&+\left(h\mathcal{N}^{-1}-\frac{1}{2}\epsilon h^2\mathcal{N}^{-1}-\frac{1}{2}\epsilon^2h^2h_{zz}\mathcal{N}\right)\tau_{air}\\&+\left(-\frac{1}{2}\epsilon h^2h_z+\frac{1}{6}\epsilon^2h^3h_z\right)\mathcal{G}_r+\left(\frac{1}{2}h^2-\frac{1}{6}\epsilon h^3\right)\mathcal{G}_z.\end{aligned}\tag{2.40}$$

We now define the volume flux across the cross section of film as

$$Q(z,t)=\int_{\frac{1}{\epsilon}-h(z,t)}^{\frac{1}{\epsilon}}rw(r,z,t)\mathrm{d}r.$$

From the expression of the axial velocity $w(r,z,t)$ (2.37), the integral can be evaluated as

$$\begin{aligned}\epsilon Q(z,t) =&\left(\frac{1}{3}\frac{\epsilon^2}{(1-\epsilon h)^2}h^3h_z\mathcal{N}+\frac{1}{3}\epsilon^2h^3h_{zzz}\mathcal{N}^3\right)\sigma\\&+\left(\frac{1}{2}h^2\mathcal{N}^{-1}-\frac{2}{3}\epsilon h^3\mathcal{N}^{-1}+\frac{1}{3}\frac{\epsilon}{(1-\epsilon h)}h^3\mathcal{N}-\frac{1}{3}\frac{\epsilon^2}{(1-\epsilon h)}h^4\mathcal{N}+\frac{1}{3}\epsilon^2h^3h_{zz}\mathcal{N}^3\right)\sigma_z\\&+\left(\frac{1}{2}h^2\mathcal{N}^{-1}-\frac{2}{3}\epsilon h^3\mathcal{N}^{-1}-\frac{1}{3}\epsilon^2h^3h_{zz}\mathcal{N}\right)\tau_{air}\\&+\left(-\frac{1}{3}\epsilon h^3h_z+\frac{1}{3}\epsilon^2h^4h_z\right)\mathcal{G}_r+\left(\frac{1}{3}h^3-\frac{1}{3}\epsilon h^4\right)\mathcal{G}_z.\end{aligned}\tag{2.41}$$

Utilizing the above expressions for the axial and radial surface velocity u^s (2.39) and w^s (2.40) and the volume flux integral (2.41), the kinematic boundary condition (2.23) can be further represented as an alternative form of the evolution equation for film thickness as

$$h_t + \frac{1}{(1-\epsilon h)}\epsilon Q_z(z,t) = 0. \tag{2.42}$$

This is the well-known thin film equation. The equation describes the leading-order approximation to the kinematics and dynamics of a Newtonian thin film lining on the interior surface of an airway.

2.4 Cross-sectional Average

In deriving the cross-sectional average approximation for the bulk surfactant transport, we follow the formulation of Jensen & Grotberg [1993] and Jensen *et al.* [1994]. The cross-sectional average of any function $\Psi(r,z)$ is defined as

$$\bar{\Psi}(z) = \frac{2\pi}{\mathcal{A}} \int_{\frac{1}{\epsilon}-h(z)}^{\frac{1}{\epsilon}} r\Psi(r,z)dr, \tag{2.43}$$

where $\mathcal{A}$ is the cross-sectional area of the liquid film,

$$\mathcal{A}(z,t) = \pi \left[\left(\frac{1}{\epsilon}\right)^2 - \left(\frac{1}{\epsilon} - h(z,t)\right)^2 \right].$$

Using the Leibnitz rule, the derivative of $\bar{\Psi}$ is

$$\left(\bar{\Psi}\right)_z = \left(\overline{\Psi_z}\right) + \frac{2\pi}{\mathcal{A}} \left(\frac{1}{\epsilon} - h\right) \left[(\Psi)_{r=\frac{1}{\epsilon}-h} - \bar{\Psi} \right].$$

Since $\mathcal{P}e_b\epsilon^2 \ll 1$ (see the typical values in Table 2.2), the surfactant molecules diffuse rapidly across the liquid film in a nondimensional time of $O(\mathcal{P}e_b\epsilon^2)$, as revealed in the transport equation for the bulk surfactant (2.30). So that for $t \gg O(\mathcal{P}e_b\epsilon^2)$, the bulk surfactant concentration C may be decomposed into two parts, a cross-sectionally averaged component and a small fluctuation in r direction:

$$C(r,z,t) = \bar{C}(z,t) + \mathcal{P}e_b\epsilon^2 C_1(r,z,t), \tag{2.44}$$

where the cross-sectional average of the fluctuation C_1 is equal to zero,

$$\bar{C}_1 \equiv \frac{2\pi}{\mathcal{A}} \int_{\frac{1}{\epsilon}-h}^{\frac{1}{\epsilon}} r C_1(r,z,t) dr = 0. \tag{2.45}$$

Substituting the expression of C in (2.44) into the sorption kinetics (2.27) and neglecting the higher-order terms give

$$\begin{aligned} J &= \frac{1}{\mathcal{P}e_b}\frac{1}{\mathcal{K}}\frac{1}{\mathcal{J}}\frac{1}{\epsilon}\left(\frac{\beta}{1+\beta}\right)\left[\bar{C}\left(1+\frac{1-\Gamma}{\beta}\right)-\Gamma\right] \\ &= \frac{1}{\mathcal{K}}\mathcal{N}\left[C_{1r}+\frac{1}{\mathcal{P}e_b}h_z\bar{C}_z\right]_{r=\frac{1}{\epsilon}-h}+O(\epsilon^2). \end{aligned} \tag{2.46}$$

This can be used to solve for the radial derivative of fluctuated bulk concentration at the film surface as

$$(C_{1r})_{r=\frac{1}{\epsilon}-h} = -\frac{1}{\mathcal{P}e_b}h_z\bar{C}_z + \frac{1}{\mathcal{P}e_b}\frac{1}{\mathcal{J}}\frac{1}{\mathcal{N}}\frac{1}{\epsilon}\left(\frac{\beta}{1+\beta}\right)\left[\bar{C}\left(1+\frac{1-\Gamma}{\beta}\right)-\Gamma\right]. \tag{2.47}$$

When the surface and bulk concentrations reach the local equilibrium, there is no sorption flux, i.e. $J=0$, and from (2.46)

$$\bar{C} = \frac{\beta\Gamma}{1+\beta-\Gamma}. \tag{2.48}$$

Similarly, substituting the decomposition (2.44) into the surfactant transport equations (2.29) and (2.30) gives rise to

$$\begin{aligned} \Gamma_t &+ \left[\frac{\epsilon}{(1-\epsilon h)}u^s\Gamma + \mathcal{N}^2(w^s\Gamma)_z\right] + \frac{\epsilon}{(1-\epsilon h)}\mathcal{N}^2\Gamma(u^s+h_z w^s) \\ &= \frac{1}{\mathcal{P}e_s}\mathcal{N}^2\Gamma_{zz} + \frac{1}{\mathcal{P}e_b}\frac{1}{\mathcal{K}}\frac{1}{\mathcal{J}}\frac{1}{\epsilon}\left(\frac{\beta}{1+\beta}\right)\left[\bar{C}\left(1+\frac{1-\Gamma}{\beta}\right)-\Gamma\right]+O(\epsilon^2), \end{aligned} \tag{2.49}$$

and

$$\bar{C}_t + w\bar{C}_z + \mathcal{P}e_b\epsilon^2\left(C_{1t}+uC_{1r}+wC_{1z}\right) = r^{-1}(rC_{1r})_r + \frac{1}{\mathcal{P}e_b}\bar{C}_{zz}+O(\epsilon^2). \tag{2.50}$$

Taking the cross-sectional averaging of equation (2.50) and using the equilibrium boundary condition (2.47) at interface and the no-penetration boundary condition $C_z = 0$ at the airway wall result in

$$\begin{aligned} \bar{C}_t + \bar{w}\bar{C}_z =& \frac{1}{\mathcal{P}e_b}\bar{C}_{zz} + \frac{1}{\mathcal{P}e_b}\frac{2-\epsilon h}{2h}h_z\bar{C}_z \\ &- \frac{1}{\mathcal{P}e_b}\frac{1}{\mathcal{J}}\frac{1}{\mathcal{N}}\frac{1}{\epsilon}\left(\frac{\beta}{1+\beta}\right)\left(\frac{2-\epsilon h}{2h}\right)\left[\bar{C}\left(1+\frac{1-\Gamma}{\beta}\right)-\Gamma\right], \end{aligned} \tag{2.51}$$

where the cross-sectionally averaged axial velocity is defined as

$$\begin{aligned}\bar{w}(z,t) =& \frac{1}{\mathcal{A}(z,t)} \int_{\frac{1}{\epsilon}-h(z,t)}^{\frac{1}{\epsilon}} 2\pi r w(r,z,t) \mathrm{d}r \\ =& \left(\frac{1}{3} \frac{\epsilon^2}{(1-\epsilon h)^2} h^2 h_z \mathcal{N} + \frac{1}{3} \epsilon^2 h^2 h_{zzz} \mathcal{N}^3 \right) \sigma \\ &+ \left(\frac{1}{2} h \mathcal{N}^{-1} - \frac{5}{12} \epsilon h^2 \mathcal{N}^{-1} + \frac{1}{3} \frac{\epsilon}{(1-\epsilon h)} h^2 \mathcal{N} - \frac{1}{6} \frac{\epsilon^2}{(1-\epsilon h)} h^3 \mathcal{N} + \frac{1}{3} \epsilon^2 h^2 h_{zz} \mathcal{N}^3 \right) \sigma_z \\ &+ \left(\frac{1}{2} h \mathcal{N}^{-1} - \frac{5}{12} \epsilon h^2 \mathcal{N}^{-1} - \frac{1}{3} \epsilon^2 h^2 h_{zz} \mathcal{N} \right) \tau_{air} \\ &+ \left(-\frac{1}{3} \epsilon h^2 h_z + \frac{1}{6} \epsilon^2 h^3 h_z \right) \mathcal{G}_r + \left(\frac{1}{3} h^2 - \frac{1}{6} \epsilon h^3 \right) \mathcal{G}_z. \end{aligned} \tag{2.52}$$

After the cross-sectional averaging approximation, the transport equations for the surface and bulk surfactants, (2.49) and (2.51), depend only on z and t.

The surfactant transport equations, (2.49) and (2.51), govern the evolutions of the surface concentration $\Gamma(z,t)$ and the averaged bulk concentration $\bar{C}(z,t)$, and are coupled through the sorption kinetics linking Γ and $\bar{C}$ at the interface.

Chapter 3

Numerical Method

3.1 Time Integration Scheme

The leading-order equations, (2.42), (2.49) and (2.51), govern the evolution of the film thickness $h(z,t)$ and the distributions of surfactant concentrations at the interface $\Gamma(z,t)$ and in the bulk phase $C(z,t)$. In these equations, the radial and axial surface velocities, u^s and w^s, are given by (2.39) and (2.40), and the average axial velocity $\bar{w}$ is given by (2.52). These coupled nonlinear partial differential equations are solved numerically. Third-order Adams-Bashforth scheme is used for numerical time integration. Expressing the evolution equations, (2.42), (2.49) and (2.51), in a general form as

$$\frac{\partial \Phi}{\partial t} = \mathrm{F}(\Phi, t),$$

the third-order Adams-Bashforth scheme can then be written as

$$\frac{\Phi_i^{n+1} - \Phi_i^n}{\Delta t} = \frac{1}{12}\left[23\mathrm{F}\left(\Phi_i^n, t^n\right) - 16\mathrm{F}\left(\Phi_i^{n-1}, t^{n-1}\right) + 5\mathrm{F}\left(\Phi_i^{n-2}, t^{n-2}\right)\right],$$

where n is the temporal discretization index, j is the spatial discretization index, and Δt is the time interval. The spatial derivatives are approximated by second-order central difference scheme.

Based on the dimensions of human airways reported in Weibel [1963] (see also Table 1.1), the typical length of airway is less than eight times of the radius in all airway generations except in the trachea. Therefore, the length of airway in the model is assumed

to be eight times of the radius R, and accordingly the nondimensional axial coordinate ranges from 0 to 8. The number of grid points employed in the computational domain is 80 with the spatial interval $\Delta z = 0.1$, which is sufficient to resolved most of the film disturbance and surfactant distribution. The time interval is chosen to be $\Delta t = 0.001$, such that the Courant-Friedrichs-Lewy condition is satisfied.

3.2 Initial Conditions

The initial thickness of the undisturbed film is assumed to be uniform such that $h(z,0) = 1$. To simulate the transport of an instilled dose, following the simulation of Jensen & Grotberg [1992] and Craster & Matar [2000], the initial distribution of the surfactant at the interface is prescribed by

$$\Gamma(z,0) = \Gamma_{pre} + (\Gamma_{exo} - \Gamma_{pre}) \exp(-5z^2) \quad \text{for } 0 \leq z \leq 8, \tag{3.1}$$

providing a smooth approximation to the surfactant surface concentration, where Γ_{exo} is the concentration of the instilled exogenous surfactant and the concentration of the pre-existing surfactant Γ_{pre} is assumed to be uniform at the entire film lining. In order to examine the influences of initial condition on the simulations, we also use the following distribution for certain computations as

$$\Gamma(z,0) = \begin{cases} \Gamma_{pre} + (\Gamma_{exo} - \Gamma_{pre}) \cos^2(0.5\pi z) & \text{for } 0 \leq z \leq 1 \\ \Gamma_{pre} & \text{for } 1 < z \leq 8, \end{cases} \tag{3.2}$$

which is similar to the that used by Espinosa & Kamm [1999]. For the soluble surfactant, the initial concentration in the substrate $\bar{C}$ is assumed to be 0, such that $\bar{C}(z,0) = 0$.

The initial conditions for the film thickness $h(z,0)$ and the surfactant concentration at the interface $\Gamma(z,0)$ for $\Gamma_{exo} = 1.0$ and $\Gamma_{pre} = 0.1$ are plotted in Figure 3.1.

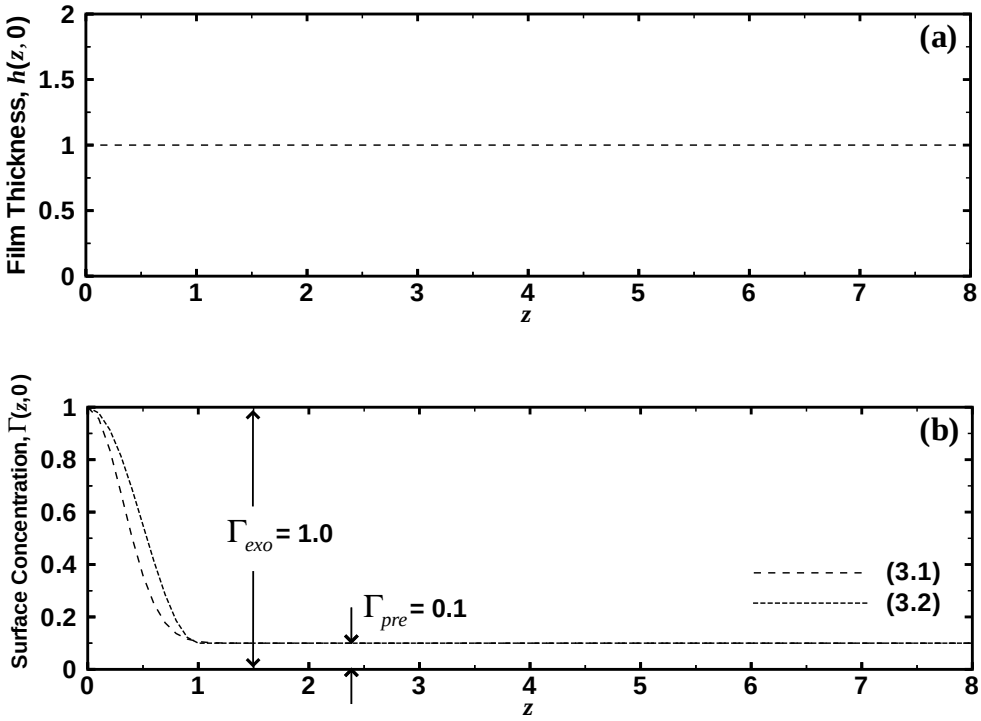

Figure 3.1: Initial conditions for (a) the film thickness $h(z,0)$ and (b) the surfactant surface concentration $\Gamma(z,0)$ for $\Gamma_{exo} = 1.0$ and $\Gamma_{pre} = 0.1$. In Figure (b), the dashed line represents the surfactant distribution described by (3.1), and the dotted line represents that described by (3.2).

3.3 Boundary Conditions

With the prescribed initial surfactant distributions, the boundary conditions for surfactant distribution is assumed vanished surfactant flux at $z = 0$, which implies that the surfactant concentration is symmetric about $z = 0$. When the effects of the axial gravity and the stress due to air flow do not exist, the induced Marangoni flow is also symmetric about $z = 0$. Accordingly, the surface axial velocity w^s, the average axial velocity $\bar{w}$ and the volume flux Q all vanish at $z = 0$, which leads to the condition that the derivatives of film thickness h_z and h_{zzz} also equal to zero. Thus, the boundary conditions for the surfactant surface and bulk concentrations Γ and $\bar{C}$ and the film height h can be expressed as

$$\Gamma_z(0,t) = 0, \quad \bar{C}_z(0,t) = 0, \quad h_z(0,t) = 0 \quad \text{and} \quad h_{zzz}(0,t) = 0.$$

Similarly, the same boundary conditions are imposed at the end of the domain, $z = 8$. Note that the transport of surfactant is terminated before reaching the end of the modeled domain in order to avoid any effects from the downstream of the airway.

Chapter 4

Results

4.1 Film Disturbance and Surfactant Spread in Various Generations of Airways

The pulmonary airways in anatomy are classified into 23 generations of branches from the trachea (generation 0) to the alveolar sacs (generation 23). The dimensions for the conducting zone of adult airways, the first 16 generations, are listed in Table 1.1. For neonatal airways, the dimensions are approximately one-third of that for adult airways from the trachea to generation 14 [Hislop *et al.*, 1972; Espinosa & Kamm, 1999]. The film thickness h_0 is approximately 10 μm for all branches [Widdicombe, 2002]. Accordingly, for all airway generations, the ratio of film thickness to airway radius ϵ ranges from 1×10^{-3} to 5×10^{-2} for adults and from 3×10^{-3} to 1×10^{-1} for neonates. To exemplify the transport of surfactant in various generations of airways, four representative ratios of film thickness to airway radius, $\epsilon = 0.001$, 0.01, 0.05 and 0.1, are simulated. The surfactant is assumed to be insoluble with the concentration of instilled exogenous surfactant $\Gamma_{exo} = 1$, and the concentration of preexisting surfactant $\Gamma_{pre} = 0$. The other parameters are fixed and chosen as $\mu = 0.01$ g/cm s, $\tau_{air} = 0$ and $\mathcal{G}_r = \mathcal{G}_z = 0$.

Time varying profiles of the film thickness $h(z,t)$ and the surface surfactant concentration $\Gamma(z,t)$ are shown in Figures 4.1 and 4.2, respectively. Immediately after the instillation of the insoluble surfactant, a steep shock develops right behind the leading

edge of the surfactant monolayer. The film height behind the shock decreases attributed to mass conservation. Accompanying the propagation of the film disturbance, the surfactant spreads forward with a rapid decrease of concentration at $z = 0$. For the four values of ϵ considered, the steepness of the shock decreases as ϵ increases. On the other hand, the spreading speed of surfactant is virtually unaffected.

To further reveal the effect of the ratio of film thickness to airway radius ϵ on the film disturbance induced by Marangoni flow, Figure 4.3 shows the temporal evolutions of (a) the peak film thickness h_{peak}, (b) the axial position of the peak z_{peak}, and (c) the trough film thickness h_{trough} appearing at $z = 0$. As depicted in Figure 4.1, as soon as the surfactant begins to spread, a shock-like solitary wave develops immediately with its peak thickness h_{peak} increases drastically to more than one and half of the undisturbed film thickness (Figure 4.3(a)). As time proceeds, the peak thickness slowly approaches an asymptotic value. The asymptotic peak thickness is higher for the airway of smaller ϵ (i.e. larger radius), which denotes that the disturbance induced by Marangoni flow in a larger airway would be more pronounced than that in a smaller one for the same level of instilled surfactant dose. Such a solitary wave propagates with a higher nondimensional forwarding speed for airways at lower generations as indicated by the change of axial position of the peak thickness plotted in Figure 4.3(b). The trough thickness h_{trough} behind the solitary wave reduces as time progresses as shown in Figure 4.3(c). However, the decreasing rate of trough thickness is unchanged for the four values of ϵ considered.

In comparison with the film disturbance, the concentration of surfactant spreading on the thin film is virtually unaffected in various generations of airway as shown in Figure 4.2. The properties of the temporal evolutions of the surfactant concentration are plotted in Figure 4.4. In Figure 4.4, the length of monolayer L_{mono} (a) is defined as the position of surfactant monolayer front where the surfactant concentration is equal to 0.01, and the spreading velocity of surfactant monolayer $\mathrm{d}L_{mono}/\mathrm{d}t$ (b) is obtained by time differentiating the frontal position of surfactant monolayer. The length of surfactant monolayer

increases monotonically with time. The spreading velocity is maximum at the moment when the surfactant dose is instilled due to the highest surface-tension gradient. Because of the rapid depression in the concentration gradient, the spreading velocity quickly decelerates to a small level. The length of the surfactant monolayer is slightly more extensive in the airway of smaller ϵ. The spreading velocity, however, is unaffected by the value of ϵ. The initial rapid spread of surfactant monolayer results in an abrupt drop of the concentration at $z = 0$, $\Gamma(0, t)$, as shown in Figure 4.4(c). Similar to the spreading velocity of surfactant monolayer $\mathrm{d}L_{mono}/\mathrm{d}t$, the dropping rate $\mathrm{d}\Gamma(0, t)/\mathrm{d}t$ decreases quickly from an extremely high initial value to a diminished level (Figure 4.4(d)).

Different initial distributions of surfactant have been used in previous studies [Jensen & Grotberg, 1992; Espinosa *et al.*, 1993; Craster & Matar, 2000]. For a fixed quantity of surfactant, the initial distribution can be described using various smooth functions. In all the simulation results discussed so far, the initial surfactant distribution is described by an exponential function (3.1). To examine the possible effect of initial condition on the simulation results, we repeat the simulations for the airways of $\epsilon = 0.001$, 0.01, 0.05 and 0.1, and use different initial condition (3.2), which has previously been used by Espinosa *et al.* [1993]. Other parameters are chosen to be the same. Figures 4.5 and 4.6 show the evolutions of the film deformation and the surfactant spreading for the simulations using the cosine-function initial condition (3.2). Similar to the results demonstrated in Figures 4.1 and 4.2, the film disturbance induced by Marangoni effect is more substantial in the lower-generation airway, but no obvious effect is observed on the spreading rate of surfactant. However, there is a significant difference in the disturbance waveforms between the two initial conditions. In Figures 4.5(a) and (b), small disturbances form behind the main disturbed solitary wave, which do not appear in the results using the exponential-function initial condition (3.1). In the previous study of Espinosa *et al.* [1993], they also observed small waves behind the main disturbance in their simulations in the lower-generation airway. They further demonstrated that these small waves would disappear using finer

computational mesh. They, therefore, concluded that these small disturbances are produced numerically and are not from a physical mechanism. The function describing the initial surfactant distribution may affect the simulated waveform of film disturbance. This can be avoided by choosing a smooth functional representation of the initial condition. The results of surfactant spreading, however, are independent of the choice of the initial surfactant distribution.

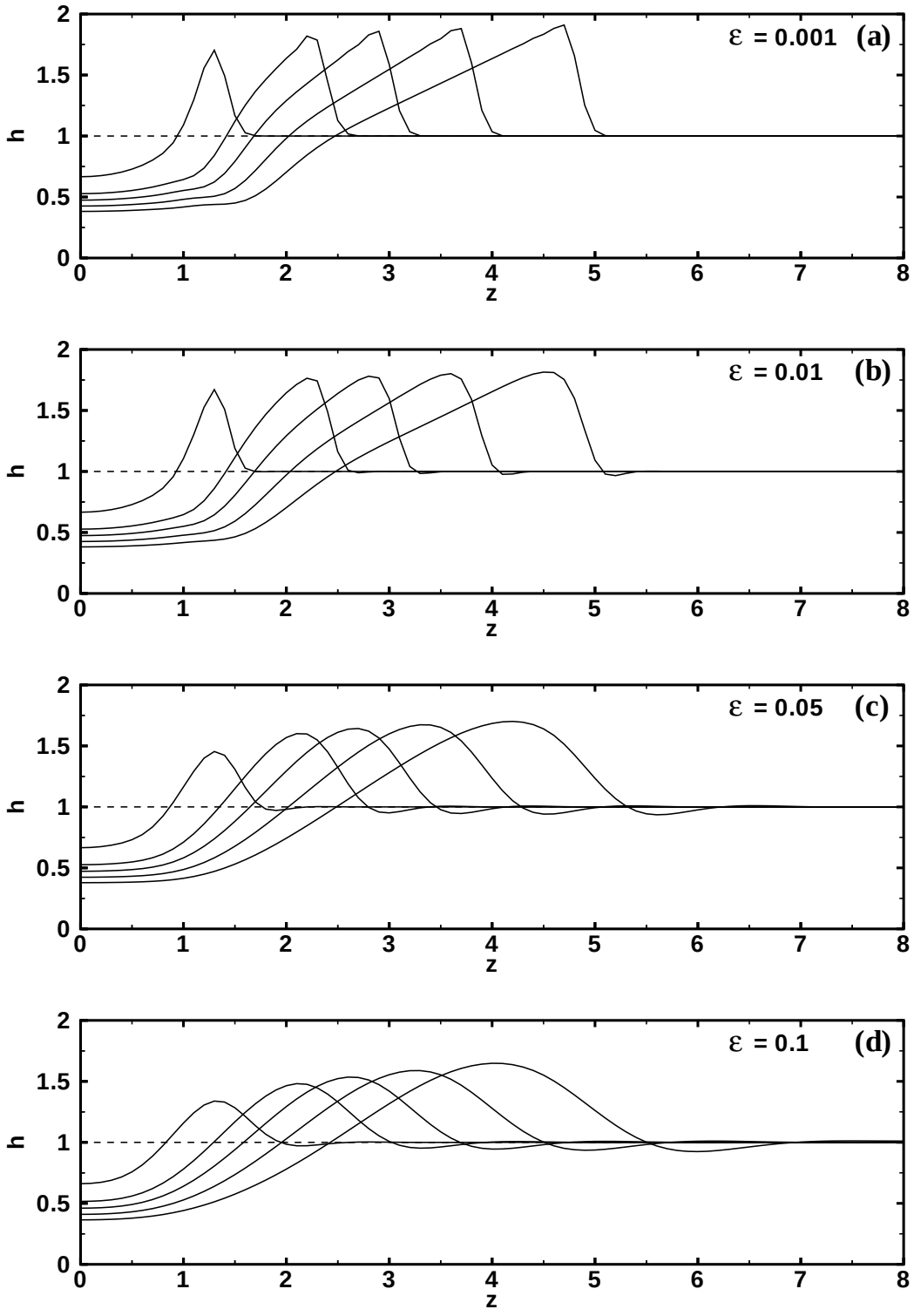

Figure 4.1: Time varying profiles of film thickness $h(z,t)$ for the ratio of film thickness to airway radius $\epsilon =$ (a) 0.001, (b) 0.01, (c) 0.05 and (d) 0.1, at time $t = 0$ (dashed line), 1, 5, 10, 20 and 40. Parameter values are $\Gamma_{exo} = 1$, $\Gamma_{pre} = 0$, $\mu = 0.01$ g/cm s, $\tau_{air} = 0$ and $\mathcal{G}_r = \mathcal{G}_z = 0$.

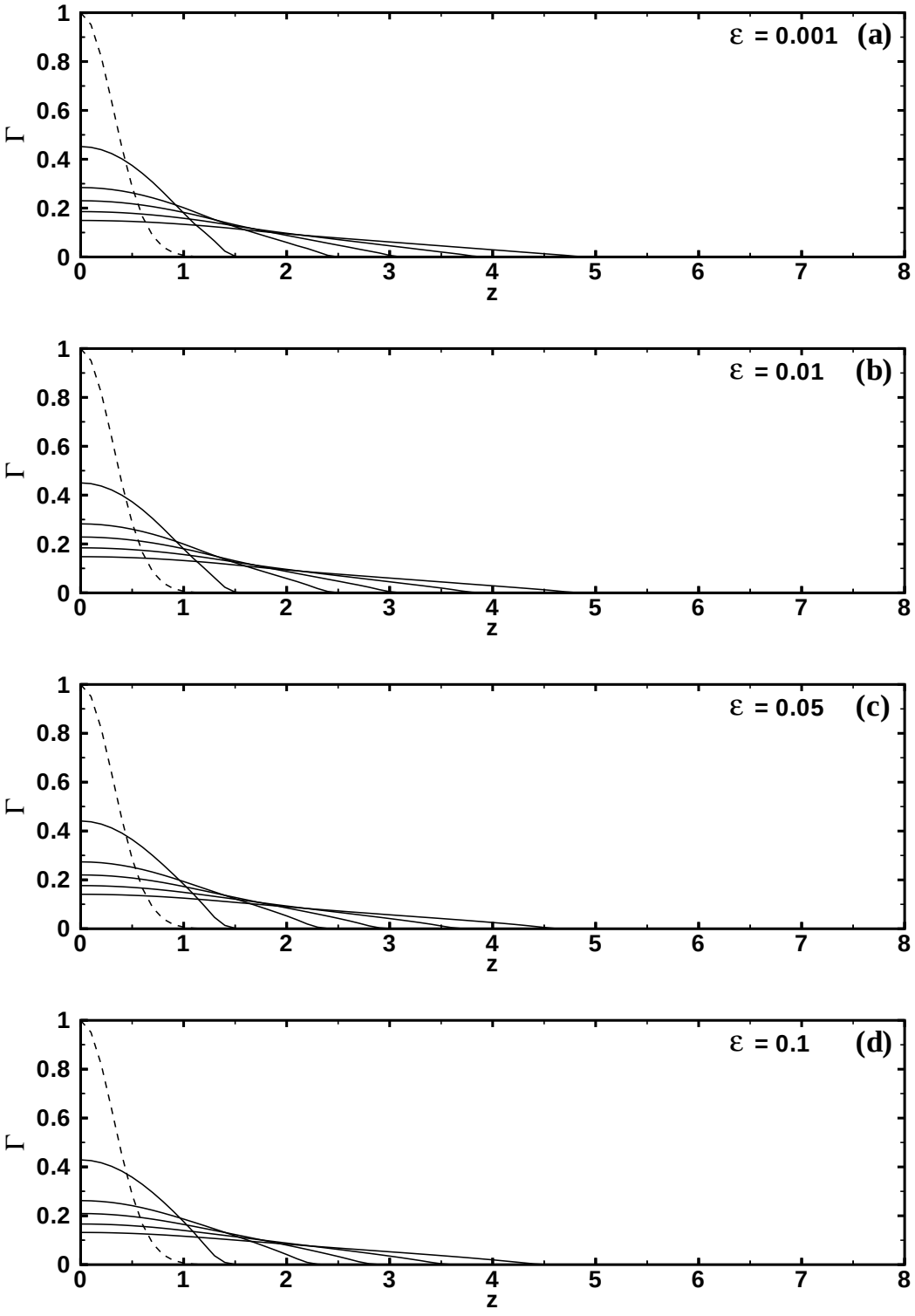

Figure 4.2: Time varying profiles of surface surfactant concentration $\Gamma(z,t)$ for the ratio of film thickness to airway radius ϵ = (a) 0.001, (b) 0.01, (c) 0.05 and (d) 0.1, at time $t = 0$ (dashed line), 1, 5, 10, 20 and 40. Parameter values are $\Gamma_{exo} = 1$, $\Gamma_{pre} = 0$, $\mu = 0.01$ g/cm s, $\tau_{air} = 0$ and $\mathcal{G}_r = \mathcal{G}_z = 0$.

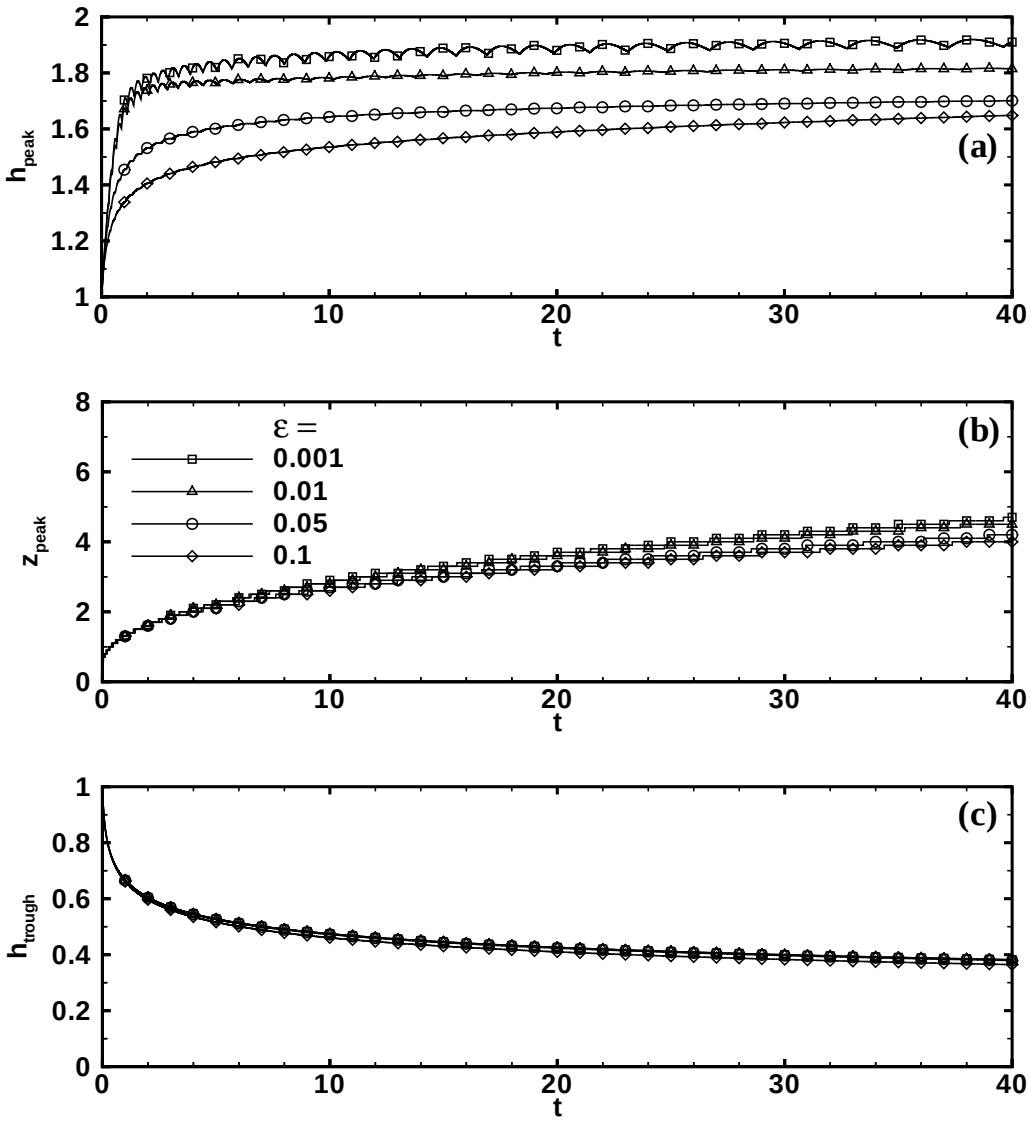

Figure 4.3: Temporal evolutions of (a) the peak film thickness, h_{peak}, (b) the axial position of peak film thickness, z_{peak}, and (c) the trough film thickness, h_{trough}, for various ratios of film thickness to airway radius $\epsilon = 0.001$, 0.01, 0.05 and 0.1.

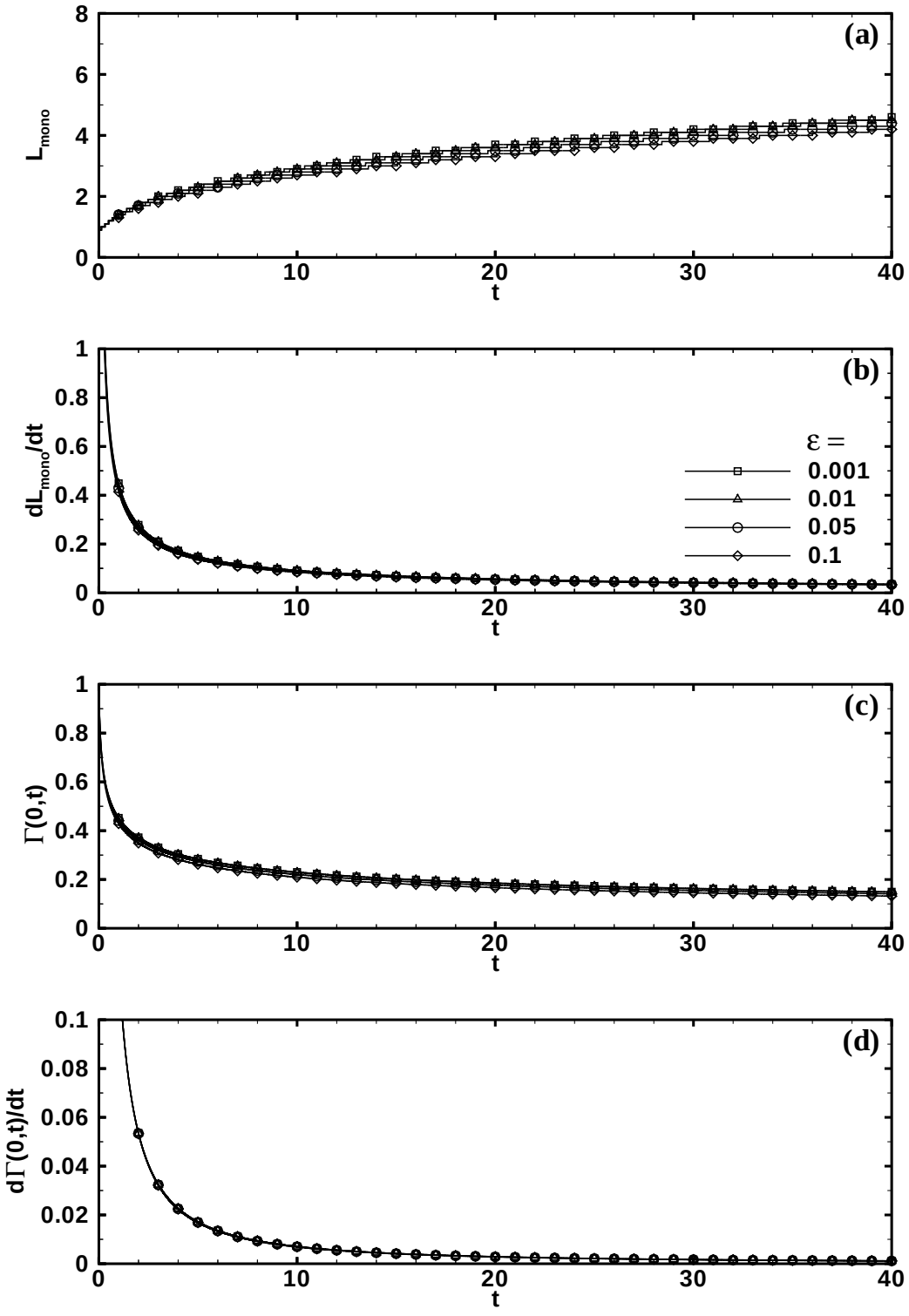

Figure 4.4: Temporal evolutions of (a) the length of surfactant monolayer, L_{mono}, (b) the spreading velocity of surfactant monolayer, $\mathrm{d}L_{mono}/\mathrm{d}t$, (c) the surfactant concentration at $z = 0$, $\Gamma(0, t)$, and (d) the dropping rate, $\mathrm{d}\Gamma(0, t)/\mathrm{d}t$, for various ratios of film thickness to airway radius $\epsilon = 0.001$, 0.01, 0.05 and 0.1.

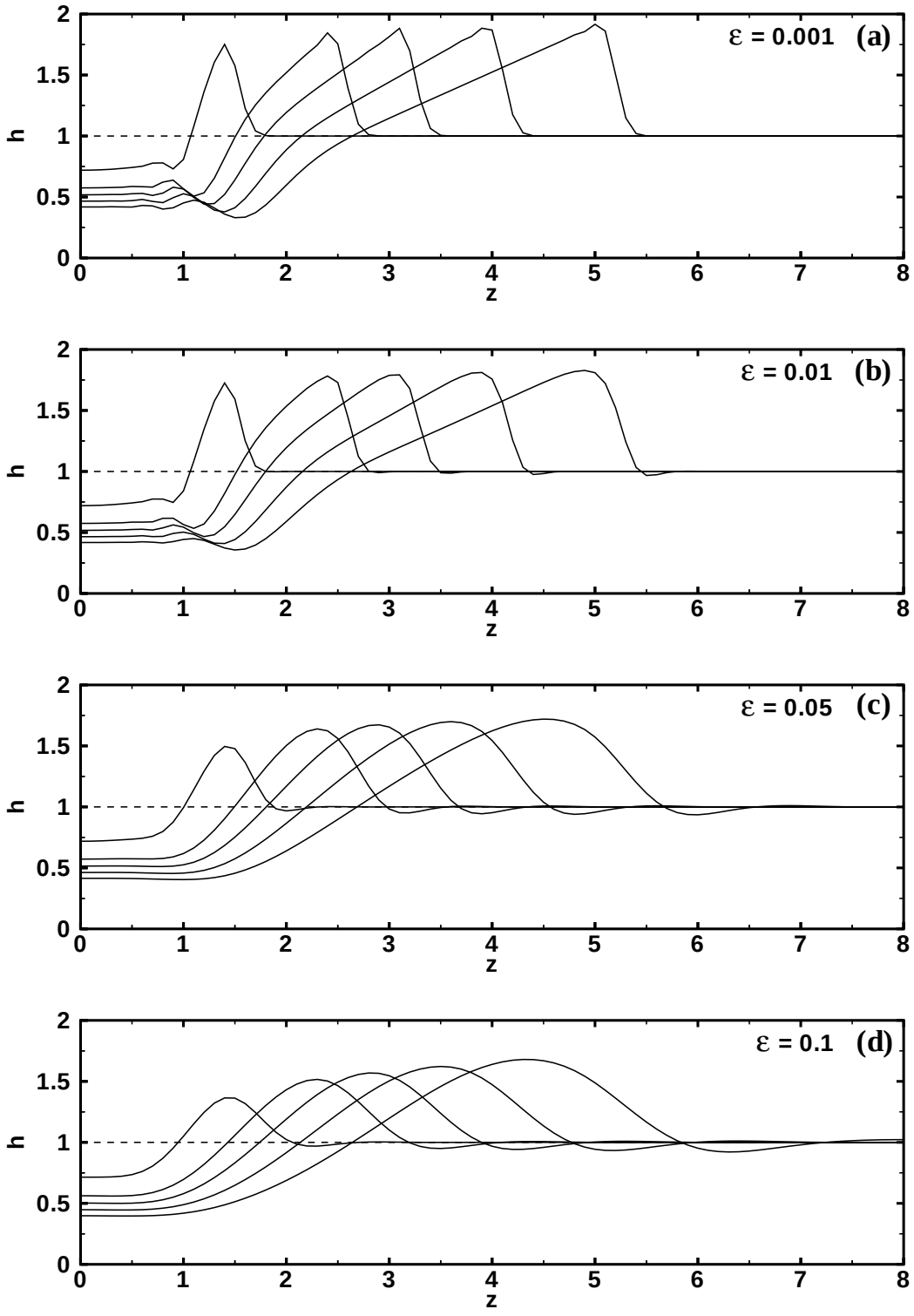

Figure 4.5: Time varying profiles of film thickness $h(z,t)$ for the ratio of film thickness to airway radius $\epsilon =$ (a) 0.001, (b) 0.01, (c) 0.05 and (d) 0.1, at time $t = 0$ (dashed line), 1, 5, 10, 20 and 40. Parameter values are $\Gamma_{exo} = 1$, $\Gamma_{pre} = 0$, $\mu = 0.01$ g/cm s, $\tau_{air} = 0$ and $\mathcal{G}_r = \mathcal{G}_z = 0$.

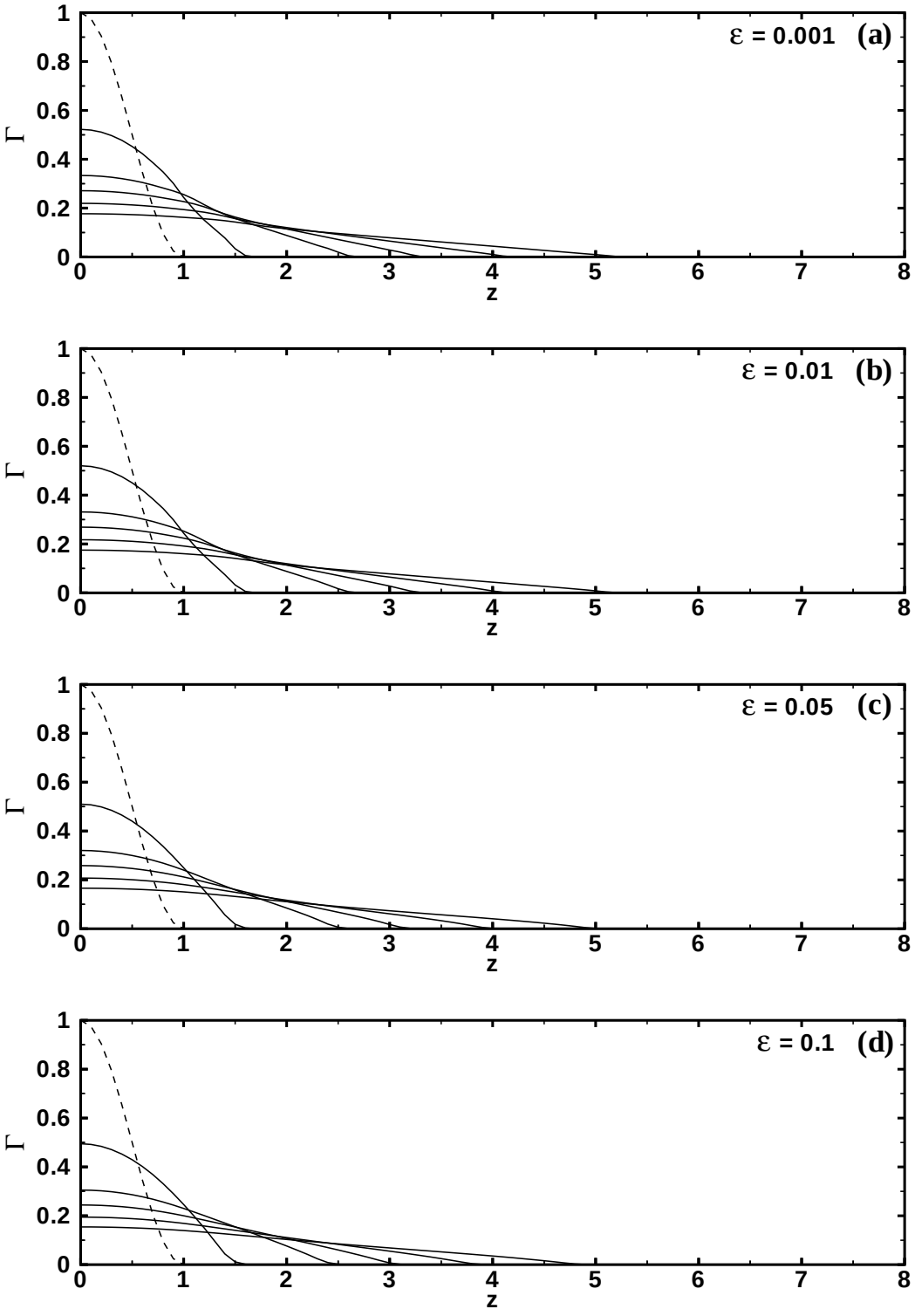

Figure 4.6: Time varying profiles of surface surfactant concentration $\Gamma(z,t)$ for the ratio of film thickness to airway radius ϵ =1 (a) 0.00, (b) 0.01, (c) 0.05 and (d) 0.1, at time $t = 0$ (dashed line), 1, 5, 10, 20 and 40. Parameter values are $\Gamma_{exo} = 1$, $\Gamma_{pre} = 0$, $\mu = 0.01$ g/cm s, $\tau_{air} = 0$ and $\mathcal{G}_r = \mathcal{G}_z = 0$.

4.2 Effect of the Initial Exogenous Surfactant Strength

Whether a stronger surfactant dose results in better curative effect is critical in clinical therapy due to the high cost of SRT, which is approximately $1000 to $2000 for a single treatment [Merritt *et al.*, 1995]. To study the effect of the initial exogenous surfactant strength on surfactant transport, various concentrations of exogenous surfactant, $\Gamma_{exo} = 1$, 0.8, 0.6 and 0.4, are considered in the simulations for the airway of $\epsilon = 0.01$. The effects of the gravity, the shear stress due to air flow and the endogenous surfactant are all neglected in the present case. Figures 4.7 and 4.8 show the temporal developments of the film disturbance and the spread of exogenous surfactant, respectively, for the four values of Γ_{exo} considered. Similar waveforms of the disturbed films are observed for various values of Γ_{exo}. However, as the results reveal, reducing the exogenous surfactant strength also decreases the initial Marangoni stress and, consequently, retards the spread of surfactant as well as the propagation of film disturbed wave. The temporal evolutions of the local disturbance characteristics shown in Figure 4.9 also evidence the impact of the exogenous surfactant strength on film disturbance. The rise of the peak height h_{peak} and the depression of the trough thickness h_{trough} are all intensified accompanying the acceleration of the monolayer spreading. Nevertheless, the higher strength of exogenous surfactant only enhances the early period of monolayer spreading. As shown in Figures 4.10(b) and (d), the spreading velocity of the surfactant monolayer, $\mathrm{d}L_{mono}/\mathrm{d}t$, and the dropping rate of surfactant concentration at $z = 0$, $\mathrm{d}\Gamma(0,t)/\mathrm{d}t$, diminish to similar levels for various values of initial concentration of the surfactant dose. The results, therefore, indicate that increasing the strength of exogenous surfactant dose not necessarily proportionally improve the efficiency of monolayer spreading.

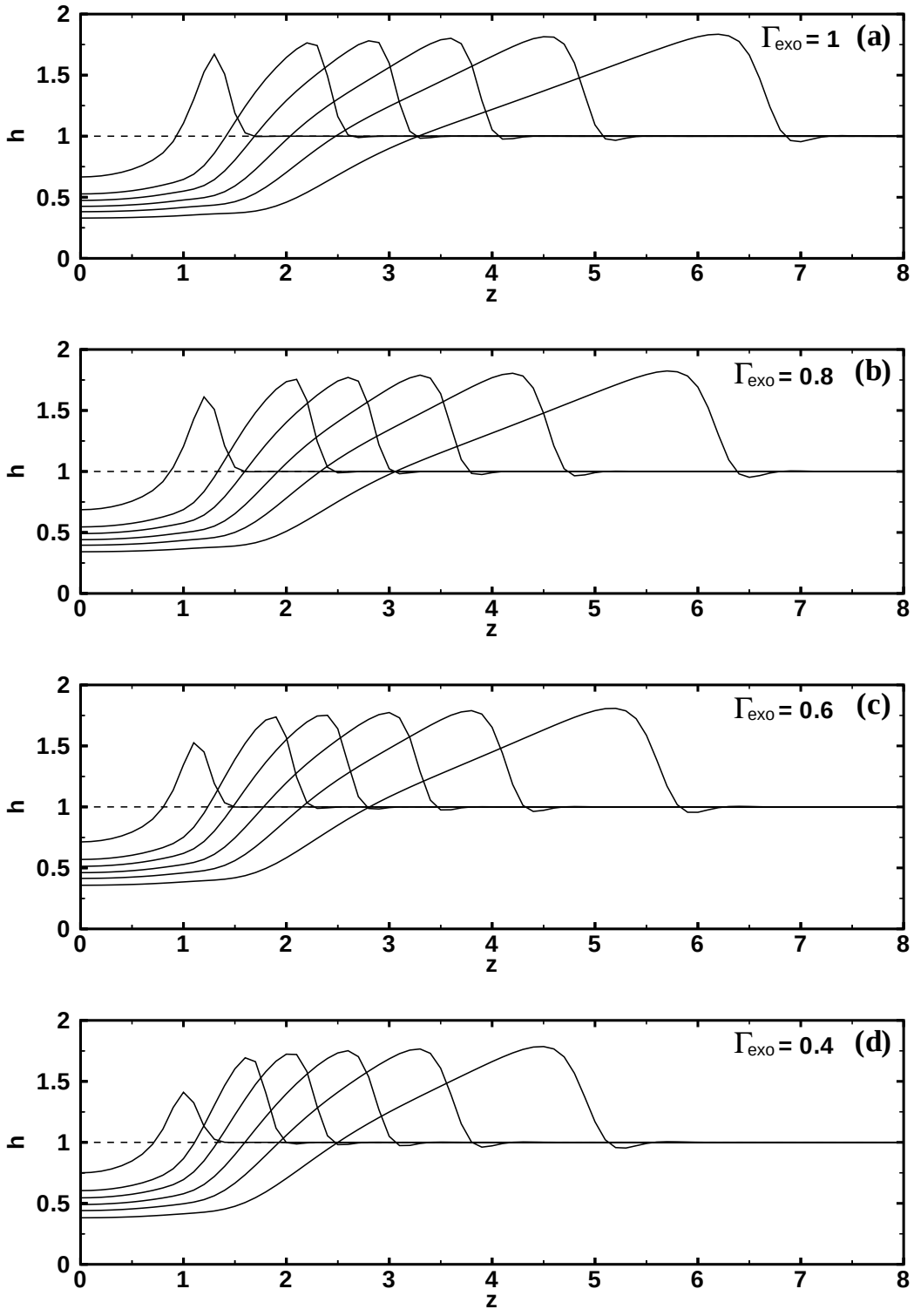

Figure 4.7: Time varying profiles of film thickness $h(z,t)$ for the concentration of exogenous surfactant Γ_{exo} = (a) 1, (b) 0.8, (c) 0.6 and (d) 0.4, at time $t = 0$ (dashed line), 1, 5, 10, 20, 40 and 100. Parameter values are $\epsilon = 0.01$, $\Gamma_{pre} = 0$, $\mu = 0.01$ g/cm s, $\tau_{air} = 0$ and $\mathcal{G}_r = \mathcal{G}_z = 0$.

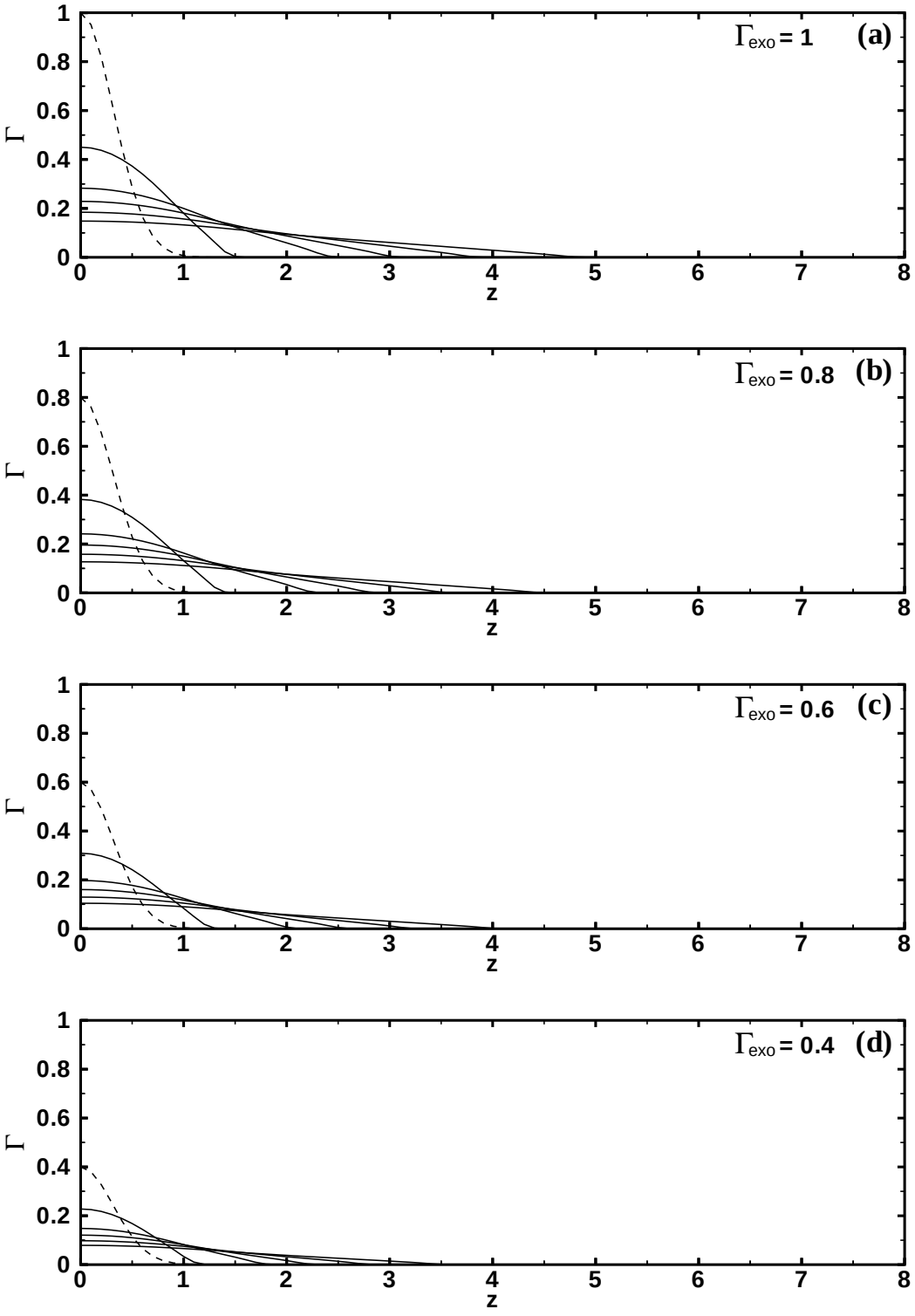

Figure 4.8: Time varying profiles of surface surfactant concentration $\Gamma(z,t)$ for the concentration of exogenous surfactant Γ_{exo} = (a) 1, (b) 0.8, (c) 0.6 and (d) 0.4, at time $t = 0$ (dashed line), 1, 5, 10, 20, 40 and 100. Parameter values are $\epsilon = 0.01$, $\Gamma_{pre} = 0$, $\mu = 0.01$ g/cm s, $\tau_{air} = 0$ and $\mathcal{G}_r = \mathcal{G}_z = 0$.

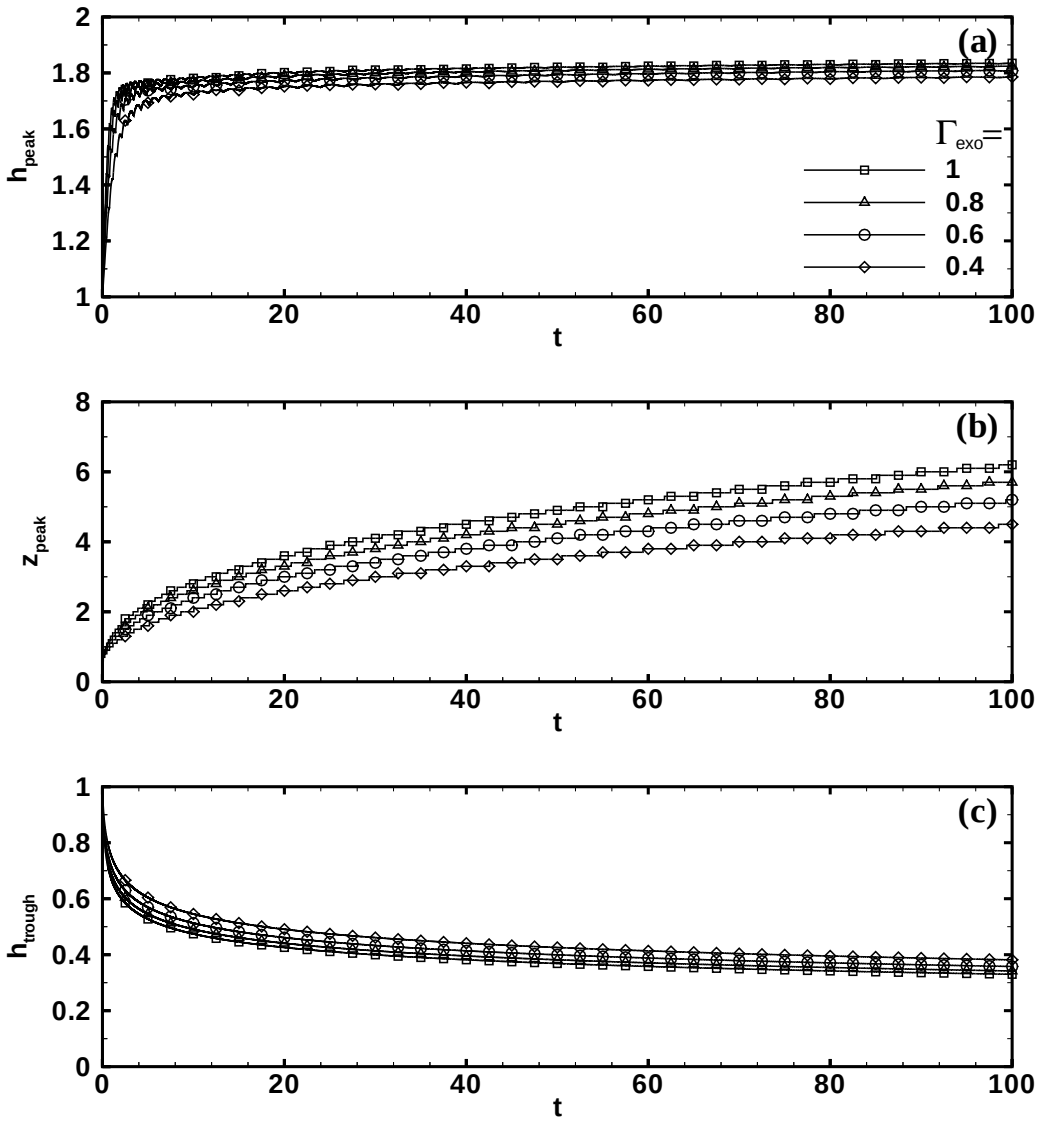

Figure 4.9: Temporal evolutions of (a) the peak film thickness, h_{peak}, (b) the axial position of peak film thickness, z_{peak}, and (c) the trough film thickness, h_{trough}, for various initial concentrations of exogenous surfactant $\Gamma_{exo} = 1$, 0.8, 0.6 and 0.4.

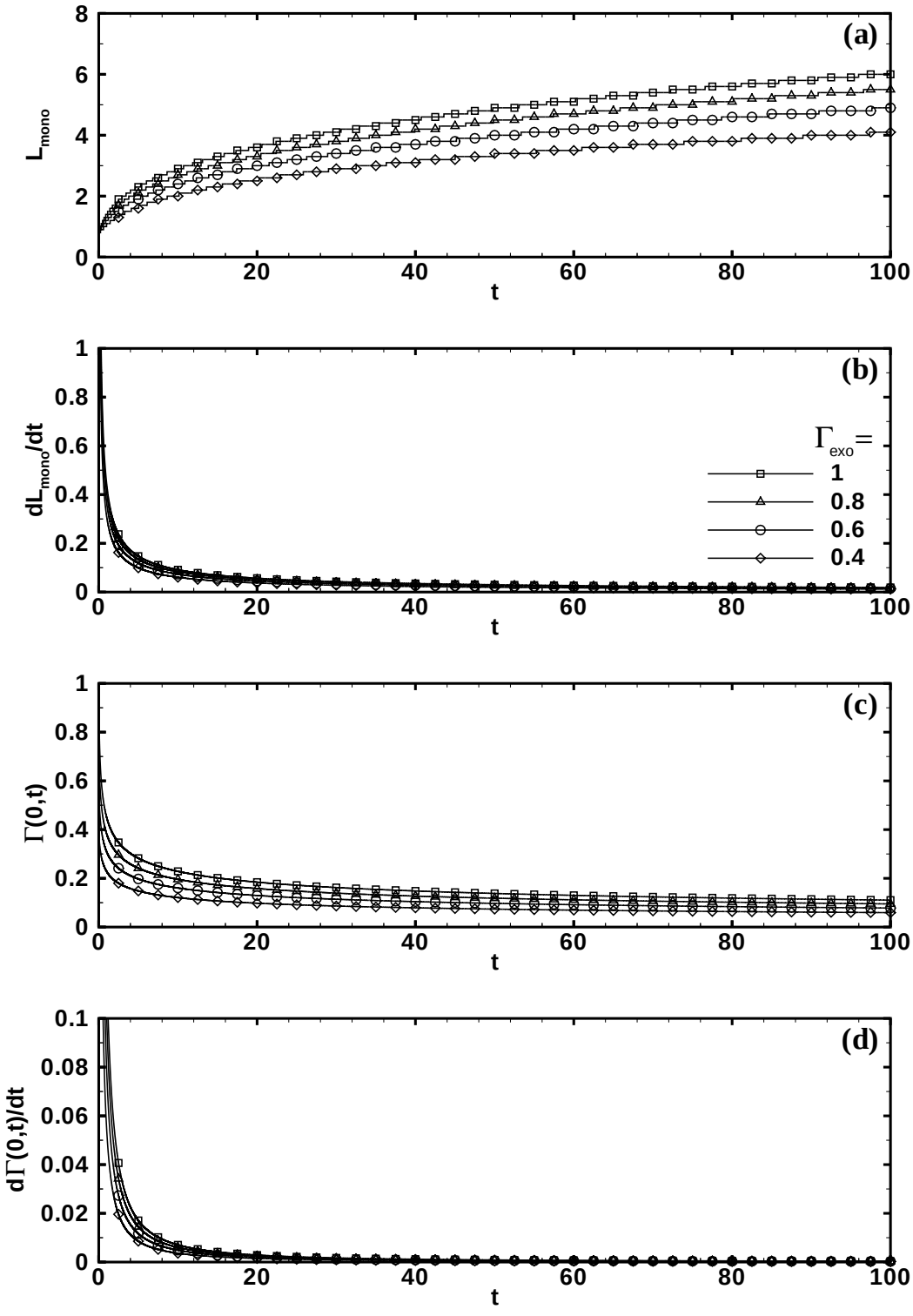

Figure 4.10: Temporal evolutions of (a) the length of surfactant monolayer, L_{mono}, (b) the spreading velocity of surfactant monolayer, $\mathrm{d}L_{mono}/\mathrm{d}t$, (c) the surfactant concentration at $z = 0$, $\Gamma(0, t)$, and (d) the dropping rate, $\mathrm{d}\Gamma(0, t)/\mathrm{d}t$, for various initial concentrations of exogenous surfactant $\Gamma_{exo} = 1$, 0.8, 0.6 and 0.4.

4.3 Effect of the Preexisting Surfactant

Clinical studies show that infants suffering from RDS have obvious responses to the first administration of exogenous surfactant dose. But the following instillations are not as effective as the first one [Long *et al.*, 1991]. This means that the presence of preexisting surfactant can possibly slow down the spread of exogenous surfactant. The sources of the preexisting surfactant are from the residual of previous doses or from the type II alveolar cells secreting. Such an issue has been addressed before [Espinosa *et al.*, 1993; Grotberg *et al.*, 1995]. Here we consider four values of preexisting surfactant concentrations, $\Gamma_{pre} = 0$, 0.01, 0.05 and 0.1, which distribute uniformly on the entire film initially. The developments of the film disturbance and the surfactant spread are illustrated in Figures 4.11 and 4.12, and the temporal evolutions of the film thickness and the concentration properties are plotted in Figures 4.13 and 4.14, respectively. The existence of preexisting surfactant moderates the steep shock of film disturbance (Figure 4.11). The peak film thickness h_{peak} raises to its maximum immediately after the instillation of surfactant dose and then decreases slowly due to the presence of preexisting surfactant, as shown in Figure 4.13(a). Both the peak film thickness h_{peak} and its propagation speed decrease as the concentration of preexisting surfactant increases as depicted in Figures 4.13(a) and (b). Nevertheless, contradictory effect of the preexisting surfactant on the advancing speed of the film disturbance is observed. Although the steepness and the peak thickness of the disturbed solitary wave are drastically reduced with the presence of preexisting surfactant, the extent of the disturbance, however, is moved forward. Such a prolonging effect also appears in the spreading of surfactant where the leading edge of surfactant monolayer seems to advance faster on the film with preexisting surfactant. Espinosa *et al.* [1993], therefore, concluded that the presence of preexisting surfactant increases the spreading rate of the exogenous surfactant. Grotberg *et al.* [1995], however, reached the opposite conclusion by arguing that the higher spreading rate of surfactant is attributed to the compression of preexisting surfactant concentration in regions ahead of the leading edge

of advancing exogenous surfactant monolayer. This conclusion can also be reinforced by the decreasing trend of concentration at $z = 0$ (Figure 4.14(c) and (d)), which reflects the spreading rate of instilled exogenous surfactant. For the faster spreading of instilled surfactant, the decreasing rate of the local concentration at $z = 0$ should also be higher. Nevertheless, for the simulation with $\Gamma_{pre} = 0.05$, the level of concentration at $z = 0$ is always slightly higher than that with $\Gamma_{pre} = 0$. In addition, there is no obvious change in the dropping rate of $\Gamma(0, t)$ with various levels of preexisting surfactant (Figure 4.14(d)). The existence of preexisting surfactant indeed reduces the spreading rate of the exogenous surfactant. However, the spreading of exogenous surfactant causes the raising of the concentration of preexisting surfactant ahead of the advancing leading edge. This makes the preexisting surfactant to propagate faster than the leading edge of exogenous surfactant.

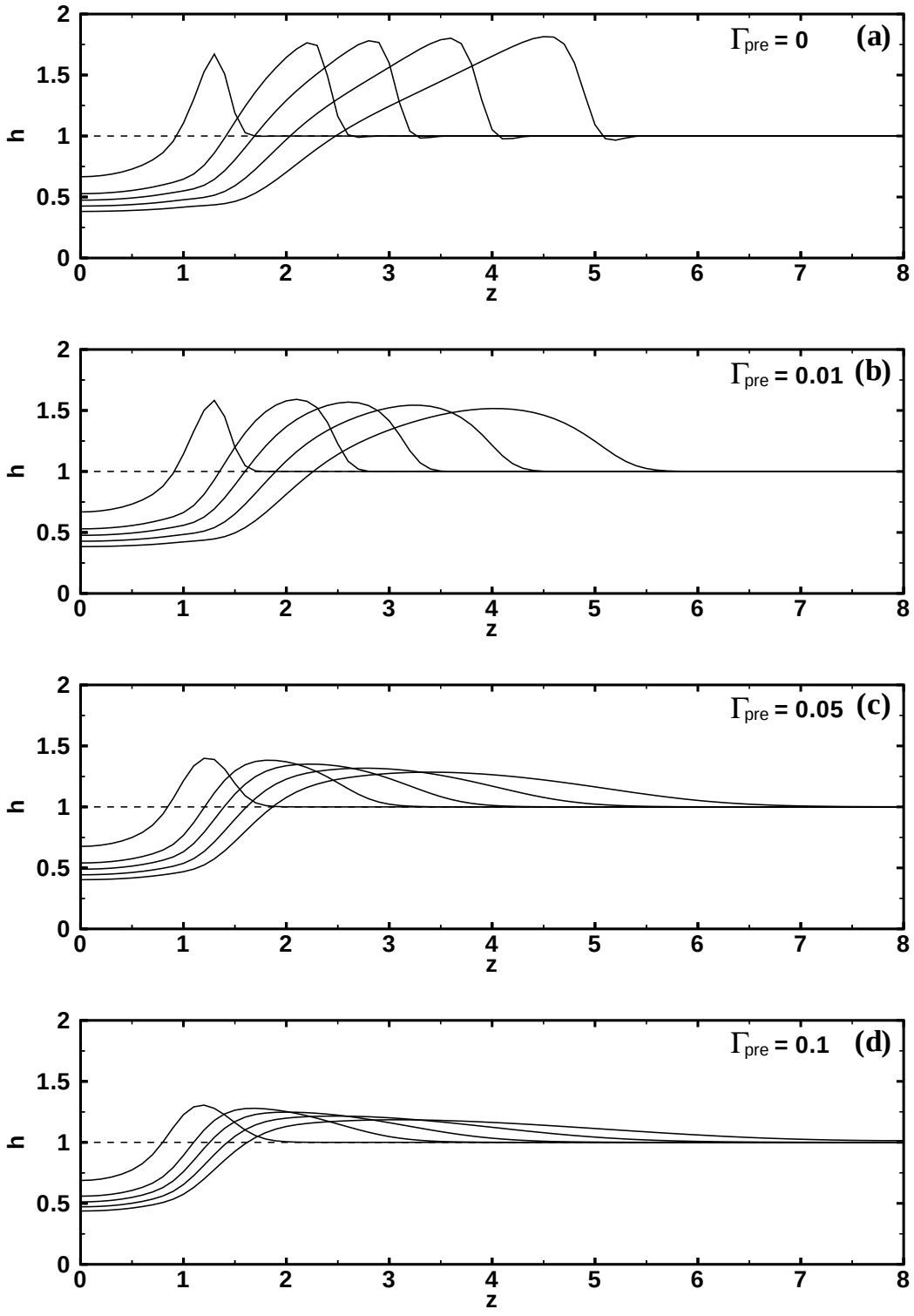

Figure 4.11: Time varying profiles of film thickness $h(z,t)$ for the concentrations of pre-existing surfactant Γ_{pre} = (a) 0, (b) 0.01, (c) 0.05 and (d) 0.1, at time $t = 0$ (dashed line), 1, 5, 10, 20 and 40. Parameter values are $\epsilon = 0.01$, $\Gamma_{exo} = 1$, $\mu = 0.01$ g/cm s, $\tau_{air} = 0$ and $\mathcal{G}_r = \mathcal{G}_z = 0$.

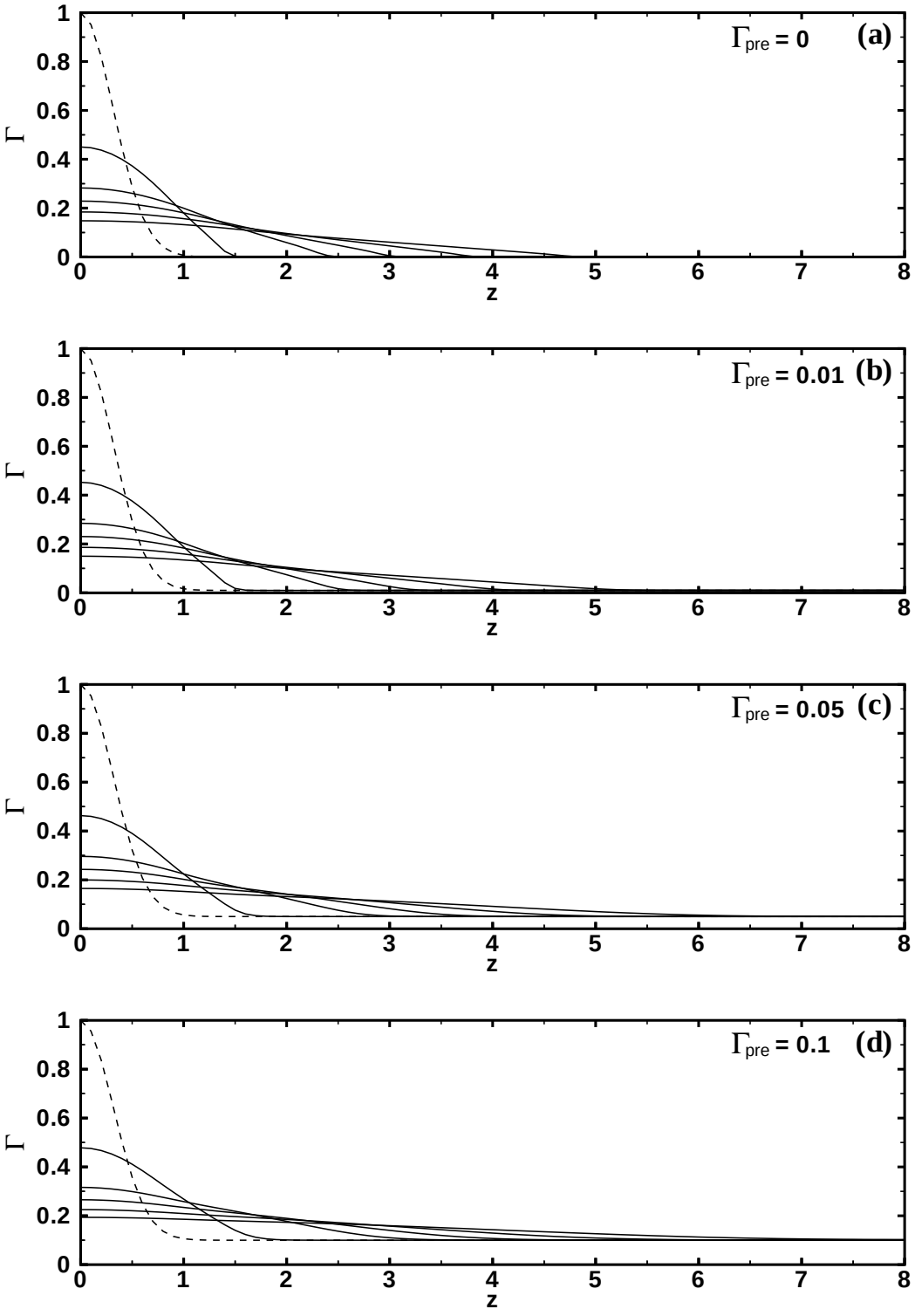

Figure 4.12: Time varying profiles of surface surfactant concentration $\Gamma(z,t)$ for the concentrations of preexisting surfactant Γ_{pre} = (a) 0, (b) 0.01, (c) 0.05 and (d) 0.1, at time $t = 0$ (dashed line), 1, 5, 10, 20 and 40. Parameter values are $\epsilon = 0.01$, $\Gamma_{exo} = 1$, $\mu = 0.01$ g/cm s, $\tau_{air} = 0$ and $\mathcal{G}_r = \mathcal{G}_z = 0$.

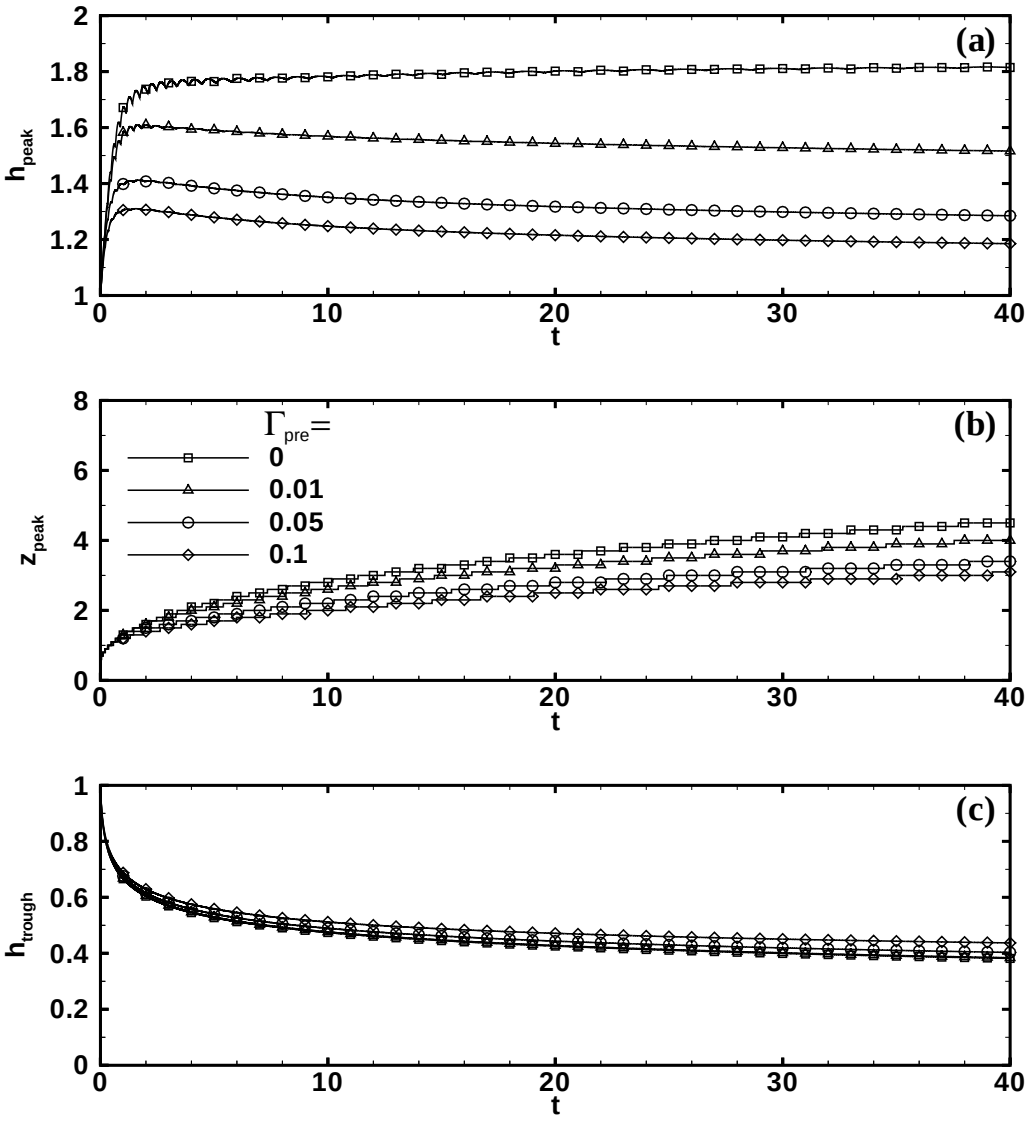

Figure 4.13: Temporal evolutions of (a) the peak film thickness, h_{peak}, (b) the axial position of peak film thickness, z_{peak}, and (c) the trough film thickness, h_{trough}, for various concentrations of preexisting surfactant $\Gamma_{pre} = 0$, 0.01, 0.05 and 0.1.

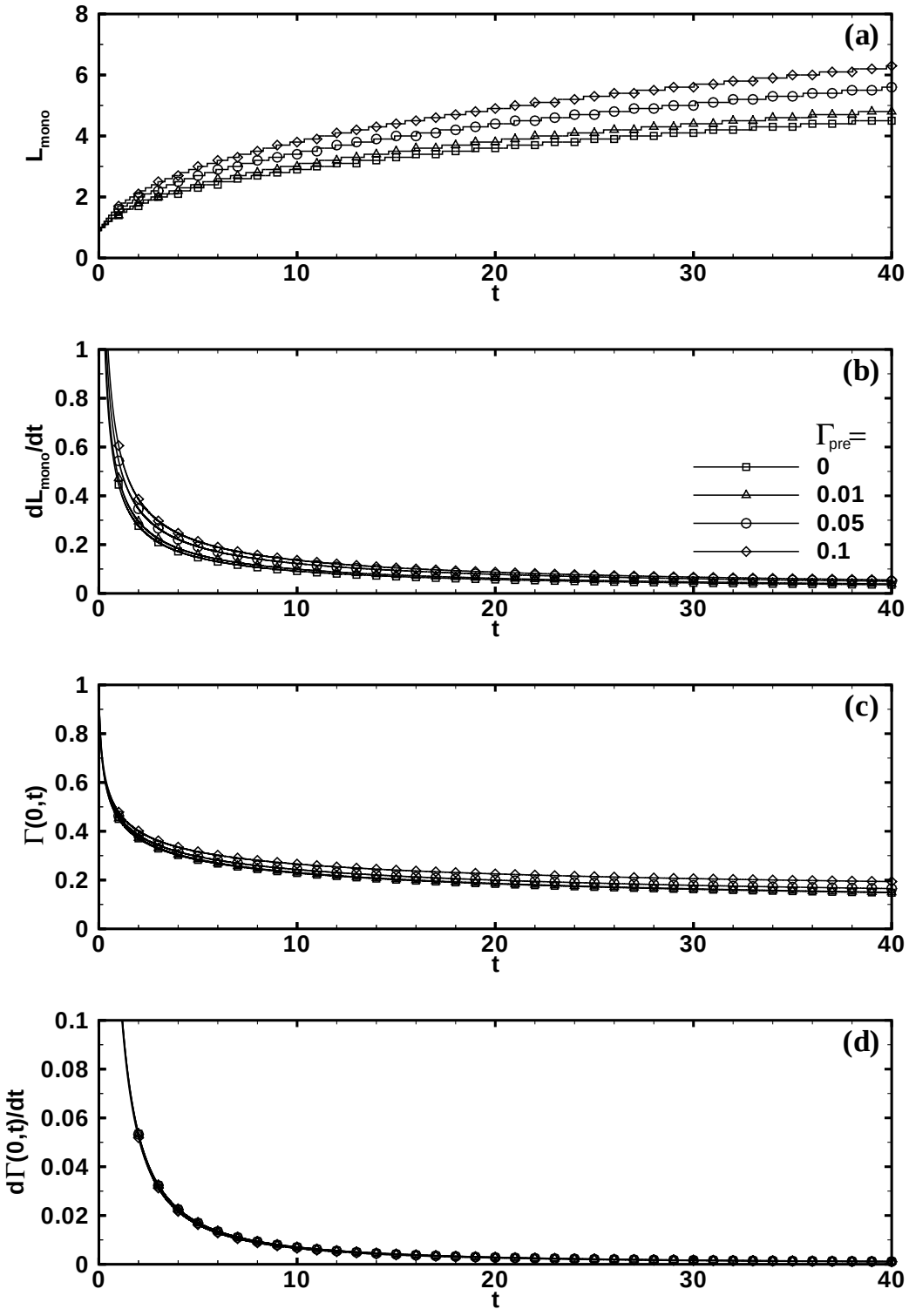

Figure 4.14: Temporal evolutions of (a) the length of surfactant monolayer, L_{mono}, (b) the spreading velocity of surfactant monolayer, $\mathrm{d}L_{mono}/\mathrm{d}t$, (c) the surfactant concentration at $z = 0$, $\Gamma(0,t)$, and (d) the dropping rate, $\mathrm{d}\Gamma(0,t)/\mathrm{d}t$, for various concentrations of preexisting surfactant $\Gamma_{pre} = 0$, 0.01, 0.05 and 0.1.

4.4 Effect of the Film Viscosity

The airway surface liquid is a bilayer system with the mucus layer overlying the periciliary liquid layer. The periciliary sol surrounding the cilia is a watery liquid with the viscosity similar to that of water and may be the only form of airway surface liquid present at birth and in completely healthy adult airways [Bhaskar *et al.*, 1985; Widdicombe, 2002]. However, the irritation of the surface of trachea and bronchi stimulates secretion of mucus. Furthermore, pulmonary diseases, such as asthma, chronic bronchitis, cystic fibrosis, and other inflammatory airway diseases probably cause airway mucus accumulation and changes in the balance of mucus-secreting and water-secreting elements [Widdicombe, 2002]. Therefore, the viscosity of airway surface liquid ranges from 0.01 to 100 g/cm s, where the lower value is that of water, and the higher range reflects the ill conditions [Silberberg, 1983; Craster & Matar, 2000]. To examine the effect of the viscosity of airway surface liquid, four values of film viscosity $\mu = 0.01$, 1, 10 and 100 g/cm s are computed. The corresponding surface Péclet numbers are $\mathcal{P}e_s = 7 \times 10^5$, 7×10^3, 7×10^2 and 7×10^1 (see Table 2.2). The other parameters are fixed and chosen as $\epsilon = 0.01$, $\Gamma_{exo} = 1$, $\Gamma_{pre} = 0$, $\tau_{air} = 0$ and $\mathcal{G}_r = \mathcal{G}_z = 0$.

Numerical solutions of the film disturbance and the surfactant spreading are shown in Figures 4.15 and 4.16, respectively. With the decreasing value of $\mathcal{P}e_s$, the shock of the film disturbed solitary wave broadens and decays with time as shown in Figure 4.15. The peak film thickness h_{peak} decreases (Figure 4.17(a)) and the propagation of the solitary wave slows down (Figure 4.17(b)) as $\mathcal{P}e_s$ reduces below a critical value where the viscous force becomes predominate. As shown in Figures 4.18(a) and (b), temporal evolutions of the length of surfactant monolayer, L_{mono}, and the spreading velocity, $\mathrm{d}L_{mono}/\mathrm{d}t$, increase with the raising value of the film viscosity μ (i.e. the decreasing value of $\mathcal{P}e_s$). The profound effect of the film viscosity on the transport of surfactant can be more appreciated by examining the surfactant spreading properties shown in Figure 4.18 using the dimensional time scale. The dimensional characteristic time scale $\mathcal{T} = (\mu R^2)/(\sigma_m h_0)$

is proportional to the value of film viscosity μ. The barely distinguishable properties of dimensional temporal evolutions of the surfactant distribution for various film viscosities, therefore, imply that the surfactant spreading rate would decrease with the increasing film viscosity. This means that for the airways suffering pulmonary diseases, the required delivery time of surfactant will increase approximately proportional to the viscosity of film lining.

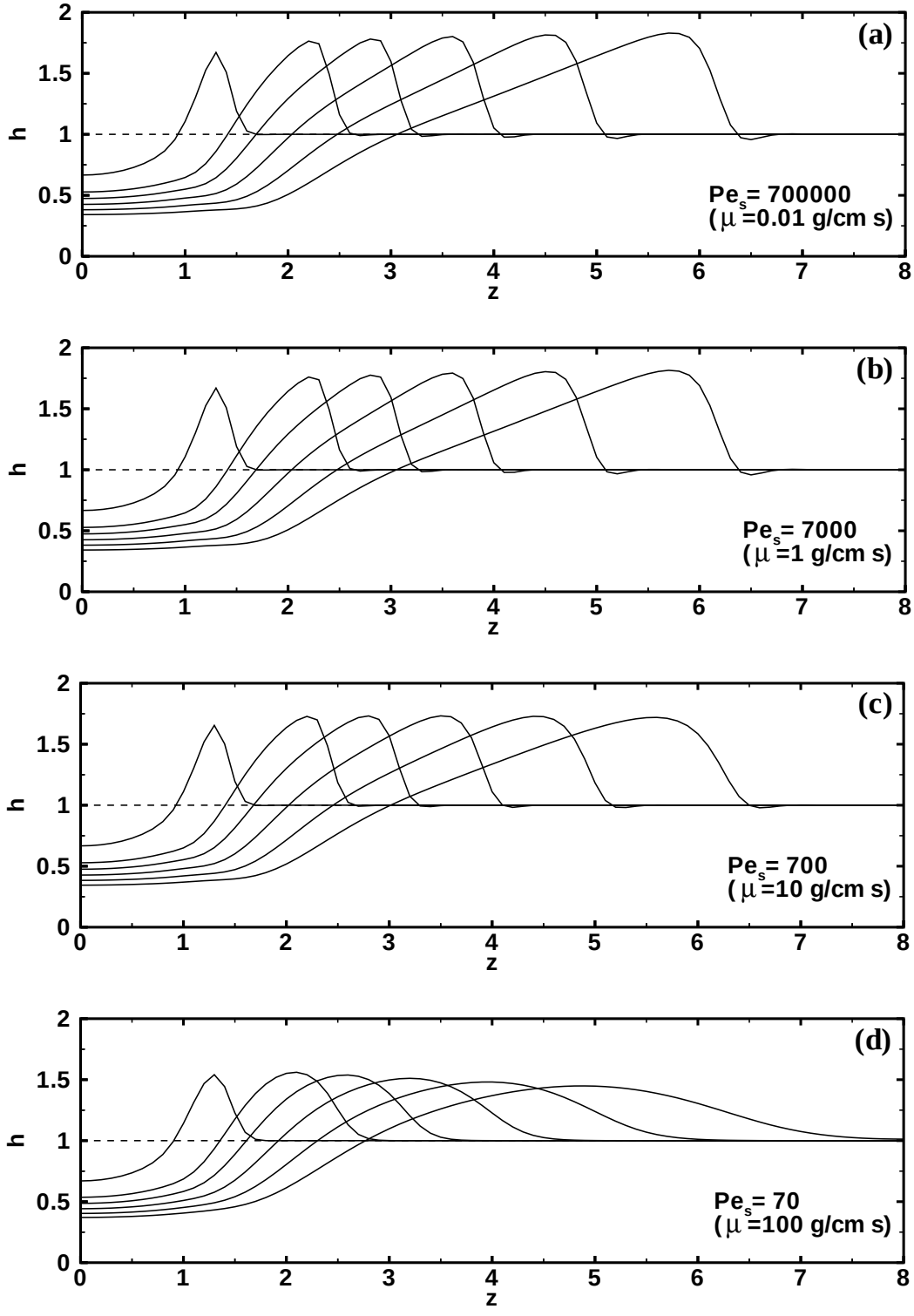

Figure 4.15: Time varying profiles of film thickness $h(z,t)$ for the film viscosity $\mu =$ (a) 0.01, (b) 1, (c) 10 and (d) 100 g/cm s, at time $t = 0$ (dashed line), 1, 5, 10, 20, 40 and 80. Parameter values are $\epsilon = 0.01$, $\Gamma_{exo} = 1$, $\Gamma_{pre} = 0$, $\tau_{air} = 0$ and $\mathcal{G}_r = \mathcal{G}_z = 0$.

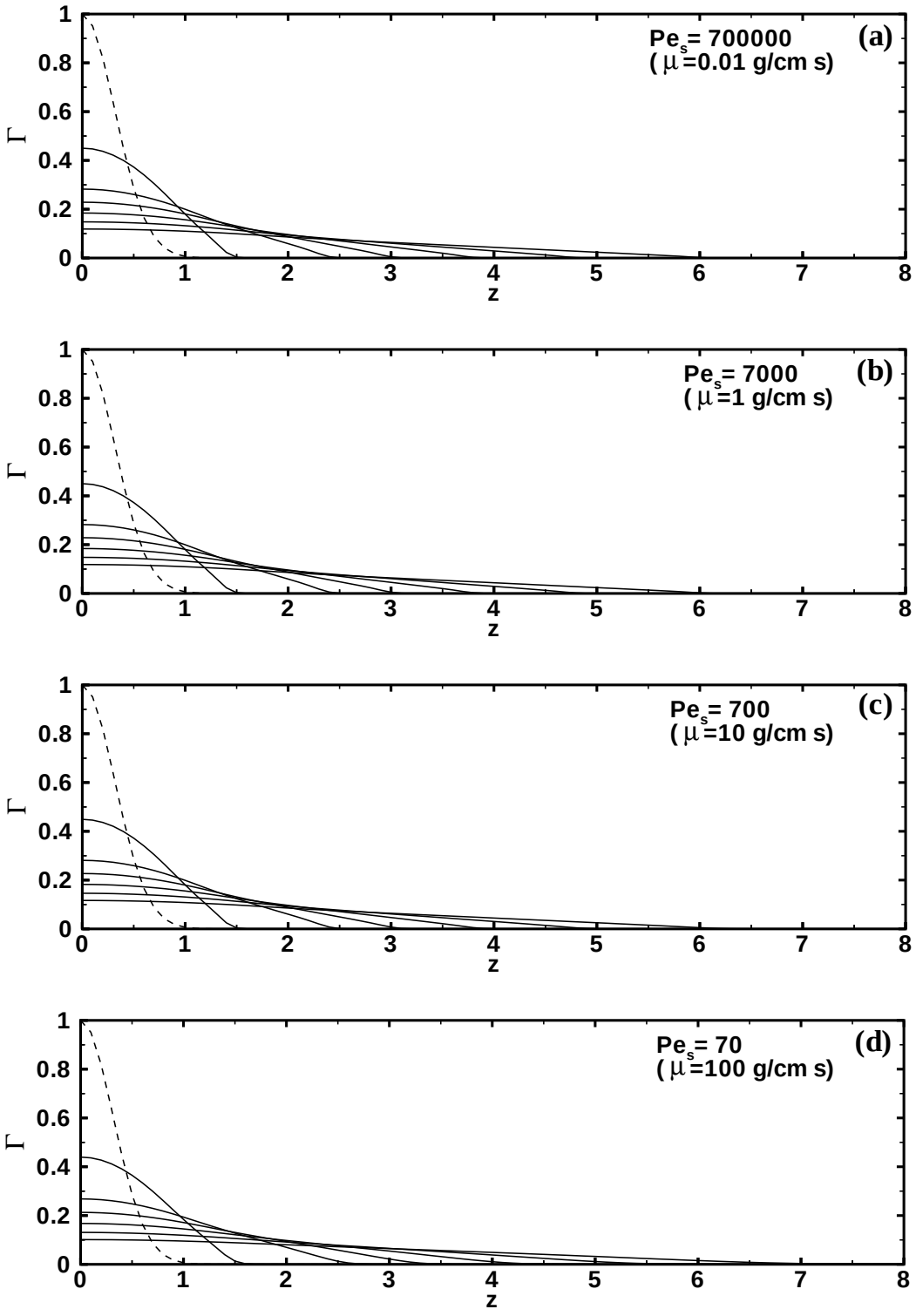

Figure 4.16: Time varying profiles of surface surfactant concentration $\Gamma(z,t)$ for the film viscosity μ = (a) 0.01, (b) 1, (c) 10 and (d) 100 g/cm s, at time $t = 0$ (dashed line), 1, 5, 10, 20, 40 and 80. Parameter values are $\epsilon = 0.01$, $\Gamma_{exo} = 1$, $\Gamma_{pre} = 0$, $\tau_{air} = 0$ and $\mathcal{G}_r = \mathcal{G}_z = 0$.

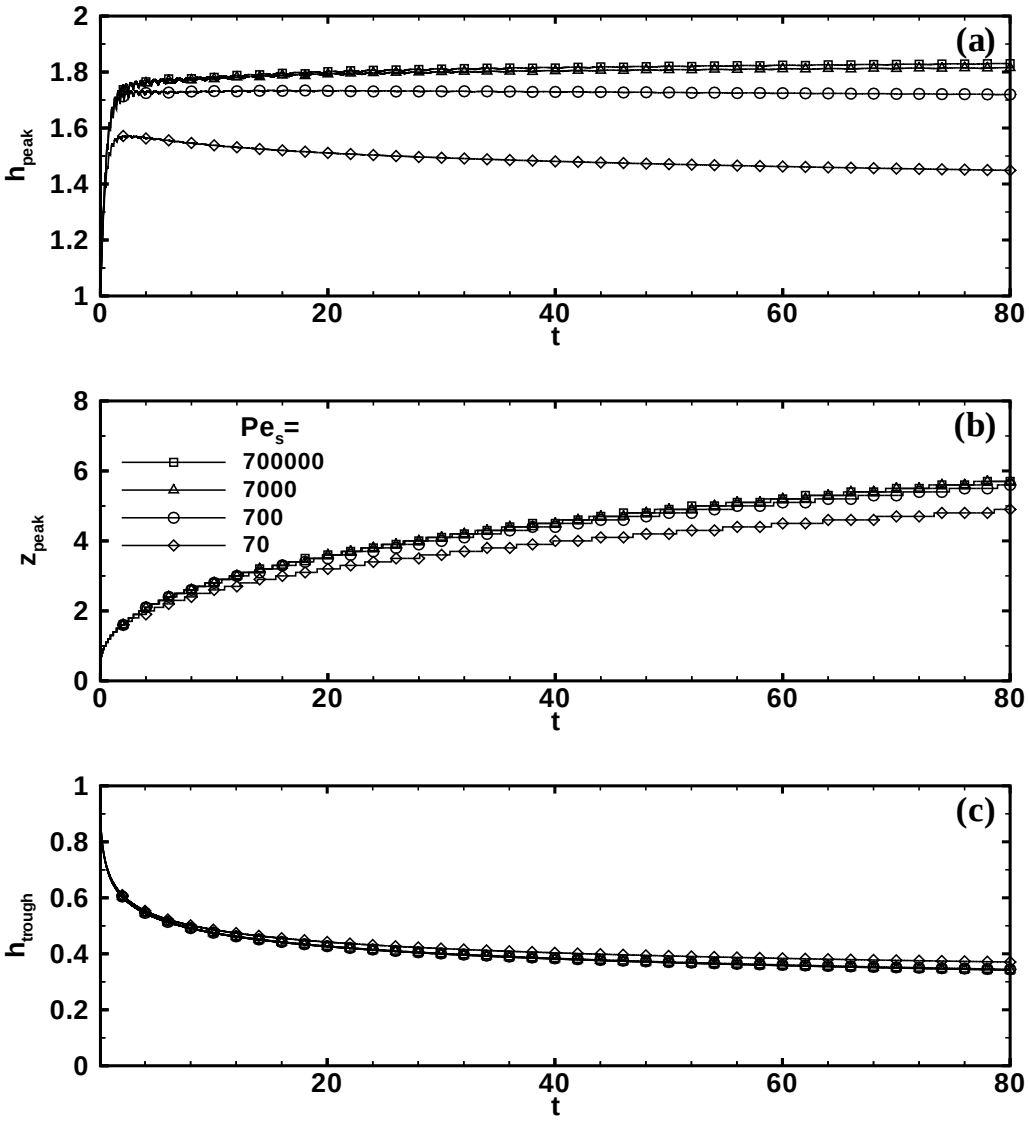

Figure 4.17: Temporal evolutions of (a) the peak film thickness, h_{peak}, (b) the axial position of peak film thickness, z_{peak}, and (c) the trough film thickness, h_{trough}, for various film viscosities $\mu = 0.01$, 1, 10 and 100 g/cm s.

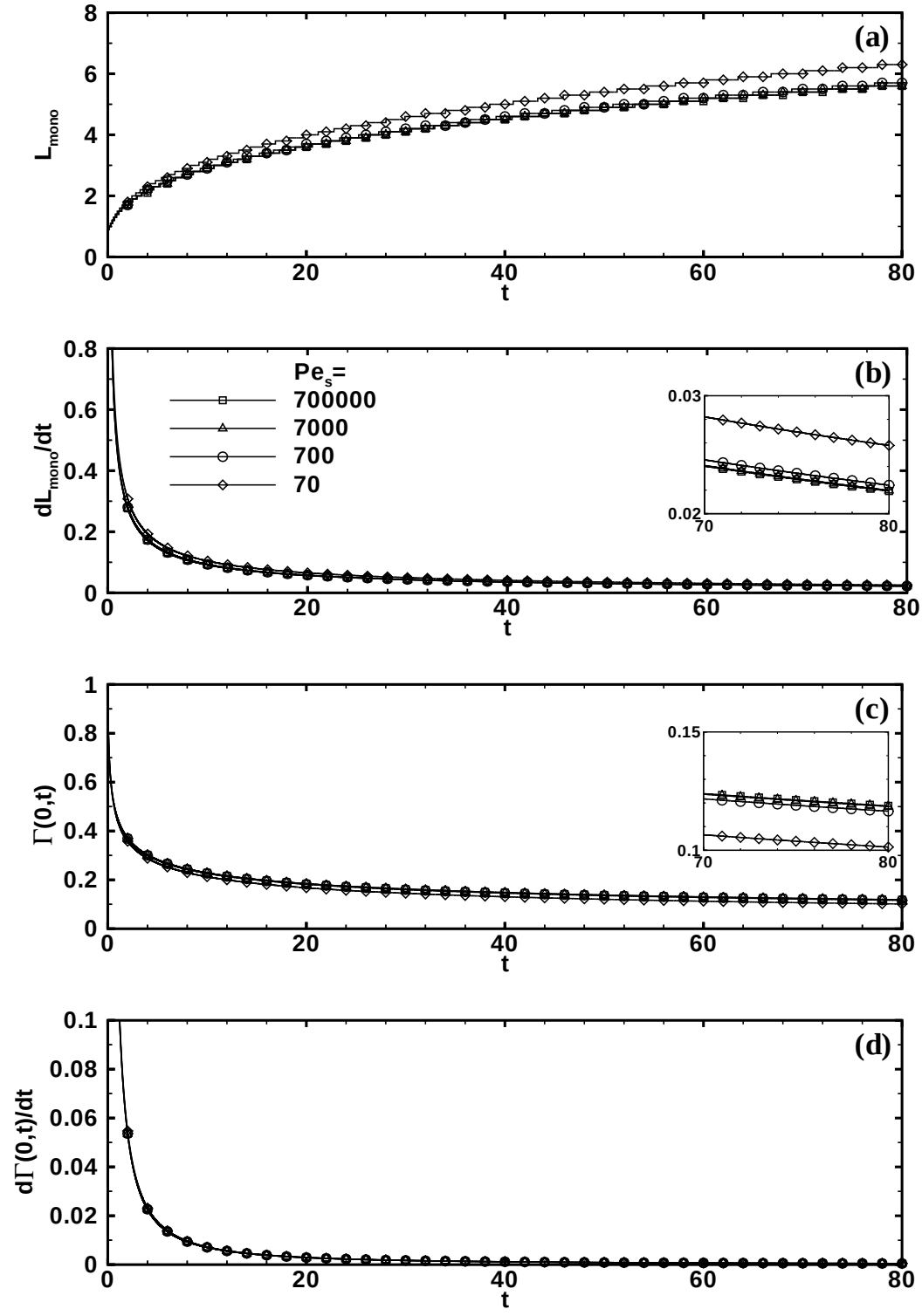

Figure 4.18: Temporal evolutions of (a) the length of surfactant monolayer, L_{mono}, (b) the spreading velocity of surfactant monolayer, $\mathrm{d}L_{mono}/\mathrm{d}t$, (c) the surfactant concentration at $z = 0$, $\Gamma(0, t)$, and (d) the dropping rate, $\mathrm{d}\Gamma(0, t)/\mathrm{d}t$, for various film viscosities $\mu = 0.01$, 1, 10 and 100 g/cm s.

4.5 Effect of the Air-Flow Induced Shear Stress

For the common procedure of SRT, the infant is ventilated for a short period of time after the injection of each surfactant dose to promote the spreading of surfactant. The main purpose of the air ventilation is to push forward the liquid plug occluding the large airway. However, the air ventilation also generates shear stress on the film surface in airways, which may possibly affect the spreading of surfactant induced by Marangoni effect. To examine the influences of the air ventilation on the surfactant transport, the shear stress due to air flow is also considered in the model. The air-flow shear stress is estimated following Espinosa & Kamm [1999], and the detailed derivation is presented in Appendix C. The nondimensional time varying air volume into the lung $V(t)$ (discarding the tilde) is prescribed according to

$$V(t) = \begin{cases} -V_T \cos\left(\dfrac{2\pi t}{2\tau_0 f}\right) & \text{for inspiration} \\ V_T \cos\left[\dfrac{2\pi t}{2\tau_0(1-f)}\right] & \text{for expiration,} \end{cases} \tag{4.1}$$

where $2V_T$ is the nondimensional tidal volume, τ_0 is the nondimensional time for one breath, and f is the fraction of τ_0 for inspiration. For example, $f = 0.5$ provides a symmetric breathing cycle, whereas $f = 0.25$ gives an asymmetric cycle with shorter inspiration and produces a higher forward shear stress. The air flux in the airway is given by $\mathrm{d}V(t)/\mathrm{d}t$. A schematic of an asymmetric breathing cycle is illustrated in Figure 4.19 with the breathing period τ_0, the tidal volume V_T and the inspiration fraction $f = 0.25$. The local shear stress due to air flow exerted on the airway lining at generation n is given as (see Appendix C)

$$\tau_{air}(t) = \frac{4\mu_a h_0}{\pi \mu R 2^n} \frac{\mathrm{d}V(t)}{\mathrm{d}t} \begin{cases} 1 & \text{for } \mathcal{R}e_a < 50 \\ (0.566 + 0.06\mathcal{R}e_a^{1/2}) & \text{for } \mathcal{R}e_a > 50, \end{cases} \tag{4.2}$$

with the local Reynolds number of air

$$\mathcal{R}e_a = \frac{\rho_a \sigma_m h_0}{\pi \mu \mu_a 2^{n-1}} \frac{\mathrm{d}V(t)}{\mathrm{d}t},$$

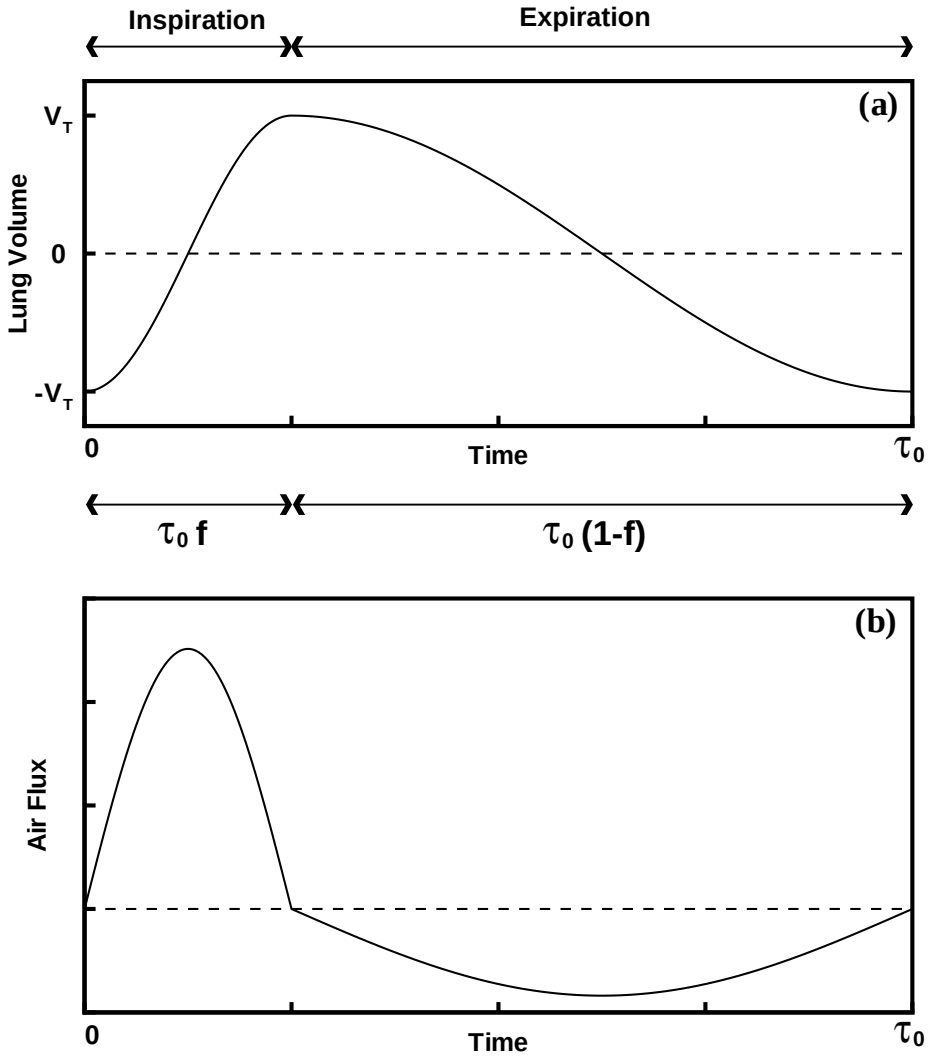

Figure 4.19: Schematic of an asymmetric breathing cycle with the inspiration fraction $f = 0.25$, the breathing period τ_0 and the tidal volume $2V_T$: (a) the time varying lung volume and (b) the air flux in the airway.

where $\mu_a = 1.2 \times 10^{-4}$ g/cm s and $\rho_a = 0.001$ g/cm^3 are the viscosity and density of saturated air. Therefore, the time varying shear stress $\tau_{air}(t)$ in generation-n airway during one-breath time τ_0 can be obtained form (4.1) and (4.2). The typical dimensional one-breath time for infants ranges from 1 to 2 s. For the airways considered in the present study, the characteristic time scale $\mathcal{T} \cong 1.43 \times 10^{-5}$ to 1.29×10^{-2} s, which results in the nondimensional one-breath time $\tau_0 \cong 10^2$ to 10^5. In the higher generation airways, the corresponding τ_0 is of the order larger than $O(10^3)$. This is much longer than the time for the surfactant front to reach the downstream end of the modeled airway. Thus, the air stress considered in the model is assumed to be constant and is taken as the maximum positive value during inspiration and the minimum negative value during expiration.

The typical clinical parameters for neonatal SRT are [Espinosa & Kamm, 1999; Cassidy *et al.*, 2001] : the dimensional tidal volume $2V_T \times R^3 \cong 6$ to 6.6 ml, the dimensional one-breath time $\tau_0 \times \mathcal{T} \cong 2$ s, and the fraction for inspiration $f \cong 0.25$ to 0.33, where R is the airway radius, and $\mathcal{T}$ is the dimensional characteristic time scale. We consider the air flow in four airway generations, $n = 1$, 5, 10 and 14, in the neonatal lung. The corresponding maximum forward shear stresses during inspiration estimated from equations (4.1) and (4.2) are approximately 8.77×10^{-4}, 5.96×10^{-4}, 1.10×10^{-4} and 2.76×10^{-5}. Similarly, the corresponding minimum backward shear stresses during expiration are approximately -2.13×10^{-4}, -1.89×10^{-4}, -3.68×10^{-5} and -9.21×10^{-6}. For the inspiration fraction $f = 0.25$, the air-flow induced forward shear stresses are higher than the backward shear stresses.

Because of the direction of the air flow, the symmetric condition at $z = 0$ is not applicable. Accordingly, for the simulation with the effect of air-flow induced surface stress, the computational domain is extended to $z = -8$ to 8, and only the result within the airway range $z = 0$ to 8 is considered. The simulation results of the film disturbance and the surfactant spreading are shown in Figures 4.20 and 4.21, where the solid line represents the simulation results without air-flow induced shear stress, the dash-dotted

line represents those with forward shear stress, and the dashed line represents those with backward shear stress. The forward/backward shear stress induced by air flow slightly improves/retards the film disturbed wave in the airway at generation 1 (Figure 4.20(a)). The effect of the air stress diminishes as the airway generation increases, and the film disturbance is virtually unaffected by the air stress in higher generation airways (Figures 4.20). As revealed in Figure 4.21, the surfactant spreading is also unchanged in airway at various generations.

In practice, the air-flow induced shear stress on the airway lining can be raised by increasing the tidal volume or by decreasing the one-breath time. We further examine the effect of the forward shear stress in the airway at generation 1 under the conditions of the tidal volume $2V_T \times R^3 = 0$, 6.6 and 12 ml with the fixed parameters $\tau_0 \times \mathcal{T} = 2$ s and $f = 0.25$. The corresponding nondimensional shear stresses are $\tau_{air} = 0$, 8.77×10^{-4} and 1.95×10^{-3}. The time varying profiles of the film thickness $h(z,t)$ and the surface concentration of surfactant $\Gamma(z,t)$ are plotted in Figure 4.22, where the solid line represents the condition of $2V_T \times R^3 = 0$ ml, the dashed line $2V_T \times R^3 = 6.6$ ml, and the dash-dotted line $2V_T \times R^3 = 12$ ml. As observed in Figures 4.22(a) and 4.23, the propagation of the film disturbance becomes slightly faster as the air-flow induced shear stress increases. With the tidal volume being increased to two times, the effect of the air stress on the surfactant spreading is still very minor (Figures 4.22(b) and 4.24). The influences on both the film disturbance and the surfactant spreading are not in accordance with the increasing rate of the air-flow shear stress.

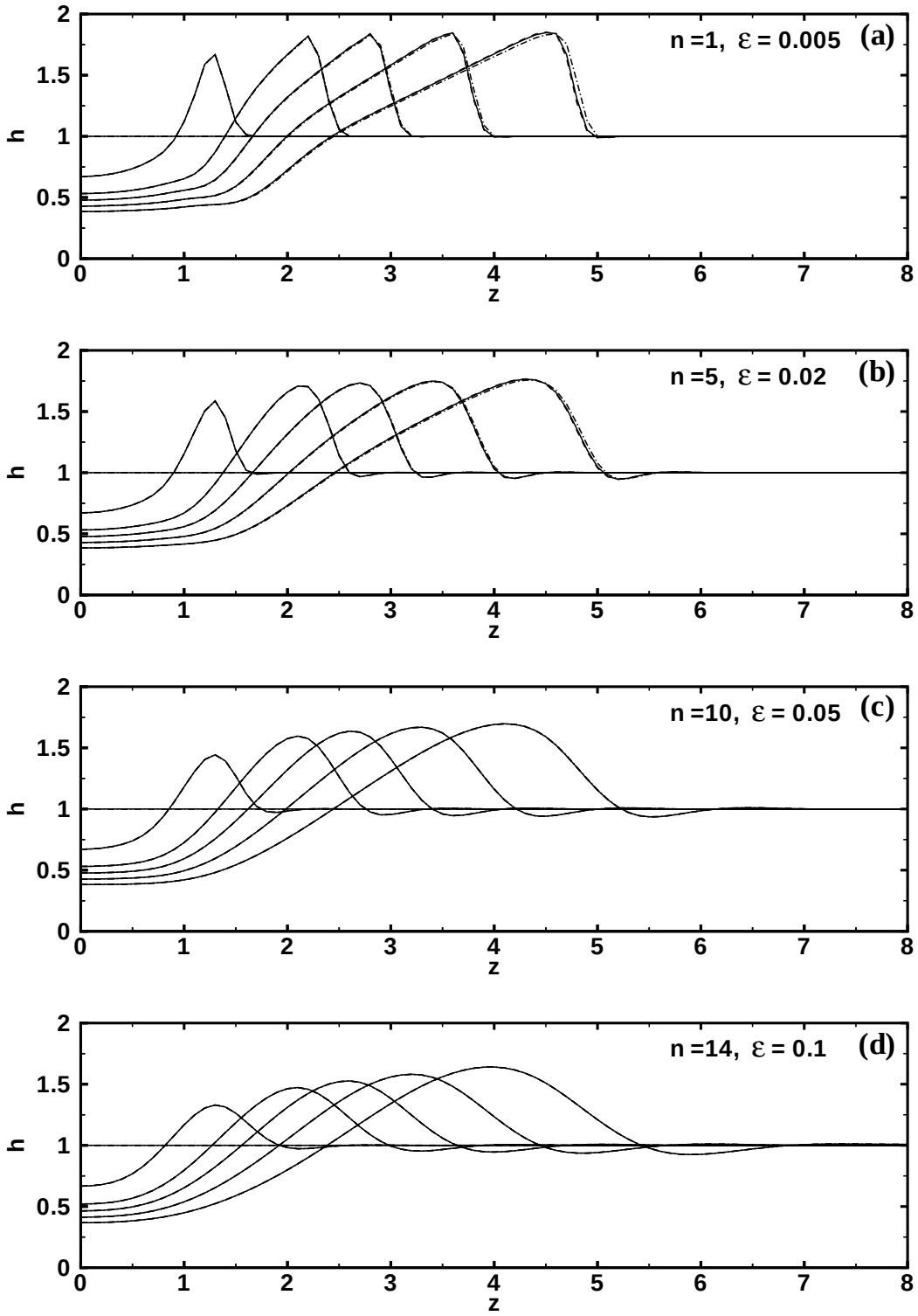

Figure 4.20: Time varying profiles of film thickness $h(z,t)$ with no shear stress (solid line) and considering forward shear stress (dash-dotted line) and backward shear stress (dashed line) in the airway at generation n = (a) 1, (b) 5, (c) 10 and (d) 14, at time t = 0, 1, 5, 10, 20 and 40. The dimensional parameters of the air flow are: $2V_T \times R^3 = 6.6$ ml, $\tau_0 \times \mathcal{T} = 2$ s and $f = 0.25$. Other parameter values are fixed as $\Gamma_{exo} = 1$, $\Gamma_{pre} = 0$, $\mu = 100$ g/cm s and $\mathcal{G}_r = \mathcal{G}_z = 0$.

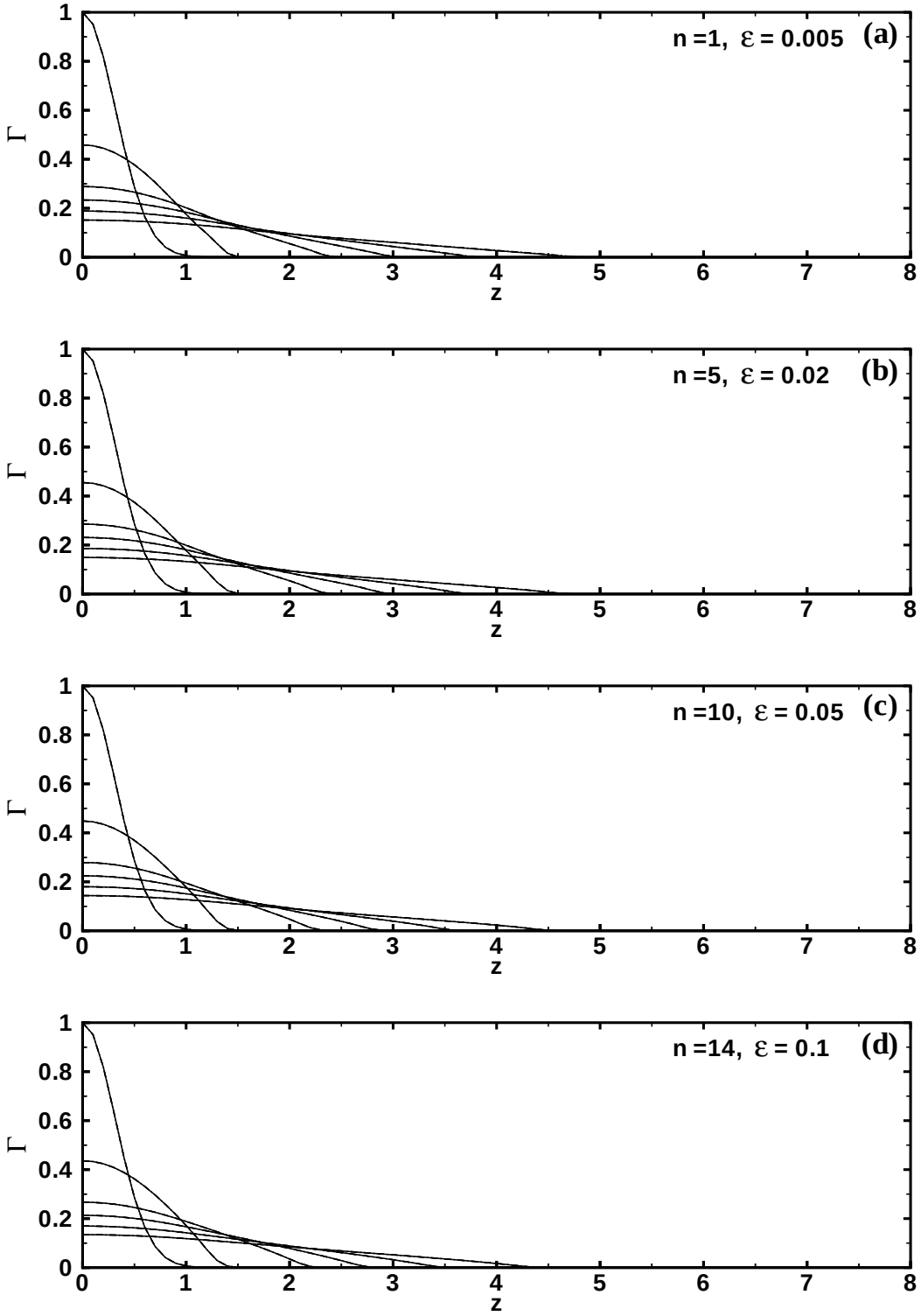

Figure 4.21: Time varying profiles of surface surfactant concentration $\Gamma(z,t)$ with no shear stress (solid line) and considering forward shear stress (dash-dotted line) and backward shear stress (dashed line) in the airway at generation n = (a) 1, (b) 5, (c) 10 and (d) 14, at time t = 0, 1, 5, 10, 20 and 40. The dimensional parameters of the air flow are: $2V_T \times R^3$ = 6.6 ml, $\tau_0 \times \mathcal{T}$ = 2 s and f = 0.25. Other parameter values are fixed as $\Gamma_{exo} = 1$, $\Gamma_{pre} = 0$, $\mu = 100$ g/cm s and $\mathcal{G}_r = \mathcal{G}_z = 0$.

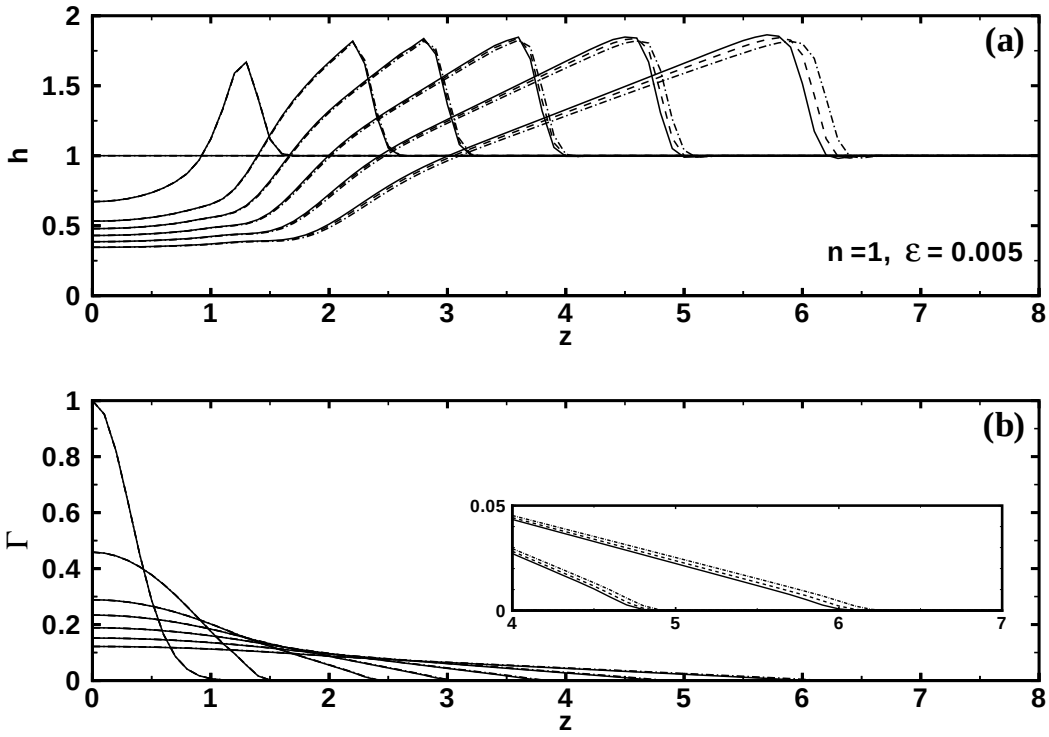

Figure 4.22: Time varying profiles of (a) film thickness $h(z,t)$ and (b) surface surfactant concentration $\Gamma(z,t)$ considering forward shear stress with the tidal volume $2V_T \times R^3$ (ml) = 0 (solid line), 6.6 (dashed line) and 12 (dash-dotted line), and $\tau_0 \times \mathcal{T} = 2$ s, $f = 0.25$ in generation 1 airway, at time $t = 0$, 1, 5, 10, 20, 40 and 80. Other parameter values are fixed as $\Gamma_{exo} = 1$, $\Gamma_{pre} = 0$, $\mu = 100$ g/cm s and $\mathcal{G}_r = \mathcal{G}_z = 0$.

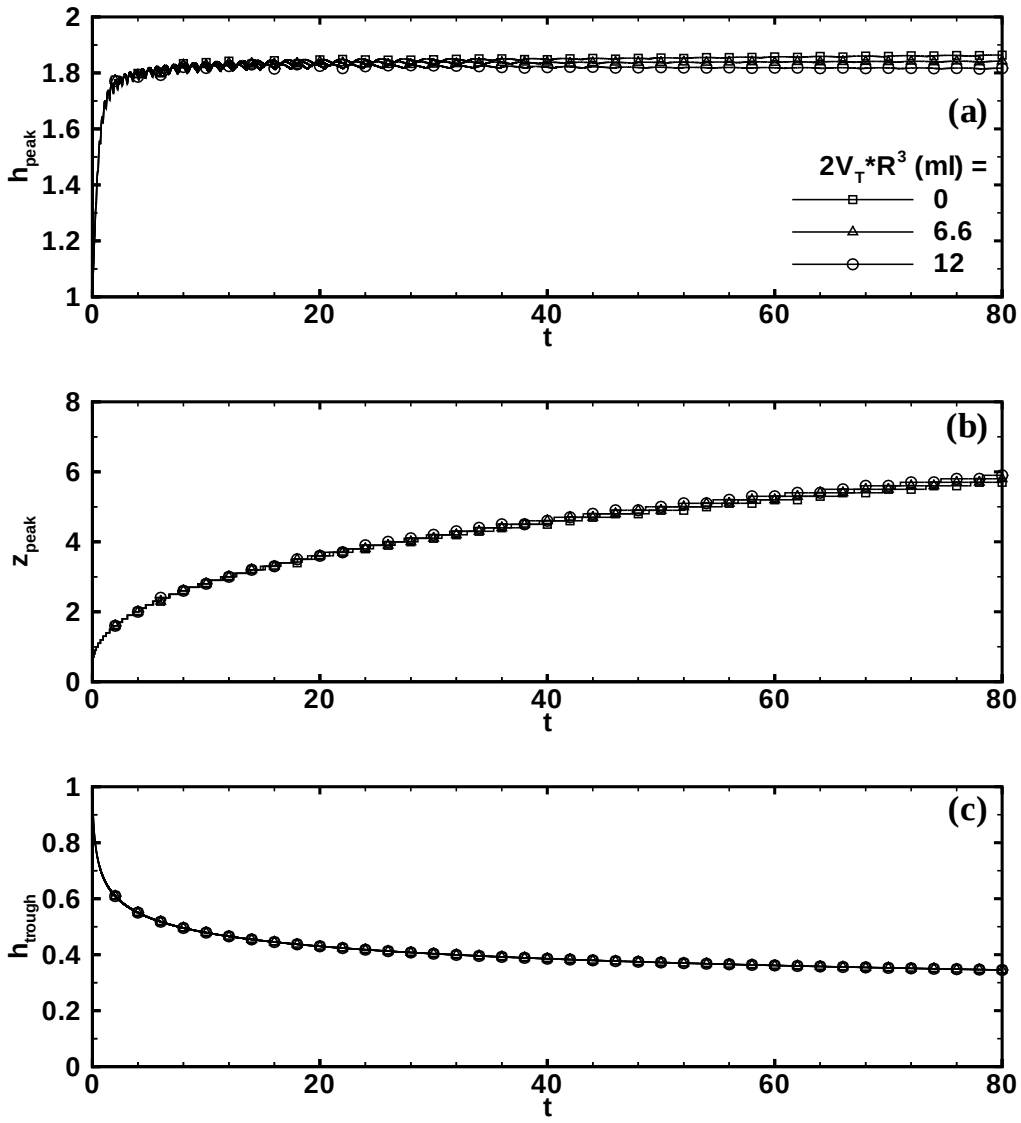

Figure 4.23: Temporal evolutions of (a) the peak film thickness, h_{peak}, (b) the axial position of peak film thickness, z_{peak}, and (c) the trough film thickness, h_{trough}, for various shear stresses with the tidal volume $2V_T \times R^3 = 0$, 6.6 and 12 ml.

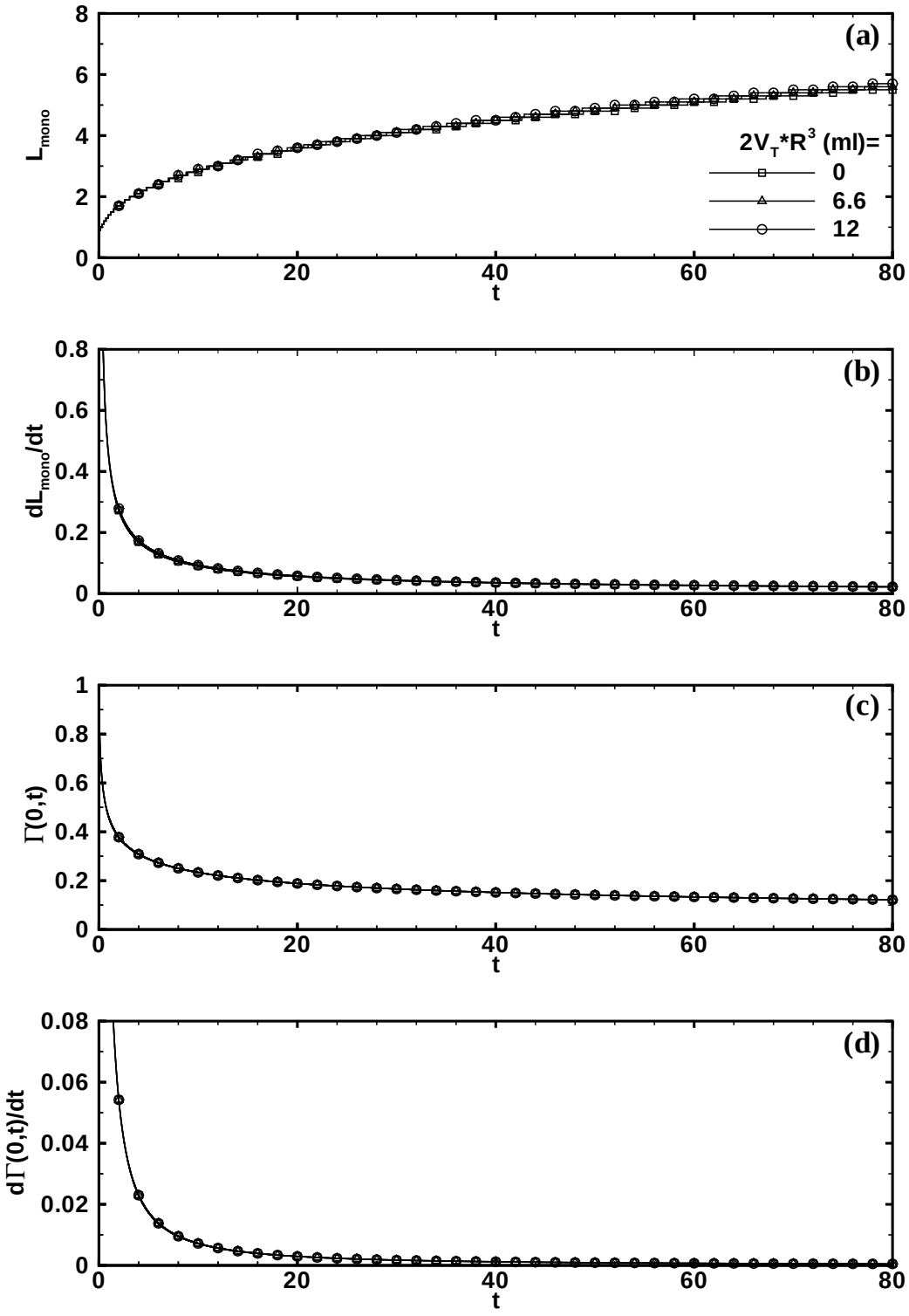

Figure 4.24: Temporal evolutions of (a) the length of surfactant monolayer, L_{mono}, (b) the spreading velocity of surfactant monolayer, $\mathrm{d}L_{mono}/\mathrm{d}t$, (c) the surfactant concentration at $z = 0.0$, $\Gamma(0,t)$, and (d) the dropping rate, $\mathrm{d}\Gamma(0,t)/\mathrm{d}t$, for various shear stresses with the tidal volume $2V_T \times R^3 = 0$, 6.6 and 12 ml.

4.6 Effect of the Surfactant Solubility

When the surfactant is soluble, the transition between the surface and bulk surfactants is governed by the sorption kinetics. A nonlinear sorption kinetics (2.46) is adapted in our model. For soluble surfactant, additional properties of relevance are the bulk Péclet number $\mathcal{P}e_b$, the equilibrium ratio between surface and bulk concentrations $\mathcal{K}$, the rato between diffusion and adsorption rates $\mathcal{J}$ and the nonlinearity of sorption kinetics β. In order to conform with the assumption in cross-sectional averaging, $\mathcal{P}e_b\epsilon^2 \ll 1$, the viscosity of thin film is chosen as $\mu = 100$ g/cm s in the following simulations. Thus, the corresponding bulk Péclet number is $\mathcal{P}e_b = 700$ and the surface Péclet number $\mathcal{P}e_s = 70$. Other parameters are fixed and chosen as $\epsilon = 0.01$, $\Gamma_{exo} = 1$, $\Gamma_{pre} = 0$, $\tau_{air} = 0$ and $\mathcal{G}_r = \mathcal{G}_z = 0$.

4.6.1 Effect of the diffusion-adsorption ratio

The diffusion-adsorption ratio $\mathcal{J}$ is a crucial property of surfactant transport in determining the kinetic resistance against adsorption/desorption to/from the surface. For small $\mathcal{J}$, the sorption kinetics is diffusion-controlled and the kinetic resistance is low and remains constant. For large $\mathcal{J}$, the resistance against adsorption increases linearly with $\mathcal{J}$ and the sorption kinetics are adsorption-controlled. In order to isolate the influence of diffusion-adsorption ratio $\mathcal{J}$ on the spreading of surfactant, we fix the equilibrium ratio $\mathcal{K} = 1$, representing that the desorption and adsorption rates are equal. A linear sorption kinetics is adopted ($\beta \to \infty$). Figures 4.25, 4.26 and 4.27 show the evolutions of the film disturbance and the surface and bulk surfactant concentrations for $\mathcal{J} = 0.01$, 1 and 100, which correspond to diffusion-controlled, dynamic (neither diffusion nor adsorption controlled) and adsorption-controlled kinetics, respectively. For $\mathcal{J} = 100$, the kinetic resistance is large enough such that the sorption rate is slow for surfactant transition to/from the bulk/surface. Therefore, little amount of surfactant is desorbed from the surface to the bulk, and the bulk surfactant concentration remains to be low in comparison with the

surface concentration (Figure 4.27(a)). The transport of surface surfactant is virtually independent of the bulk surfactant for large $\mathcal{J}$. The film disturbance (Figure 4.25(a)) is similar to that of insoluble surfactant (Figure 4.15(d)). As $\mathcal{J}$ decreases, the resistance against the sorption process also reduces. For low kinetic resistance ($\mathcal{J} = 0.01$), the surface surfactant is quickly desorbed and then diffuses to the bulk-phase. The same process happens in the opposite direction, in which the bulk surfactant quickly diffuses to the surface where it is adsorbed. Such a adsorption/desorption process diminishes the Marangoni effect and consequently decreases the gradient of surfactant surface concentration.

Figures 4.28(a) and (b) show the time varying profiles of the bulk and surface concentrations at the upstream end of airway, $\bar{C}(0,t)$ and $\Gamma(0,t)$, respectively. For $\mathcal{J} = 0.01$ (rapid sorption), $\bar{C}(0,t)$ immediately raises to the maximum value and then decreases with $\Gamma(0,t)$ at the same rate. For $\mathcal{J} = 1$ (slow sorption), the $\bar{C}(0,t)$ increases gradually and reaches the maximum value at approximately $t = 5$, after which the bulk and surface concentrations are in instantaneous equilibrium state. For $\mathcal{J} = 100$, the kinetic resistance is so large that the surfactant desorption rate is small and $\bar{C}(0,t)$ increases slowly. Incidentally, Figure 4.28(c) demonstrates that the sorption kinetics slows the spreading rate of surfactant monolayer.

Inspections of the film thickness for these three values of $\mathcal{J}$, plotted in Figure 4.29, show temporal evolutions of both the film peak thickness h_{peak} and its axial position z_{peak}. After the bulk and surface distributions are in instantaneous equilibrium, the dissolved bulk surfactant has an increasing influence on the film deformation. For lower value of $\mathcal{J}$, the width of the shock is narrower (see Figure 4.25(c)) and the film peak thickness h_{peak} develops to higher than two times of the undisturbed film thickness (Figure 4.29(a)). The propagation of the film disturbed wave, however, is retarded by the sorption kinetics as observed in Figure 4.29(b). Jensen & Grotberg [1993] demonstrated that the advection of dissolved surfactant appears to cause fluid to be driven into this shock from its upstream end, and this "squeezing" process enhances film elevations.

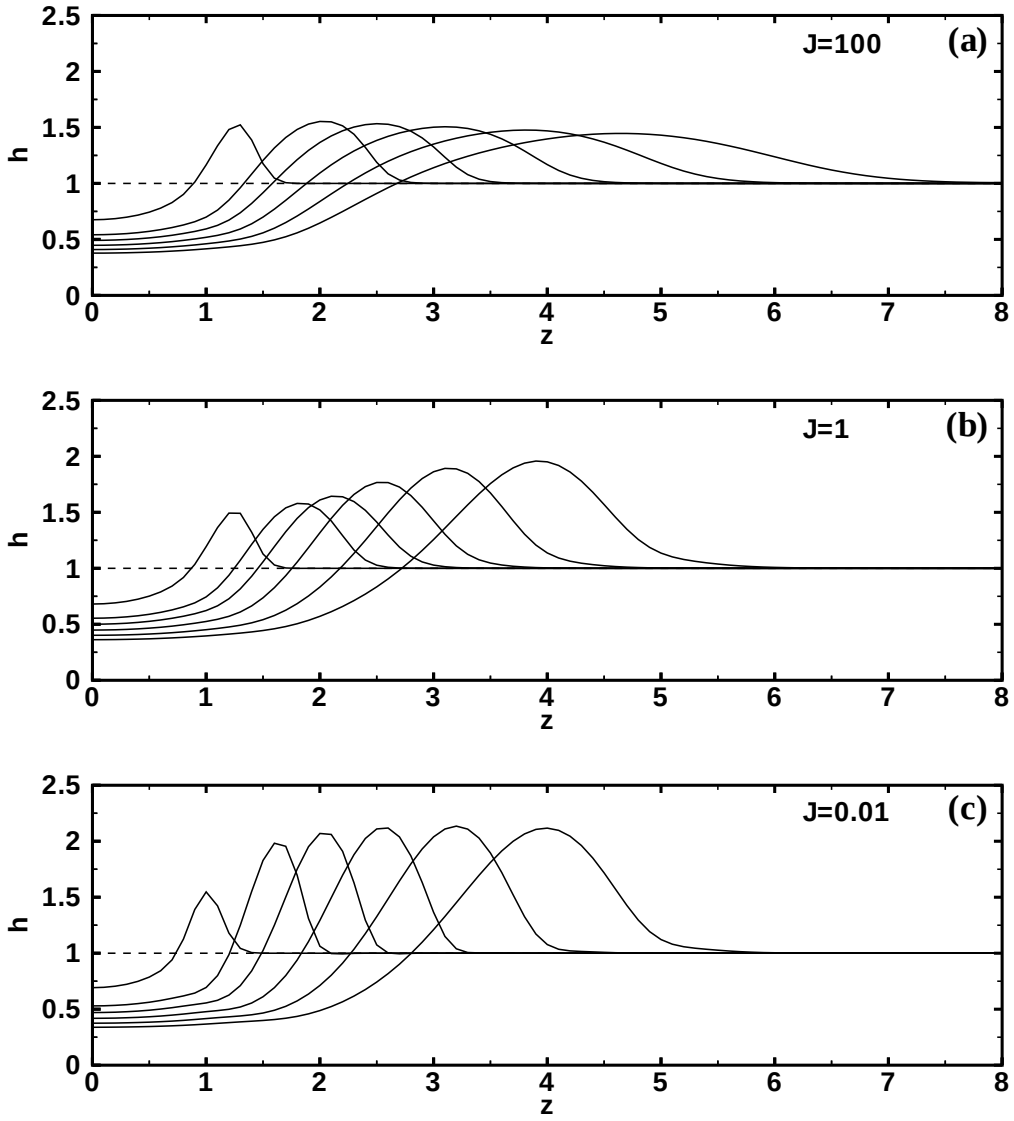

Figure 4.25: Time varying profiles of film thickness $h(z,t)$ for the diffusion-adsorption ratio $\mathcal{J}$ = (a) 100, (b) 1 and (c) 0.01, illustrated at times $t = 0$ (dashed line), 1, 5, 10, 20, 40, 80. Other parameter values are fixed and chosen as $\beta \to \infty$, $\mathcal{K} = 1$, $\Gamma_{exo} = 1$, $\Gamma_{pre} = 0$, $\mu = 100$ g/cm s, $\tau_{air} = 0$ and $\mathcal{G}_r = \mathcal{G}_z = 0$.

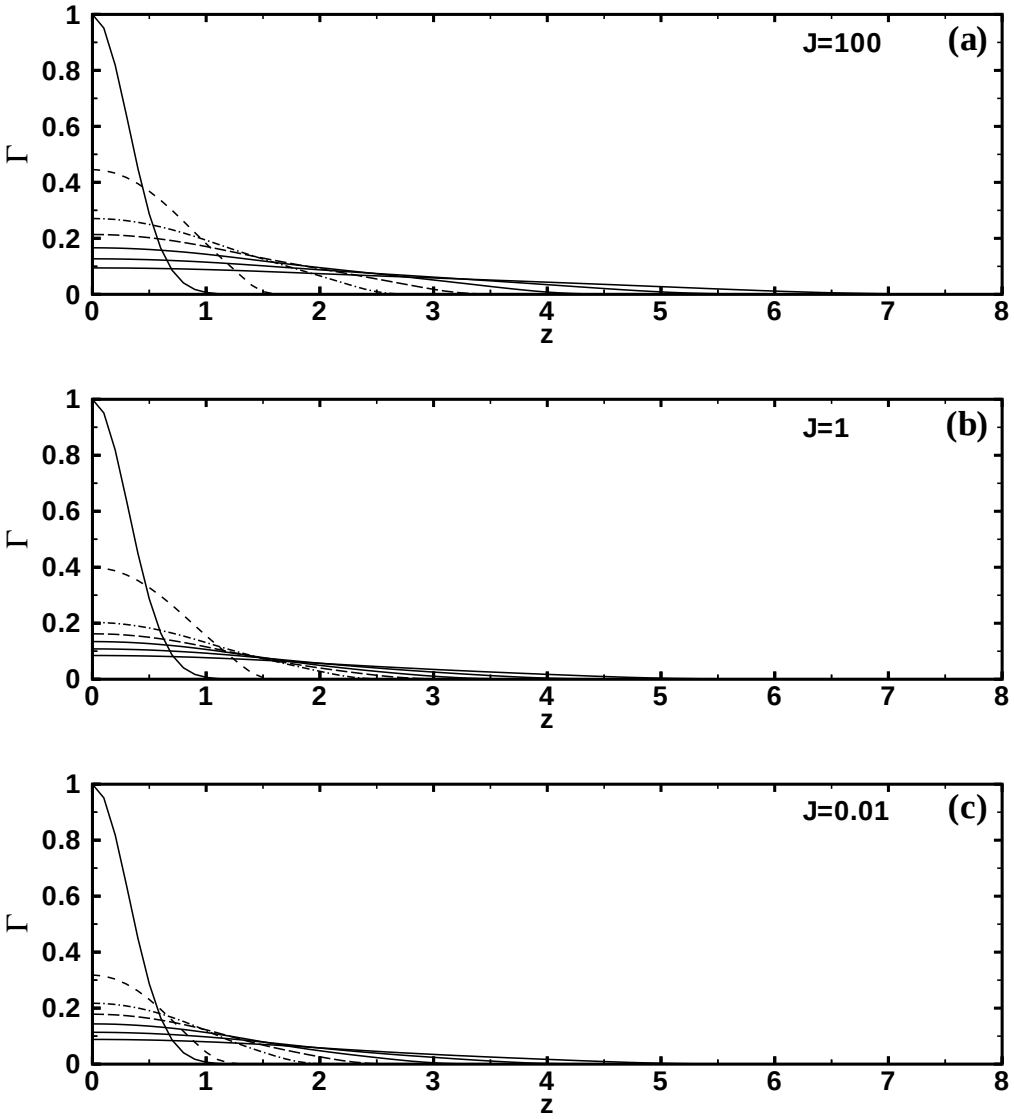

Figure 4.26: Time varying profiles of surface surfactant concentration $\Gamma(z,t)$ for the diffusion-adsorption ratio $\mathcal{J}$ = (a) 100, (b) 1 and (c) 0.01, illustrated at times $t = 0$, 1 (dashed), 5 (dash-dotted), 10 (long-dashed line), 20, 40, 80. Other parameter values are fixed and chosen as $\beta \to \infty$, $\mathcal{K} = 1$, $\Gamma_{exo} = 1$, $\Gamma_{pre} = 0$, $\mu = 100$ g/cm s, $\tau_{air} = 0$ and $\mathcal{G}_r = \mathcal{G}_z = 0$.

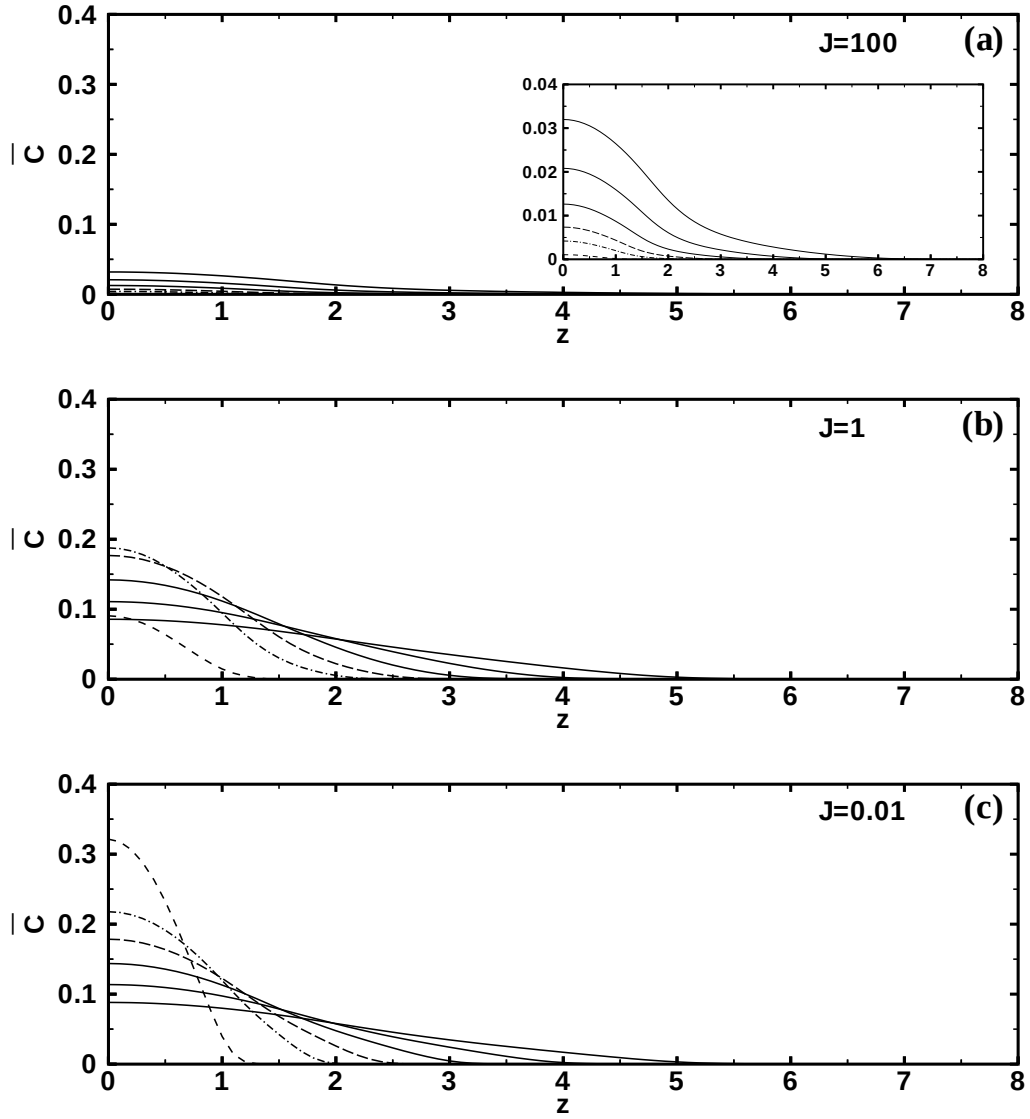

Figure 4.27: Time varying profiles of bulk surfactant concentration $\bar{C}(z,t)$ for the diffusion-adsorption ratio $\mathcal{J}$ = (a) 100, (b) 1 and (c) 0.01, illustrated at times $t = 0$, 1 (dashed), 5 (dash-dotted), 10 (long-dashed line), 20, 40, 80. Other parameter values are fixed and chosen as $\beta \to \infty$, $\mathcal{K} = 1$, $\Gamma_{exo} = 1$, $\Gamma_{pre} = 0$, $\mu = 100$ g/cm s, $\tau_{air} = 0$ and $\mathcal{G}_r = \mathcal{G}_z = 0$.

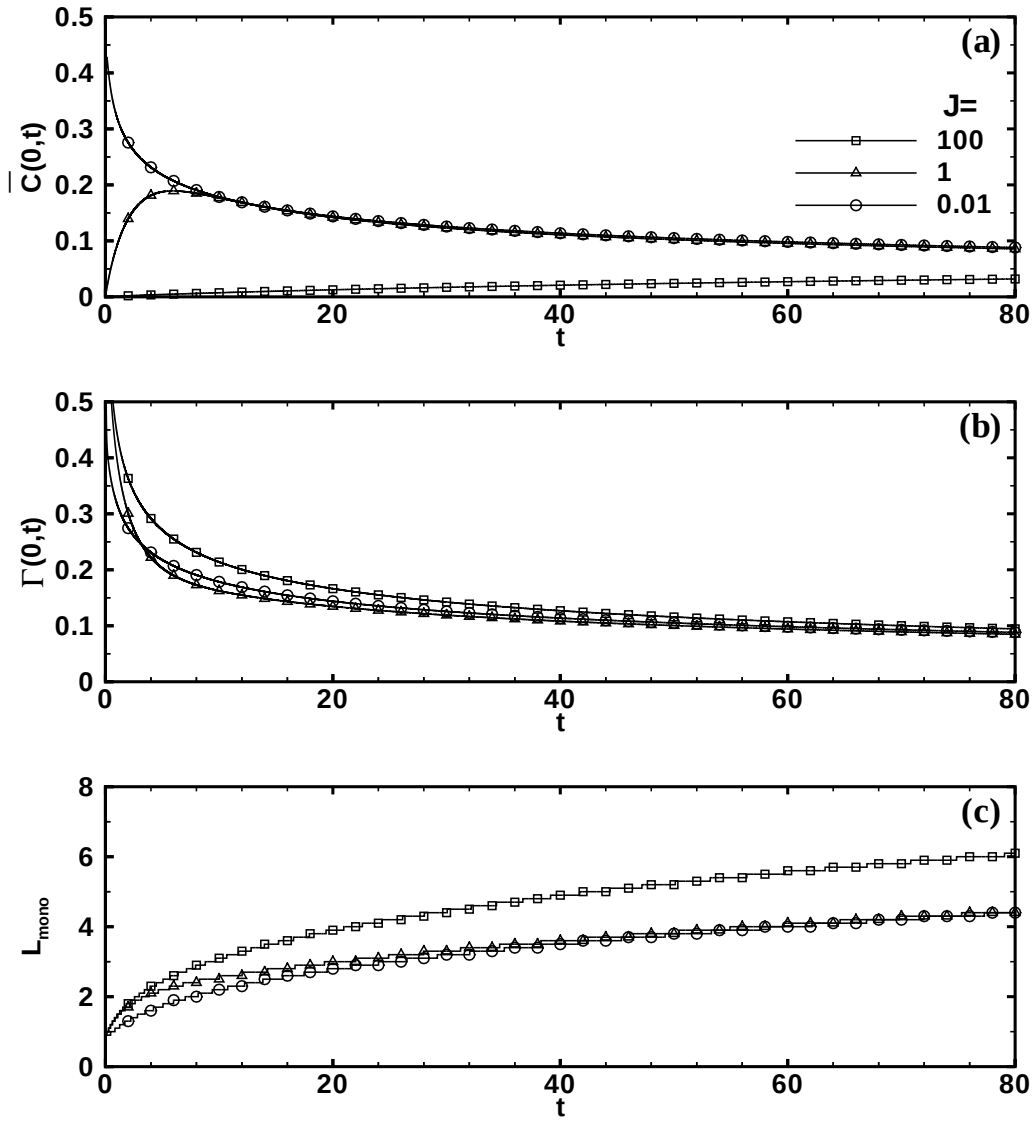

Figure 4.28: Temporal evolutions of (a) the bulk surfactant concentration at $z = 0$, $\bar{C}(0,t)$, (b) the surface surfactant concentration at $z = 0$, $\Gamma(0,t)$, and (c) the monolayer length, L_{mono}, for $\mathcal{J} = 100$, 1 and 0.01.

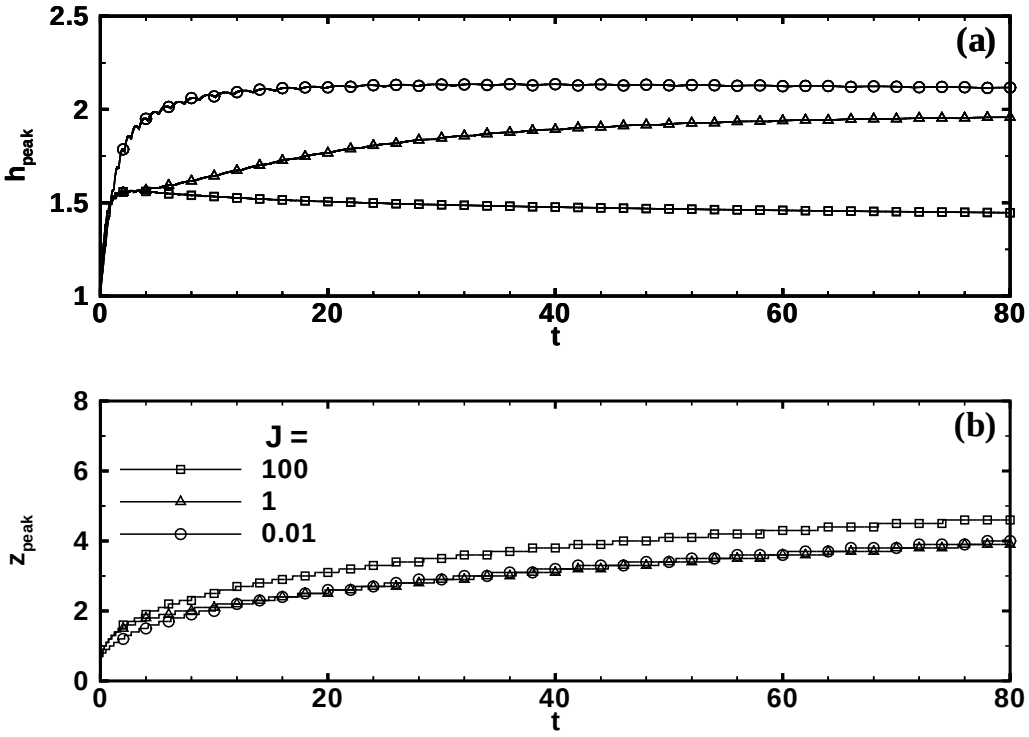

Figure 4.29: Temporal evolutions of (a) the peak film thickness, h_{peak}, and (b) the axial position of peak film thickness, z_{peak}, for $\mathcal{J} = 100$, 1 and 0.01.

4.6.2 Effect of the kinetic nonlinearity

All the simulations we have discussed so far for soluble surfactant are based on the linear sorption kinetics and the linear equation of state ($\beta \to \infty$). Here, we fix the diffusion-adsorption ratio and the equilibrium ratio, such that $\mathcal{J} = \mathcal{K} = 1$, and vary β, thus examine the effect of sorption kinetic nonlinearity. Four values of the nonlinearity of sorption kinetics $\beta = \infty$ (linear sorption), 5, 1 and 0.5, are considered. The corresponding relationships between the average bulk concentration $\bar{C}$ and the surface concentration Γ based on the nonlinear (Langmuir) isotherm (2.48) are illustrated in Figure 4.30. For the nonlinear sorption kinetics, the dependence of surface tension σ on surface concentration Γ also becomes nonlinear according to the Gibbs' equation. In Figure 4.31, we also show the variations of surface tension σ as a function of surface concentration Γ according to the nonlinear equation of state (2.32) for different values of β. For all values of β, the nondimensional surface tension is unit for vanishing surface concentration $\Gamma \to 0$. For linear sorption kinetics ($\beta \to \infty$), the reduction rate of surface tension remains constant for varying surface concentration. In contrast, for nonlinear equation of state, the surface tension σ decreases exponentially with increasing surface concentration Γ as the sorption kinetics become nonlinear. This means that, for nonlinear kinetics, the reduction rate of surface tension increases with the raising surfactant surface concentration. However, for the value of β less than 0.5, the surface tension decreases to a negative value as the surface concentration $\Gamma \to 1$, which violates the physical mechanism. Therefore, the value of β must be chosen higher than 0.5 in this model.

Figures 4.32, 4.33, 4.34 and 4.35 depict the effects of nonlinear sorption kinetics and equation of state on the evolutions of the film deformation, the surface and averaged-bulk concentrations, and the induced surface tension. As revealed in Figure 4.33, the evolution of the surface concentration Γ is independent on the values of β. However, for high nonlinearity of sorption kinetics (i.e. small β), the averaged bulk concentration $\bar{C}$ desorbed from the film surface decreases (Figure 4.34(d)). The elevated film height attributed

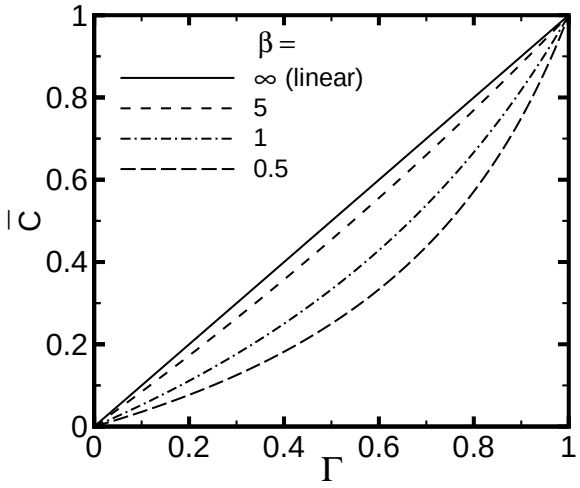

Figure 4.30: The equilibrium relation between the average bulk concentration $\bar{C}$ and the surface concentration Γ, based on the nonlinear (Langmuir) isotherm (2.48) for varying kinetic nonlinearity β.

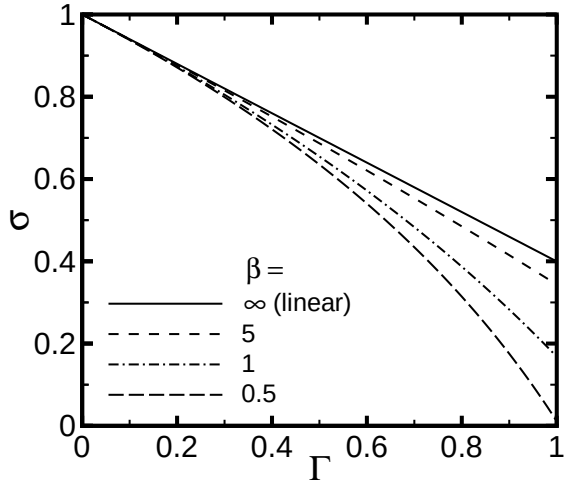

Figure 4.31: Surface tension σ as a function of surface concentration Γ for varying kinetic nonlinearity β according to the nondimensional nonlinear equation of state (2.32), and the Marangoni number $\mathcal{M}a = 0.6$.

to squeezing process induced by the advection of the bulk-phase surfactant [Jensen & Grotberg, 1993] is also reduced (Figure 4.32). As shown in temporal evolution of the peak film thickness h_{peak} (Figure 4.36(a)), the squeezing process diminishes with increasing sorption kinetics nonlinearity (i.e. decreasing β). In addition, for high nonlinearity of equation of state (i.e. small value of β), the induced surface-tension variation is larger in comparison with that using linear equation of state (Figure 4.35). As a result, the Marangoni effect is also more significant for nonlinear sorption kinetics. In conclusion, the nonlinearity of sorption kinetics increase the resistance against the adsorption/desorption and diminish the impact of surfactant solubility on delaying the spreading of monolayer.

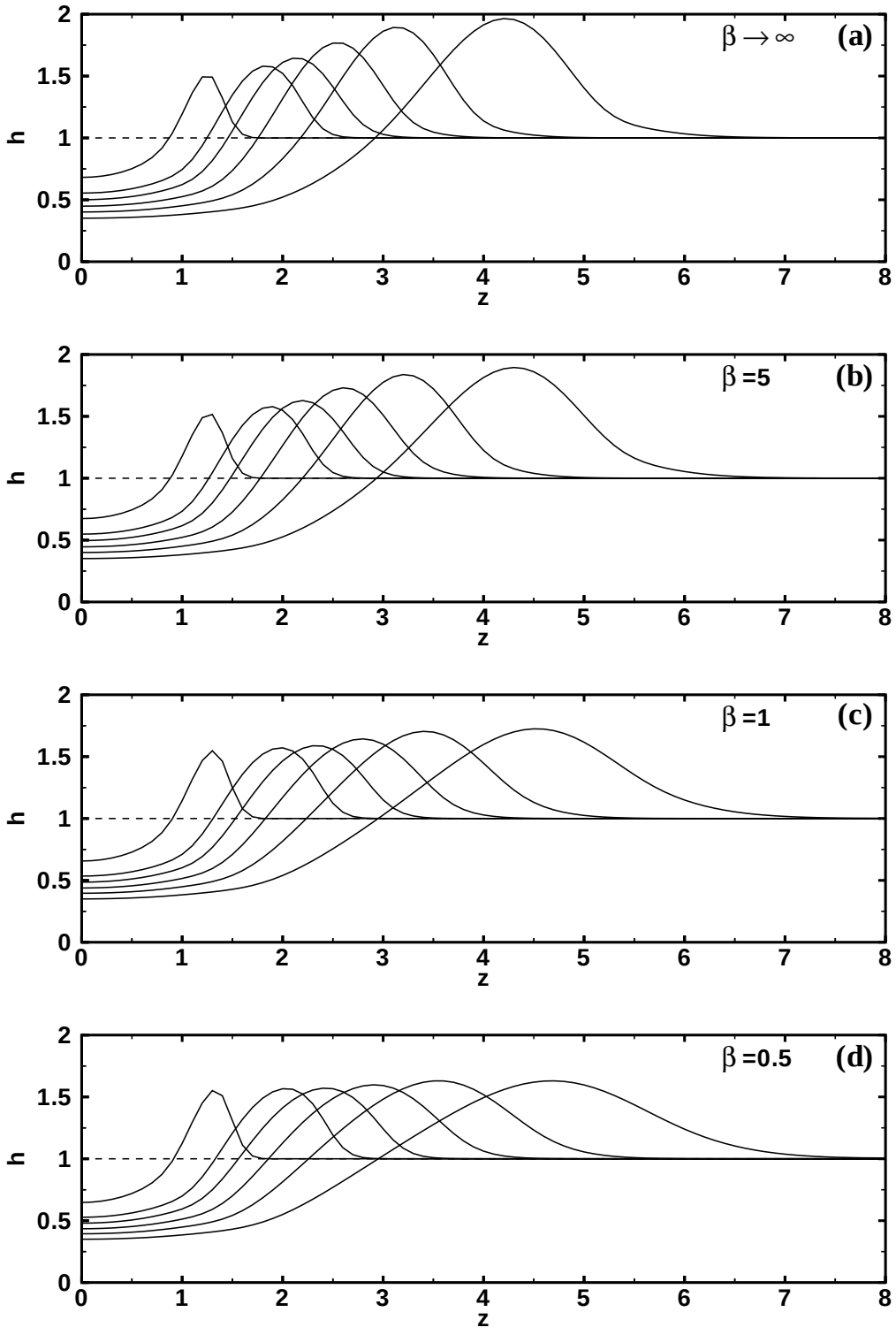

Figure 4.32: Time varying profiles of film thickness $h(z,t)$ for the kinetic nonlinearity (a) $\to \infty$ (linear), and $\beta =$ (b) 5, (c) 1, (d) 0.5, illustrated at times $t = 0$ (dashed line), 1, 5, 10, 20, 40, 100. Other parameter values are fixed and chosen as $\mathcal{J} = \mathcal{K} = 1$, $\Gamma_{exo} = 1$, $\Gamma_{pre} = 0$, $\mu = 100$ g/cm s, $\tau_{air} = 0$ and $\mathcal{G}_r = \mathcal{G}_z = 0$.

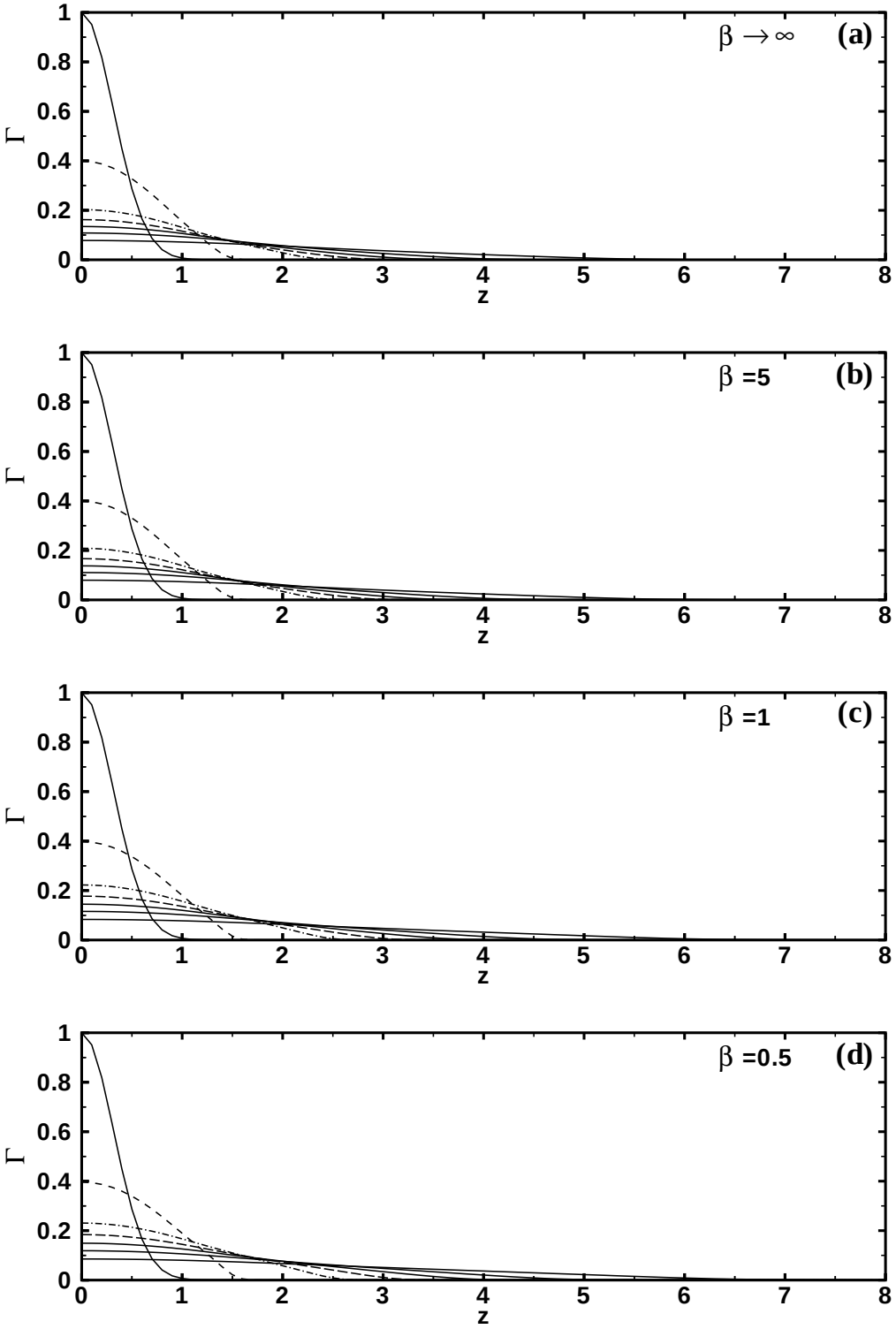

Figure 4.33: Time varying profiles of surface surfactant concentration $\Gamma(z,t)$ for the kinetic nonlinearity (a) $\to \infty$ (linear), and $\beta =$ (b) 5, (c) 1, (d) 0.5, illustrated at times $t = 0$, 1 (dashed), 5 (dash-dotted), 10 (long-dashed line), 20, 40, 100. Other parameter values are fixed and chosen as $\mathcal{J} = \mathcal{K} = 1$, $\Gamma_{exo} = 1$, $\Gamma_{pre} = 0$, $\mu = 100$ g/cm s, $\tau_{air} = 0$ and $\mathcal{G}_r = \mathcal{G}_z = 0$.

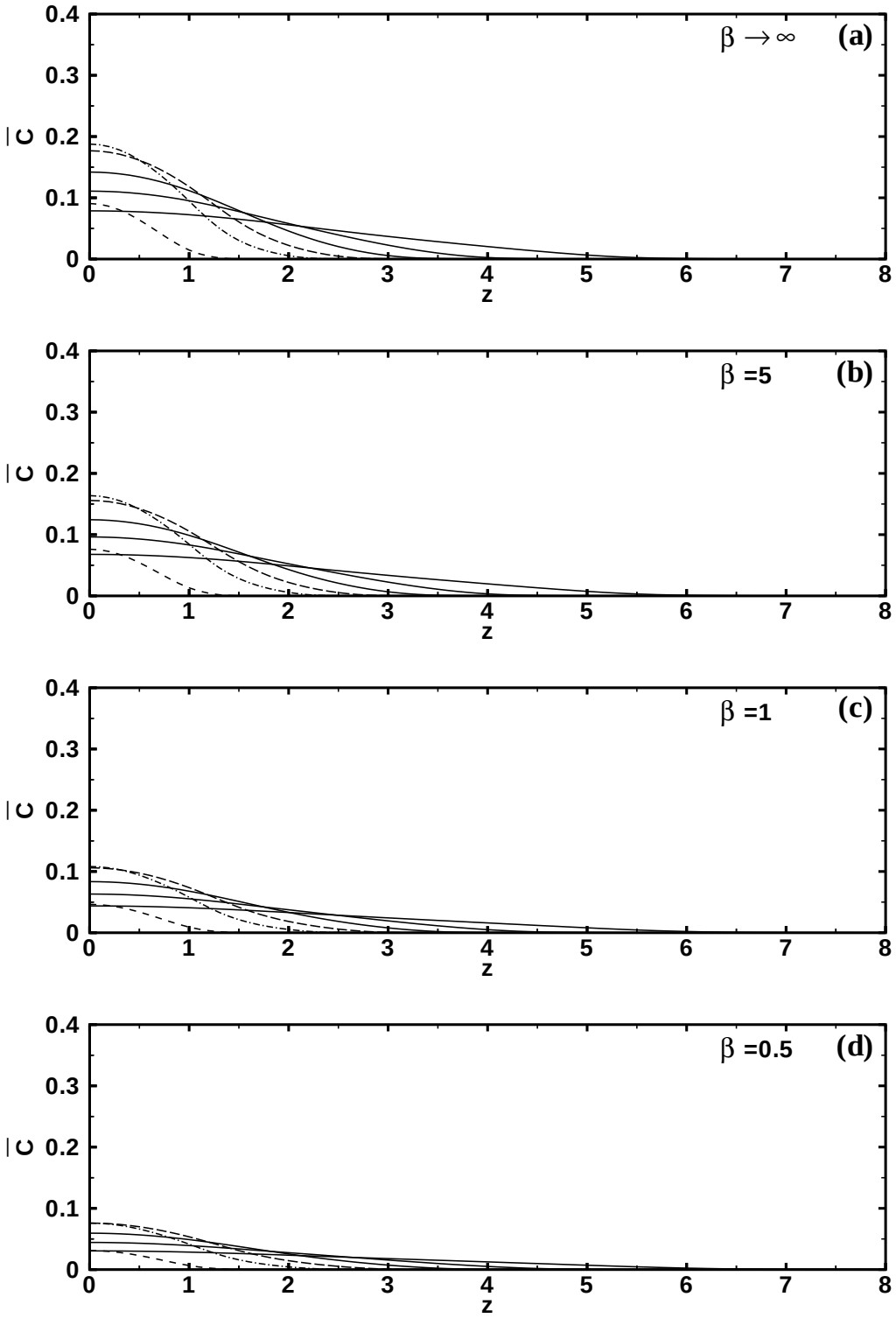

Figure 4.34: Time varying profiles of bulk surfactant concentration $\bar{C}(t)$ for the kinetic nonlinearity (a) $\to \infty$ (linear), and $\beta =$ (b) 5, (c) 1, (d) 0.5, illustrated at times $t = 0$, 1 (dashed), 5 (dash-dotted), 10 (long-dashed line), 20, 40, 100. Other parameter values are fixed and chosen as $\mathcal{J} = \mathcal{K} = 1$, $\Gamma_{exo} = 1$, $\Gamma_{pre} = 0$, $\mu = 100$ g/cm s, $\tau_{air} = 0$ and $\mathcal{G}_r = \mathcal{G}_z = 0$.

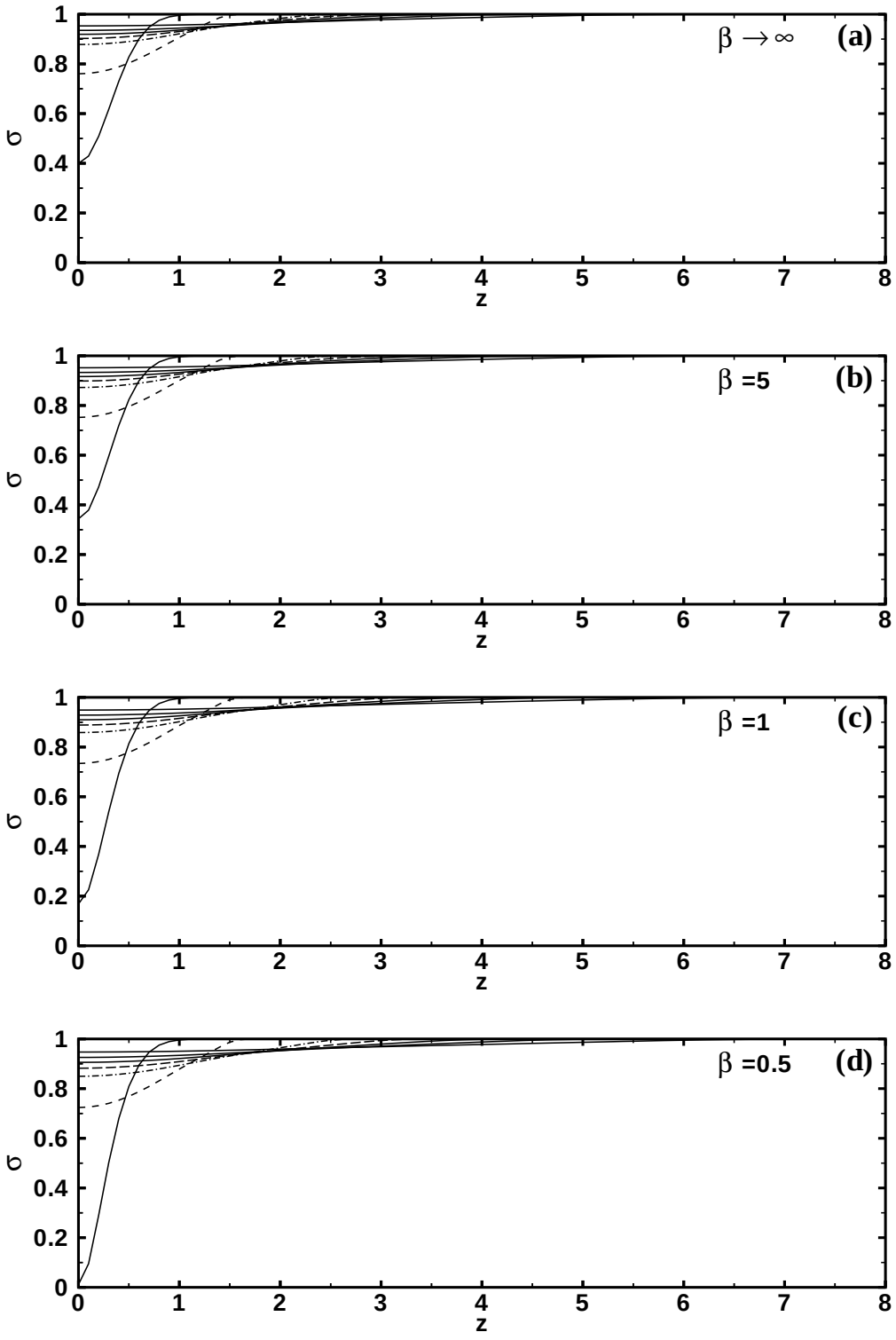

Figure 4.35: Time varying profiles of surface tension $\sigma(z,t)$ for the kinetic nonlinearity (a) $\to \infty$ (linear), and $\beta =$ (b) 5, (c) 1, (d) 0.5, illustrated at times $t = 0$, 1 (dashed), 5 (dash-dotted), 10 (long-dashed line), 20, 40, 100. Other parameter values are fixed and chosen as $\mathcal{J} = \mathcal{K} = 1$, $\Gamma_{exo} = 1$, $\Gamma_{pre} = 0$, $\mu = 100$ g/cm s, $\tau_{air} = 0$ and $\mathcal{G}_r = \mathcal{G}_z = 0$.

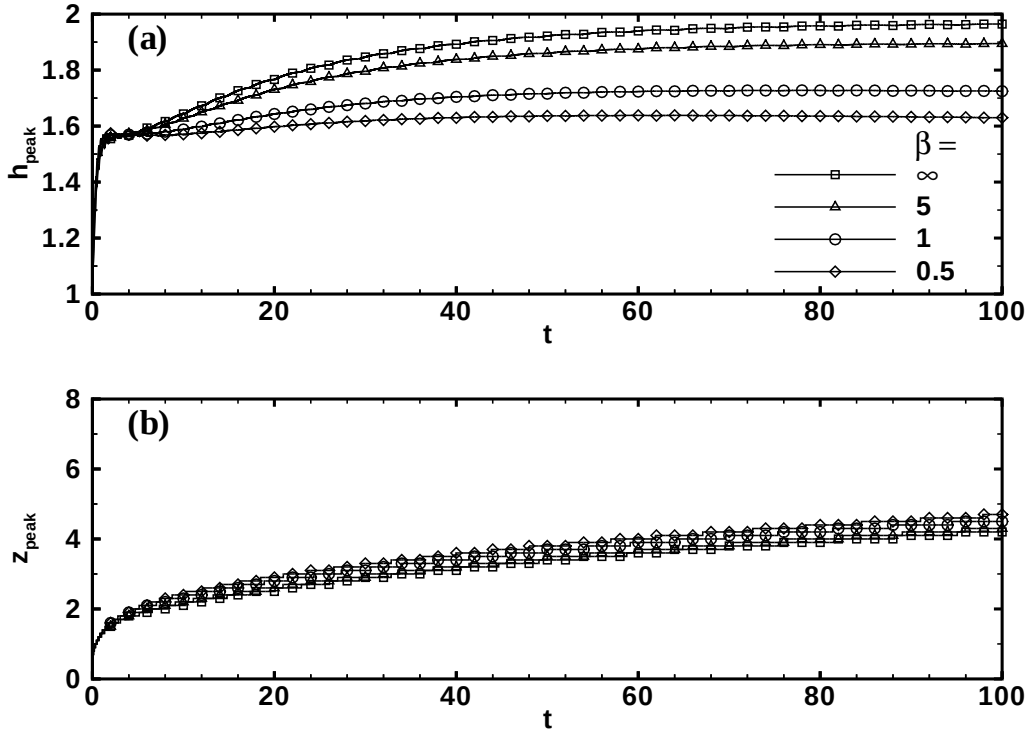

Figure 4.36: Temporal evolutions of (a) the peak film thickness, h_{peak}, and (b) the axial position of peak film thickness, z_{peak}, for $\beta \to \infty$ (linear), 5, 1 and 0.5.

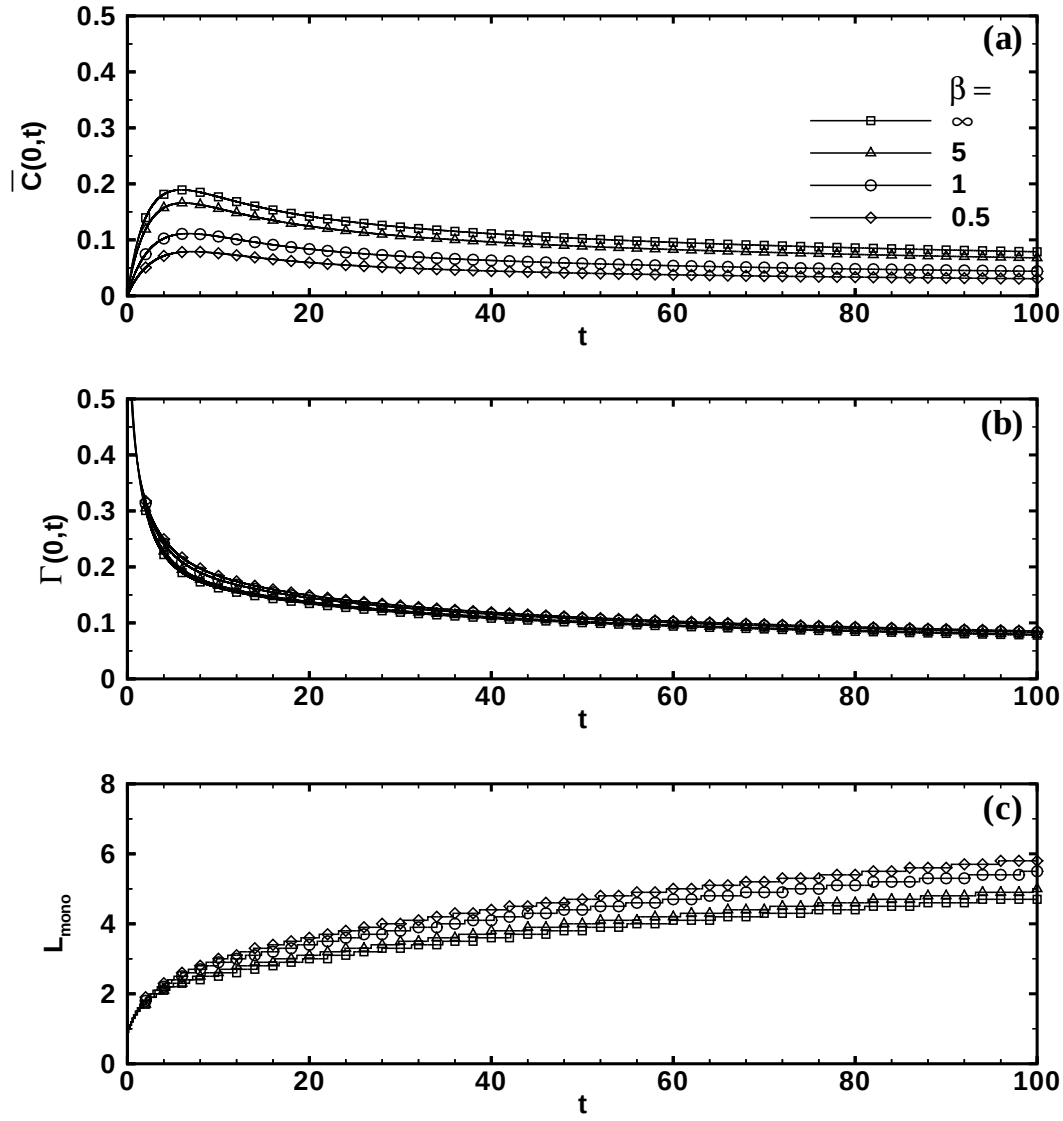

Figure 4.37: Temporal evolutions of (a) the bulk surfactant concentration at $z = 0$, $\bar{C}(0,t)$, (b) the surface surfactant concentration at $z = 0$, $\Gamma(0,t)$, and (c) the monolayer length, L_{mono}, for $\beta \to \infty$ (linear), 5, 1 and 0.5.

Chapter 5

Conclusions

The delivery of surfactant into the lung through the airways involves a variety of hydrodynamic, physico-chemical and physiological factors. Accurate estimation of the delivery time requires a thorough understanding of the localized spreading of surfactant on a pulmonary airway lining. In this study, we examine in detail the potential impacts of various parameters on the transport of exogenous surfactant and the induced film disturbance, including: the airway generation (the ratio of film thickness to airway radius), the strength of exogenous surfactant, the existence of preexisting surfactant, the viscosity of liquid lining, the shear stress from air flow and the surfactant solubility. The transport process is modeled by assuming small ratio of film thickness to airway radius, and the evolution of the viscous film is therefore governed by the balance between the viscous and Marangoni forces. The coupling between the surfactant surface spreading and the film deformation is governed by the equation of state, which relates the surface surfactant concentration to the surface tension. For soluble surfactant, nonlinear Langmuir isotherm is employed for the sorption kinetics between the surface and bulk-phase surfactants, and a nonlinear equation of state is derived from the Gibbs' equation.

Numerical simulation of the physico-chemical coupled model reveals that the surfactant spreads rapidly from the initial instillation of surfactant due to the large gradient in the localized distribution of concentration. As the surfactant spreads, the thin film lining is push away from the upstream end of airway to the downstream end through the the

Marangoni effect. A shock-like disturbance develops at the leading edge of the surfactant monolayer, across which is an abrupt transient in film thickness and a corresponding discontinuity in shear stress. The surfactant spreading is virtually independent on the airway generation. However, the disturbed shock is steeper in low-generation airway. For insoluble surfactant, fitting of the surfactant monolayer length L_{mono} from the numerical results indicates that a non-dimensional similarity time scale of $t^{0.31}$ exists in the surfactant spreading. Similar results have also been found by Espinosa *et al.* [1993] and Jensen & Grotberg [1992].

Film Rupture The solitary, shock-like disturbance forms near the leading edge of the surfactant monolayer advances with the surfactant spreading. Accompanying the raise of the peak height of shock-like disturbance h_{peak}, severe thinning of film occurs near the upstream end of airway forming a depressed trough. Film rupture ultimately develops when the depressed trough height continues to decrease as the shock-like disturbed wave propagates forward. Such a rupture in airway lining terminates the transport of surfactant [Gaver & Grotberg, 1992] and should be avoided in clinical therapy. Although the film will eventually reconnected, the treatment is delayed. Our simulations reveal that although the trough film height h_{trough} depresses drastically at the early transient stage, it tends to approach an asymptotic thickness as time processes. As the front of the disturbed wave reaches the downstream end of the airway, the trough height h_{trough} decreases to approximately 30% of the initial film thickness, which demonstrates that such severe thinning of the film dose not lead to film rupture within a finite time. This result is consistent with the conclusion of Jensen & Grotberg [1992] drawn for a planar thin lining that the viscous and Marangoni forces alone are insufficient to induce film rupture. When this severe thinning induced by Marangoni effect develops continuously, the intermolecular force becomes significant. Jensen & Grotberg [1992], therefore, included van der Waals forces in their model to explained the dryout process observed in the experiment of Gaver & Grotberg [1992]. Given the dramatic impact of film rupture on the transport of instilled

surfactant bolus, it is worthwhile to consider the prominent mechanism associated with van der Waals force in the further work.

The Exogenous and Preexisting Surfactants Raising the strength of the instilled exogenous bolus will increase the spreading rate of surfactant. The propagation speed of the film disturbance is also enhanced although the induced waveform is essentially unchanged. The presence of preexisting surfactant, on the other hand, retards the spreading of exogenous surfactant. As the exogenous surfactant advances, the preexisting surfactant in the region ahead of exogenous monolayer is compressed. This compressed monolayer accumulates in concentration and propagates forward. Such a push-and-compress mechanism, however, is not advantageous in clinical treatment as the transport of the administered surfactant is decelerated. This is consistent with the findings of clinical trial comparing two treatment strategies: a single bolus of surfactant is intubated into the endotracheal tube followed by mechanical ventilation; and administering surfactant by several bolus injection schemes including positioning the infant to optimize the transport. No differences in the short-term efficacy were found between these treatment strategies [Zola *et al.*, 1993], which imply the preexisting surfactant distribution does not accelerate the spreading of the afterwards administered exogenous surfactant.

Solubility of Surfactant If the surfactant is soluble, the coupled transport processes are further complicated by the adsorption/desorption kinetics between the surface and substrate surfactant. The sorption kinetics reduces the degree of inhomogeneity in surfactant-concentration distribution and, consequently, diminishes the surface-tension gradient and the induced Marangoni flow. The surfactant spreading is therefore retarded and so is the film disturbance. As a result, the height of the decelerated shock-like disturbance increases significantly due to the "squeezing" effect of the film thinning. Previous study of Espinosa & Kamm [1999], who modeled the surfactant transport into the entire lung, also indicated that the sorption kinetics can eliminate the surface-tension gradient in the central airways and enhance the sharp transition at the leading edge of surfactant, which

may cause film rupture and trap up to 95% of the surfactant in the airways.

Bibliography

[1] Avery, M.E. & Mead, J. 1959, Surface properties in relation to atelectasis and hyaline membrane disease, Am. J. Dis. Child., 97: 517–523.

[2] Barnes, T.A. 1994, Core textbook of respiratory care, St Louis: Mosby.

[3] Beachey, W. 1998, Respiratory Care Anatomy and Physiology, London: Mosby.

[4] Bhaskar, K.R., O'Sullivan, D.D., Seltzer, J., Rossing, T.H., Drazen, J.M. & Reid, L.M. 1985, Density gradient study of bronchial mucus aspirates from healthy volunteers (smokers and nonsmokers) and from patients with tracheostomy, Exp. Lung Res., 9: 289–308.

[5] Boncuk-Dayanikli, P. & Taeusch, H.W. 1995, Essential and nonessential constituents of exogenous surfactants, In Robertson, B. & Taeusch, H.W., editors, Surfactant Therapy for Lung Disease, Chapter 11, pp.217–238, New York: Marcel Dekker.

[6] Borgas, M.S. & Grotberg, J.B. 1988, Monolayer flow on a thin film, J. Fluid Mech., 193: 151–170.

[7] Cassidy, K.J., Bull, J.L., Glucksberg, M.R., Dawson, C.A., Haworth, S.T., Hirschl, R., Gavriely, N. & Grotberg, J.B. 2001, A rat lung model of instilled liquid transport in the pulmonary airways, J. Appl. Physiol., 90: 1955–1967.

[8] Clements, J.A. & Tierney, D.F. 1965, Alveolar instability associated with altered surface tension, In Fenn, W.O. & Rahn, H., editors, Handbook of Physiology, section 3, Washington D.C., American Physiological Society, 2: 1567–1568.

[9] Clint, J.H. 1992, Surfactant Aggregation, London: Blackie.

[10] Corbet, A. 1993, Clinical trails of synthetic surfactant in respiratory distress syndrome of premature infants, In Long, W.A., editors, Clinics in Perinatology, pp.737, Philadelphia: Saunders.

[11] Collins, J.M., Shapiro, A.H., Kimmel, E. & Kamm, R.D. 1993, The steady expiratory pressure-flow relation in a model pulmonary bifurcation, J. Biomech. Eng., 115: 299–305.

[12] Corbet, A., Bucciarelli, R., Goldman, S., Mammel, M., Wold, D. & Long, W. 1991, Decreased mortality rate among small premature infants treated at birth with a single dose of synthetic surfactant: a multicenter controlled trail, J. Pediatr., 118: 277–284.

[13] Craster, R.V. & Matar, O.K. 2000, Surfactant transport on mucus films, J. Fluid Mech., 425: 235–258.

[14] Davis, S.H., Liu, A.-K. & Sealy, G.R. 1974, Motion driven by surface tension gradients in a tube lining, J. Fluid Mech., 62: 737–751.

[15] Edwards, D.A., Brenner, H. & Wasan, D.T. 1991, Interfacial Transport Processes and Rheology, Boston: Butterworth-Heinemann.

[16] Espinosa, F.F. & Kamm, R.D. 1999, Bolus dispersal through the lungs in surfactant replacement therapy, J. Appl. Physiol., 86(1): 391–410.

[17] Espinosa, F.F., Shapiro, A.H., Fredberg, J.J. & Kamm, R.D. 1993, Spreading of exogenous surfactant in an airway, J. Appl. Physiol., 75: 2028–2039.

[18] Fujiwara, T, Maeta, H., Chida, S., Morita, T., Watabe, Y. & Abe, T. 1980, Artificial surfactant therapy in hyaline-membrane disease, Lancet, 1: 55–59.

[19] Gaver, D.P. & Grotberg, J.B. 1992, Droplet spreading on a thin viscous film, J. Fluid Mech., 235: 399–414.

[20] Gluck, L., Kulovich, M.V., Borer, R.C., Brenner, P.H., Anderson, G.G. & Sepllacy, W.W. 1971, Diagnosis of the respiratory distress syndrome by amniocentesis, Am. J. Obstet. Gyncol., 109: 440–445.

[21] Grotberg, J.B., Halpern, D. & Jensen, O.E. 1995, Interaction of exogenous and endogenous surfactant: spreading-rate effects, J. Appl. Physiol., 78(2): 750–756.

[22] Haitsma, J.J., Lachmann, U. & Lachmann, B. 2001, Exogenous surfactant as a drug delivery agent, Adv. Drug Delivery Rev., 47: 197–207.

[23] Halpern, D. & Grotberg, J.B. 1992, Dynamics and transport of a localized soluble surfactant on a thin film, J. Fluid Mech., 237: 1–11.

[24] Halpern, D., Jensen, O.E. & Grotberg, J.B. 1998, A theoretical study of surfactant and liquid delivery into the lung, J. Appl. Physiol., 85(1): 333–352.

[25] Hawgood, S. 1989, Pulmonary surfactant apoproteins: a review of protein and genomic structure, Am. J. Physiol., 257: L13–L22.

[26] Hiemenz, P.C. 1986, Principles of Colloid and Surface Chemistry, New York: Marcel Dekker.

[27] Hislop, A., Muir, D.C.F., Jacobsen, M., Simon, G. & Reid, L. 1972, Postnatal growth and function of the pre-acinar airways, Thorax, 27: 265–274.

[28] Jensen, O.E. & Grotberg, J.B. 1992, Insoluble surfactant spreading on a thin viscous film: shock evolution and film rupture, J. Fluid Mech., 240: 259–288.

[29] Jensen, O.E. & Grotberg, J.B. 1993, The spreading of heat or soluble surfactant along a thin liquid film, Phys. Fluids A, 5(1): 58–68.

[30] Jensen, O.E., Halpern, D. & Grotberg, J.B. 1994, Transport of a passive solute by surfactant-driven flows, Chem. Engng. Sci., 49(8): 1107–1117.

[31] Jensen, O.E. & Halpern, D. 1998, The stress singularity in surfactant-driven thin-film flows, J. Fluid Mech., 372: 273–300.

[32] Jobe, A.H. 1993, Pulmonary surfactant therapy, N. Engl. J. Med., 328: 861–868.

[33] Jobe, A.H., Ueda, T., Whitsett, J.A., Trapnell, B.C. & Ikegami, M. 1996, Surfactant enhances adenovirus mediated gene expression in rabbit lungs, Gene Ther., 3: 775–779.

[34] Katkin, J.P., Husser, R.C., Langston, C. & Welty, S.E. 1997, Exogenous surfactant enhances the delivery of recombinant adenoviral vectors to the lung, Hnm. Gene Ther., 8: 171–176.

[35] Kendig, J.W., Notter, R.H., Cox, C., Reubens, L., Davis, J.M., Maniscalco, W.M., Sinkin, R.A., Bartoletti, A., Dweck, H.S., Horgan, M.J., Risemberg, H., Phelps, D.L. & Shapiro, D. 1991, A comparison of surfactant as immediate prophylaxis and as rescue therapy in newborns of less than 30 weeks gestation, N. Engl. J. Med., 324: 865–871.

[36] Khammash, H., Perlman, M., Wojtulewicz, J. & Dunn, M. 1993, Surfactant therapy in full-term neonates with severe respiratory failure, Pediatrics, 92: 135–139.

[37] Kharasch, V.S., Sweeney, T.D., Fredberg, J.J., Lehr, J., Damokosh, A.I., Avery, M.E. & Brain, J.D. 1991, Pulmonary surfactant as a vehicle for intratracheal delivery of technetium sulfur colloid and pentamidine in hamster lungs, Am. Rev. Respir. Dis., 144: 909–913.

[38] Krueger, M.A. & Gaver, D.P. 2000, A theoretical model of pulmonary surfactant multilayer collapse under oscillating area conditions, J. Colloid Interface Sci., 229: 353–364.

[39] Levitzky, M.G. 1999, Pulmonary Physiology, New York: McGraw-Hill.

[40] Lewis, J.F., Ikegami, M., Jobe, A.H. & Absolom, D. 1993, Physiologic responses and distribution of aerosolized surfactant (Survanta) in a nonuniform pattern of lung injury, Am. Rev. Respir. Dis., 147: 1364–1370.

[41] Lewis, J.F. & Jobe, A.H. 1993, Surfactant and the adult respiratory distress syndrome, Am. Rev. Respir. Dis., 147: 218–233.

[42] Long, W., Thompson, T., Sundell, H., Schumacher, R., Volberg, F. & Guthrie, R. 1991, Effects of two rescue doses of a synthetic surfactant on mortality rate and survival without bronchopulmonary dysplasia in 700- to 1350-gram infants with respiratory distress syndrome, J. Pediatr., 118: 595–605.

[43] Marieb, E.N. 2000, Human Anatomy & Physiology, Benjamin Cummings.

[44] Mercier, C.E. & Soll, R.F. 1993, Clinical trails of natural surfactant extract in respiratory distress syndrome, In Long, W.A., editors, Clinics in Perinatology, pp.711, Philadelphia: Saunders.

[45] Merritt, T.A., Turner, T., Hallman, M., Vaucher, Y. & Wilson, M.J. 1995, Outcomes of surfactant-treated infants: analysis of developmental outcomes and the economic impact of surfactant therapy, In Robertson, B. & Taeusch, H.W., editors, Surfactant Therapy for Lung Disease, Chapter 29, pp.610–620, New York: Marcel Dekker.

[46] Morley, C.J. 1991, Surfactant treatment for premature babies: a review of clinical trails, Arch. Dis. Child, 66: 445–450.

[47] Morris, J., Ingenito, E.P., Mark, L., Kamm, R.D. & Johnson, M. 2001, Dynamic behavior of lung surfactant, J. Biomech. Eng., 123(1): 106–113.

[48] Otis, D.R., Ingenito, Jr.E.P., Kamm, R.D. & Johnson, M. 1994, Dynamic surface tension of surfactant TA: experiments and theory, J. Appl. Physiol., 77(6): 2681–2688.

[49] Pison, U., Bock, J.C., Pietschmann, S., Veit, S. & Slama, K. 1995, The adult respiratory distress syndrome: pathophysiological concepts related to the pulmonary surfactant system, In Robertson, B. & Taeusch, H.W., editors, Surfactant Therapy for Lung Disease, Chapter 9, pp.169–197, New York: Marcel Dekker.

[50] Possmayer, F. 1990, The role of surfactant-associated proteins, Am. Rev. Respir. Dis., 142: 749–752.

[51] Probstein R.F. 1994, Physicochemical Hydrodynamics: An Introduction, New York: John Wiley & Sons.

[52] Robertson, B. & Taeusch, H.W. 1995, Surfactant Therapy for Lung Disease, New York: Marcel Dekker.

[53] Sakata, E.K. & Berg, J.C. 1969, Surface diffusion in monolayers, Ind. Eng. Chem. Fundamentals, 8: 570–575.

[54] Scriven, L.E. 1960, Dynamics of a fluid interface: equation of motion of Newtonian surface fluids, Chem. Engng. Sci., 12: 98–108.

[55] Silberberg, A. 1983, Biorheological matching: mucociliary interaction and epithelial clearance, Biorheology, 20: 215–222.

[56] Soll, R.F. & McQueen, M.C. 1992, Respiratory distress syndrome, In Sinclair, J.C. & Bracken, M.B., editors, Effective care of the newborn infants, pp.325–355, Oxford: Oxford University Press.

[57] Spragg, R.G., Gilliard, N., Richman, P., Smith, R.M., Hite, R.D., Pappert, D., Robertson, B., Curstedt, T. & Strayer, D. 1994, Acute effects of a single dose of porcine surfactant on patients with adult respiratory distress syndrome, Chest, 105: 195–202.

[58] Stone, H.A. 1989, A simple derivation of the time-dependent convective-diffusion equation for surfactant transport along a deforming interface, Phys. Fluids A, 2(1): 111–112.

[59] Sun, B., Herting, E., Curstedt, T. & Robertson, B. 1994, Exogenous surfactant improves lung compliance and oxygenation in adult rats with meconium aspiration, J. Appl. Physiol., 77: 1961–1971.

[60] Tsai, W.T. & Yue, D.K.Y 1995, Effects of soluble and insoluble surfactant on laminar interactions of vortical flows with a free surface, J. Fluid Mech., 289: 315–349.

[61] Vander, A.J., Sherman, J.H. & Luciano, D.S. 1994, Human Physiology, McGraw Hill.

[62] Weaver, T.A. & Whitsett, J.A. 1991, Function and regulation of expression of pulmonary surfactant-associated proteins, Biochem. J., 273: 249–264.

[63] Weibel, E.R. 1963, Morphometry of the Human Lung, New York: Academic.

[64] Widdicombe, J.H. 2002, Regulation of the depth and composition of airway surface liquid, J. Anat., 201: 313–318.

[65] Wiswell, T.E., Peabody, S.S., Davis, M.V., Slayter, Bent, R.C. & Merritt, T.A. 1994, Surfactant therapy and high-frequency jet ventilation in the management of a piglet model of the meconium aspiration syndrome, Pediatr. Res., 36: 494–500.

[66] Zhang, Y.L., Matar, O.K. & Craster R.V. 2002, Surfactant spreading on a thin weakly viscoelastic film, J. Non-Newtonian Fluid Mech., 105: 53–78.

[67] Zhang, Y.L., Matar, O.K. & Craster R.V. 2003, A theoretical study of chemical delivery within the lung using exogenous surfactant, Med. Eng. Phys., 25: 115–132.

[68] Zola, E.M., Gunkel, J.H., Chan, R.K., Lim, M.O., Knox, I., Feldman, B.H., Denson, S.E., Stonestreet, B.S., Mitchell, B.R., Wyza, M.M., Bennett, K.J. & Gold, A.J.

1993, Comparison of three dosing procedures for administration of bovine surfactant to neonates with respiratory distress syndrome, J. Pediatr., 122(3): 453–459.

Appendix A

Stress Boundary Conditions for a Newtonian Interface

A.1 Normal-stress Boundary Condition

The general form of the normal-stress boundary condition for a Newtonian interface is of the form

$$-\mathbf{n}\cdot\mathbf{P}\cdot\mathbf{nn} = \mathbf{F}^s\cdot\mathbf{nn} + 2H\sigma\mathbf{n}, \tag{A.1}$$

where $\mathbf{n}$ is the normal vector at the interface, $\mathbf{F}^s$ is the external force, the pressure tensor $\mathbf{P} = -p\,\mathbf{I} + \mu(\nabla\mathbf{V} + \nabla\mathbf{V}^\intercal)$, and the surface curvature $H = -1/2\ \nabla_s\cdot\mathbf{n}$ with the surface operator $\nabla_s = (\mathbf{I}-\mathbf{nn})\cdot\nabla$. For the geometry of axisymmetric airway lining considered, the generic normal-stress boundary condition (A.1) is expressed in the cylindrical coordinate system. Using the axisymmetric properties, each term in (A.7) can be further simplified

in component forms of the vector equations as :

$$
\begin{aligned}
&-\mathbf{n}\cdot\mathbf{P}\cdot\mathbf{nn} \\
&= -\begin{bmatrix} n_r \\ 0 \\ n_z \end{bmatrix} \cdot \begin{Bmatrix} -p+2\mu\dfrac{\partial u}{\partial r} & 0 & \mu\left(\dfrac{\partial w}{\partial r}+\dfrac{\partial u}{\partial z}\right) \\ 0 & -p+2\mu\dfrac{u}{r} & 0 \\ \mu\left(\dfrac{\partial w}{\partial r}+\dfrac{\partial u}{\partial z}\right) & 0 & -p+2\mu\dfrac{\partial w}{\partial z} \end{Bmatrix} \cdot \begin{Bmatrix} n_r^2 & 0 & n_r n_z \\ 0 & 0 & 0 \\ n_r n_z & 0 & n_z^2 \end{Bmatrix} \\
&= -\begin{bmatrix} n_r\left(-p+2\mu\dfrac{\partial u}{\partial r}\right)+n_z\mu\left(\dfrac{\partial w}{\partial r}+\dfrac{\partial u}{\partial z}\right) \\ 0 \\ n_r\mu\left(\dfrac{\partial w}{\partial r}+\dfrac{\partial u}{\partial z}\right)+n_z\left(-p+2\mu\dfrac{\partial w}{\partial z}\right) \end{bmatrix} \cdot \begin{Bmatrix} n_r^2 & 0 & n_r n_z \\ 0 & 0 & 0 \\ n_r n_z & 0 & n_z^2 \end{Bmatrix} \\
&= -\begin{bmatrix} n_r^3\left(-p+2\mu\dfrac{\partial u}{\partial r}\right)+2n_r^2 n_z\mu\left(\dfrac{\partial w}{\partial r}+\dfrac{\partial u}{\partial z}\right)+n_r n_z^2\left(-p+2\mu\dfrac{\partial w}{\partial z}\right) \\ 0 \\ n_r^2 n_z\left(-p+2\mu\dfrac{\partial u}{\partial r}\right)+2n_r n_z^2\mu\left(\dfrac{\partial w}{\partial r}+\dfrac{\partial u}{\partial z}\right)+n_z^3\left(-p+2\mu\dfrac{\partial w}{\partial z}\right) \end{bmatrix} \\
&= \begin{bmatrix} n_r p-2\mu\left[n_r^3\dfrac{\partial u}{\partial r}+n_r n_z^2\dfrac{\partial w}{\partial z}+n_r^2 n_z\left(\dfrac{\partial w}{\partial r}+\dfrac{\partial u}{\partial z}\right)\right] \\ 0 \\ n_z p-2\mu\left[n_r^2 n_z\dfrac{\partial u}{\partial r}+n_z^3\dfrac{\partial w}{\partial z}+n_r n_z^2\left(\dfrac{\partial w}{\partial r}+\dfrac{\partial u}{\partial z}\right)\right] \end{bmatrix},
\end{aligned}
\tag{A.2}
$$

$$
\mathbf{F}_s\cdot\mathbf{nn} = \begin{bmatrix} 0 \\ 0 \\ \tau_{air} \end{bmatrix} \cdot \begin{Bmatrix} n_r^2 & 0 & n_r n_z \\ 0 & 0 & 0 \\ n_r n_z & 0 & n_z^2 \end{Bmatrix} = \begin{bmatrix} n_r n_z \tau_{air} \\ 0 \\ n_z^2 \tau_{air} \end{bmatrix}, \tag{A.3}
$$

and

$$
2H\sigma\mathbf{n} = -\sigma\left(\frac{\partial n_z}{\partial z}+\frac{n_r}{r}\right)\begin{bmatrix} n_r \\ 0 \\ n_z \end{bmatrix} = \begin{bmatrix} -\sigma n_r\left(\dfrac{\partial n_z}{\partial z}+\dfrac{n_r}{r}\right) \\ 0 \\ -\sigma n_z\left(\dfrac{\partial n_z}{\partial z}+\dfrac{n_r}{r}\right) \end{bmatrix}. \tag{A.4}
$$

Combining the expressions in (A.2), (A.3) and (A.4), the normal-stress boundary condition can be represented by the two equations in r and z directions, respectively, as

r-component :

$$n_r p - 2\mu \left[n_r^3 \frac{\partial u}{\partial r} + n_r n_z^2 \frac{\partial w}{\partial z} + n_r^2 n_z \left(\frac{\partial w}{\partial r} + \frac{\partial u}{\partial z} \right) \right] = n_r n_z \tau_{air} - \sigma \left(n_r \frac{\partial n_z}{\partial z} + \frac{n_r^2}{r} \right), \quad \text{(A.5)}$$

z-component :

$$n_z p - 2\mu \left[n_r^2 n_z \frac{\partial u}{\partial r} + n_z^3 \frac{\partial w}{\partial z} + n_r n_z^2 \left(\frac{\partial w}{\partial r} + \frac{\partial u}{\partial z} \right) \right] = n_r^2 \tau_{air} - \sigma \left(n_z \frac{\partial n_z}{\partial z} + \frac{n_r n_z}{r} \right). \quad \text{(A.6)}$$

A.2 Tangential-stress Boundary Condition

The general form of the tangential-stress boundary condition for a Newtonian interface is of the form

$$-\mathbf{n}\cdot\mathbf{P}\cdot\mathbf{I}_s = \mathbf{F}^s\cdot\mathbf{I}_s + \nabla_s\sigma, \tag{A.7}$$

where the dyadic surface idemfactor $\mathbf{I}_s = (\mathbf{I}-\mathbf{nn})$, and the surface operator $\nabla_s = \mathbf{I}_s\cdot\nabla$. Similar to the normal-stress boundary condition, for the geometry of axisymmetric airway lining considered, the terms in (A.7) can be written in the tensor form as follow :

$$\begin{aligned}
&-\mathbf{n}\cdot\mathbf{P}\cdot\mathbf{I}_s \\
&= -\begin{bmatrix} n_r\left(-p+2\mu\dfrac{\partial u}{\partial r}\right)+n_z\mu\left(\dfrac{\partial w}{\partial r}+\dfrac{\partial u}{\partial z}\right) \\ 0 \\ n_r\mu\left(\dfrac{\partial w}{\partial r}+\dfrac{\partial u}{\partial z}\right)+n_z\left(-p+2\mu\dfrac{\partial w}{\partial z}\right)\end{bmatrix}\cdot\begin{Bmatrix} n_z^2 & 0 & -n_rn_z \\ 0 & 1 & 0 \\ -n_rn_z & 0 & n_r^2\end{Bmatrix} \\
&= -\begin{bmatrix} (n_z^3-n_r^2n_z)\mu\left(\dfrac{\partial w}{\partial r}+\dfrac{\partial u}{\partial z}\right)+2n_rn_z^2\mu\left(\dfrac{\partial u}{\partial r}+\dfrac{\partial w}{\partial z}\right) \\ 0 \\ (n_r^3-n_rn_z^2)\mu\left(\dfrac{\partial w}{\partial r}+\dfrac{\partial u}{\partial z}\right)+2n_r^2n_z\mu\left(\dfrac{\partial u}{\partial r}+\dfrac{\partial w}{\partial z}\right)\end{bmatrix},
\end{aligned} \tag{A.8}$$

$$\mathbf{F}_s\cdot\mathbf{I}_s = \begin{bmatrix} 0 \\ 0 \\ \tau_{air}\end{bmatrix}\cdot\begin{Bmatrix} n_z^2 & 0 & -n_rn_z \\ 0 & 1 & 0 \\ -n_rn_z & 0 & n_r^2\end{Bmatrix} = \begin{bmatrix} -n_rn_z\tau_{air} \\ 0 \\ n_r^2\tau_{air}\end{bmatrix}, \tag{A.9}$$

and

$$\nabla_s\sigma = \begin{bmatrix} -n_rn_z\dfrac{\partial\sigma}{\partial z} \\ 0 \\ n_r^2\dfrac{\partial\sigma}{\partial z}\end{bmatrix}. \tag{A.10}$$

Therefore, the tangential-stress boundary condition can be expressed into two components in r and z directions, respectively, as

r-component:

$$-(n_z^3 - n_r^2 n_z)\mu\left(\frac{\partial w}{\partial r} + \frac{\partial u}{\partial z}\right) - 2n_r n_z^2 \mu\left(\frac{\partial u}{\partial r} + \frac{\partial w}{\partial z}\right) = -n_r n_z \tau_{air} - n_r n_z \frac{\partial \sigma}{\partial z}, \qquad \text{(A.11)}$$

z-component:

$$-(n_r^3 - n_r n_z^2)\mu\left(\frac{\partial w}{\partial r} + \frac{\partial u}{\partial z}\right) - 2n_r^2 n_z \mu\left(\frac{\partial u}{\partial r} + \frac{\partial w}{\partial z}\right) = n_r^2 \tau_{air} + n_r^2 \frac{\partial \sigma}{\partial z}. \qquad \text{(A.12)}$$

Appendix B

Cross-sectional Average of Bulk Surfactant Transport Equation

The cross-sectional average of the transport equation for bulk surfactant (2.50) is

$$\frac{2\pi}{\mathcal{A}}\int_{\frac{1}{\epsilon}-h}^{\frac{1}{\epsilon}} r\left[\underbrace{\bar{C}_t}_{(1)}+\underbrace{w\bar{C}_z}_{(2)}+\underbrace{\mathcal{P}e_b\epsilon^2 C_{1t}}_{(3)}+\underbrace{\mathcal{P}e_b\epsilon^2 uC_{1r}}_{(4)}+\underbrace{\mathcal{P}e_b\epsilon^2 wC_{1z}}_{(5)}=\underbrace{r^{-1}(rC_{1r})_r}_{(6)}+\underbrace{C_{1zz}}_{(7)}\right]\mathrm{d}r.$$

Each term in the above equation is further expressed as :

$$(1): \quad \frac{2\pi}{\mathcal{A}}\int_{\frac{1}{\epsilon}-h}^{\frac{1}{\epsilon}} r\frac{\partial\bar{C}(z,t)}{\partial t}\mathrm{d}r=\frac{\partial\bar{C}(z,t)}{\partial t} \tag{B.1}$$

$$(2): \quad \frac{2\pi}{\mathcal{A}}\int_{\frac{1}{\epsilon}-h}^{\frac{1}{\epsilon}} rw(r,z,t)\frac{\partial\bar{C}(z,t)}{\partial z}\mathrm{d}r=\bar{w}\frac{\partial\bar{C}(z,t)}{\partial z} \tag{B.2}$$

$$\begin{aligned}(3): \quad & \mathcal{P}e_b\epsilon^2\frac{2\pi}{\mathcal{A}}\int_{\frac{1}{\epsilon}-h}^{\frac{1}{\epsilon}} r\frac{\partial C_1(r,z,t)}{\partial t}\mathrm{d}r \\ &=\mathcal{P}e_b\epsilon^2\left\{\frac{\partial}{\partial t}\left(\frac{2\pi}{\mathcal{A}}\int_{\frac{1}{\epsilon}-h}^{\frac{1}{\epsilon}} rC_1dr\right)+\frac{2\pi}{\mathcal{A}}\left(\frac{1}{\epsilon}-h\right)\frac{\partial h}{\partial t}\left[\bar{C}_1-(C_1)_{r=\frac{1}{\epsilon}-h}\right]\right\} \\ &=-\mathcal{P}e_b\epsilon^2\frac{2\pi}{\mathcal{A}}\left(\frac{1}{\epsilon}-h\right)\frac{\partial h}{\partial t}(C_1)_{r=\frac{1}{\epsilon}-h}\end{aligned} \tag{B.3}$$

(4) :

$$\begin{aligned}
&\mathcal{P}e_b\epsilon^2\frac{2\pi}{\mathcal{A}}\int_{\frac{1}{\epsilon}-h}^{\frac{1}{\epsilon}} ru\frac{\partial C_1(r,z,t)}{\partial r}\mathrm{d}r \\
&= \mathcal{P}e_b\epsilon^2\frac{2\pi}{\mathcal{A}}\int_{\frac{1}{\epsilon}-h}^{\frac{1}{\epsilon}} \frac{\partial(ruC_1)}{\partial r}\mathrm{d}r \\
&= \mathcal{P}e_b\epsilon^2\frac{2\pi}{\mathcal{A}}(ruC_1)_{r=\frac{1}{\epsilon}-h}^{\frac{1}{\epsilon}} \\
&= \mathcal{P}e_b\epsilon^2\frac{2\pi}{\mathcal{A}}\left[(ruC_1)_{r=\frac{1}{\epsilon}} - (ruC_1)_{r=\frac{1}{\epsilon}-h}\right] \\
&= -\mathcal{P}e_b\epsilon^2\frac{2\pi}{\mathcal{A}}\left(\frac{1}{\epsilon}-h\right)u^s(C_1)_{r=\frac{1}{\epsilon}-h}
\end{aligned} \tag{B.4}$$

(5) :

$$\begin{aligned}
&\mathcal{P}e_b\epsilon^2\frac{2\pi}{\mathcal{A}}\int_{\frac{1}{\epsilon}-h}^{\frac{1}{\epsilon}} r\frac{\partial\left[wC_1(r,z,t)\right]}{\partial z}\mathrm{d}r \\
&= \mathcal{P}e_b\epsilon^2\frac{2\pi}{\mathcal{A}}\overline{(wC_1)_z} \\
&= \mathcal{P}e_b\epsilon^2\left[\frac{\mathcal{A}}{2\pi}\frac{\partial}{\partial z}\left(\frac{2\pi}{\mathcal{A}}\overline{wC_1}\right) - \frac{2\pi}{\mathcal{A}}\left(\frac{1}{\epsilon}-h\right)\frac{\partial h}{\partial z}w^s(C_1)_{r=\frac{1}{\epsilon}-h}\right]
\end{aligned} \tag{B.5}$$

(6) :

$$\begin{aligned}
&\frac{2\pi}{\mathcal{A}}\int_{\frac{1}{\epsilon}-h}^{\frac{1}{\epsilon}}\frac{\partial}{\partial r}\left(r\frac{\partial C_1}{\partial r}\right)\mathrm{d}r \\
&= \frac{2\pi}{\mathcal{A}}\left[r\frac{\partial C_1}{\partial r}\right]_{r=\frac{1}{\epsilon}-h}^{\frac{1}{\epsilon}} \\
&= \frac{2\pi}{\mathcal{A}}\left[\frac{1}{\epsilon}\left(\frac{\partial C_1}{\partial r}\right)_{r=\frac{1}{\epsilon}} - \left(\frac{1}{\epsilon}-h\right)\left(\frac{\partial C_1}{\partial r}\right)_{r=\frac{1}{\epsilon}-h}\right] \\
&= -\frac{2\pi}{\mathcal{A}}\left(\frac{1}{\epsilon}-h\right)\left(\frac{\partial C_1}{\partial r}\right)_{r=\frac{1}{\epsilon}-h}
\end{aligned} \tag{B.6}$$

(7) :

$$\frac{1}{\mathcal{P}e_b}\frac{2\pi}{\mathcal{A}}\int_{\frac{1}{\epsilon}-h}^{\frac{1}{\epsilon}} r\frac{\partial^2\bar{C}}{\partial z^2}\mathrm{d}r = \frac{1}{\mathcal{P}e_b}\frac{\partial^2\bar{C}}{\partial z^2} \tag{B.7}$$

After taking the cross-sectional averaging, the bulk surfactant transport equation becomes

$$\begin{aligned}
&\bar{C}_t + \bar{w}\bar{C}_z - \mathcal{P}e_b\epsilon^2\frac{2\pi}{\mathcal{A}}\left(\frac{1}{\epsilon}-h\right)\left(h_t + w^s h_z + u^s\right)(C_1)_{r=\frac{1}{\epsilon}-h} + \mathcal{P}e_b\epsilon^2\frac{\mathcal{A}}{2\pi}\left(\frac{2\pi}{\mathcal{A}}\overline{wC_1}\right)_z \\
&= -\frac{2\pi}{\mathcal{A}}\left(\frac{1}{\epsilon}-h\right)(C_{1r})_{r=\frac{1}{\epsilon}-h} + \frac{1}{\mathcal{P}e_b}\bar{C}_{zz}.
\end{aligned} \tag{B.8}$$

The third term in the above equation vanishes because of the kinematic boundary condition (2.23). The term of $O(\mathcal{P}e_b\epsilon^2)$ represents the effect of shear dispersion. As what has been discussed by Jensen & Grotberg [1993], the bulk surfactant transport attributed to shear dispersion would decay with time, while the horizontal diffusion becomes significant

increasingly. The shear dispersion term in (B.8) is potentially important only in the early period of spreading, and will be neglected in the following model. Using the equilibrium boundary condition (2.47), the average bulk-surfactant transport equation (B.8) becomes

$$\begin{aligned}\bar{C}_t + \bar{w}\bar{C}_z =& \frac{1}{\mathcal{P}e_b}\bar{C}_{zz} + \frac{1}{\mathcal{P}e_b}\frac{2-\epsilon h}{2h}h_z\bar{C}_z \\ &- \frac{1}{\mathcal{P}e_b}\frac{1}{\mathcal{J}}\frac{1}{\mathcal{N}}\frac{1}{\epsilon}\left(\frac{\beta}{1+\beta}\right)\left(\frac{2-\epsilon h}{2h}\right)\left[\bar{C}\left(1+\frac{1-\Gamma}{\beta}\right)-\Gamma\right]. \end{aligned} \tag{B.9}$$

Appendix C

Shear Stress Due to Air Flow

Following Espinosa & Kamm [1999], a Poiseuille flow in a single airway is considered with the pressure $p^a = p^a(z)$. Under the condition that the thin film thickness is much smaller than the airway radius ($h \ll R$), and the surface velocity of airway lining is small in comparison with the axial air velocity ($w^s \ll w^a$), the dimensional axial velocity of the air flow is

$$w^a(r) = \frac{(r^2 - R^2)}{4\mu_a} \frac{\mathrm{d}p^a}{\mathrm{d}z}, \tag{C.1}$$

where μ_a is the viscosity of air. The dimensional air flux in generation-n airways is

$$Q^a = 2^n \left(2\pi \int_0^R r w^a \mathrm{d}r \right) = \frac{-\pi R^4 2^n}{8\mu_a} \frac{\mathrm{d}p^a}{\mathrm{d}z}, \tag{C.2}$$

where 2^n is the total number of airways at generation n for the dichotomous airway model described by Weibel [1963]. From (C.1) and (C.2), the dimensional average axial velocity of air flow becomes

$$\bar{w}^a = \frac{Q^a}{\pi R^2 2^n}. \tag{C.3}$$

Applying the experimental result of Collins *et al.* [1993], the dimensional shear stress due to air flow can be deduced from the pressure gradient,

$$\tau_{air} = \mu_a \frac{\mathrm{d}w^a}{\mathrm{d}r}\bigg|_{r=R} = -\frac{R}{2} \begin{cases} \dfrac{\mathrm{d}p^a}{\mathrm{d}z} & \text{for } \mathcal{R}e_a < 50 \\ \dfrac{\mathrm{d}p^a}{\mathrm{d}z}(0.566 + 0.06\mathcal{R}e_a^{1/2}) & \text{for } \mathcal{R}e_a > 50, \end{cases} \tag{C.4}$$

where the local Reynolds number is defined as $\mathcal{R}e_a \equiv (\rho_a Q^a)/(\pi \mu_a R 2^{n-1})$ with ρ_a the density of air. Substituting the air flux (C.2) into (C.4), the dimensional shear stress

induced by air flow becomes

$$\tau_{air} = \frac{4\mu_a Q^a}{\pi R^3 2^n} \begin{cases} 1 & \text{for } \mathcal{R}e_a < 50 \\ (0.566 + 0.06\mathcal{R}e_a^{1/2}) & \text{for } \mathcal{R}e_a > 50. \end{cases} \tag{C.5}$$

Additionally, the time varying volume into the airway for the ventilation is described by

$$V(t) = \begin{cases} -V_T \cos\left(\dfrac{2\pi t}{2\tau_0 f}\right) & \text{for inspiration} \\ V_T \cos\left[\dfrac{2\pi t}{2\tau_0(1-f)}\right] & \text{for expiration,} \end{cases} \tag{C.6}$$

where $2V_T$ is the tidal volume, τ_0 is the time for one breath, and f is the fraction of τ_0 for inspiration. The air flux Q^a can then be obtained from (C.6) by $Q^a = \mathrm{d}V(t)/\mathrm{d}t$. Non-dimensionalization using the characteristic scales in (2.19), equations (C.5) and (C.6) become

$$\tilde{\tau}_{air} = \frac{4\mu_a h_0}{\pi\mu R 2^n} \frac{\mathrm{d}\tilde{V}(\tilde{t})}{\mathrm{d}\tilde{t}} \begin{cases} 1 & \text{for } \mathcal{R}e_a < 50 \\ (0.566 + 0.06\mathcal{R}e_a^{1/2}) & \text{for } \mathcal{R}e_a > 50, \end{cases} \tag{C.7}$$

and

$$\tilde{V}(\tilde{t}) = \begin{cases} -\tilde{V}_T \cos\left(\dfrac{2\pi\tilde{t}}{2\tilde{\tau}_0 f}\right) & \text{for inspiration} \\ \tilde{V}_T \cos\left[\dfrac{2\pi\tilde{t}}{2\tilde{\tau}_0(1-f)}\right] & \text{for expiration,} \end{cases} \tag{C.8}$$

where

$$\mathcal{R}e_a = \frac{\rho_a \sigma_m h_0}{\pi\mu\mu_a 2^{n-1}} \frac{\mathrm{d}\tilde{V}(\tilde{t})}{\mathrm{d}\tilde{t}}.$$